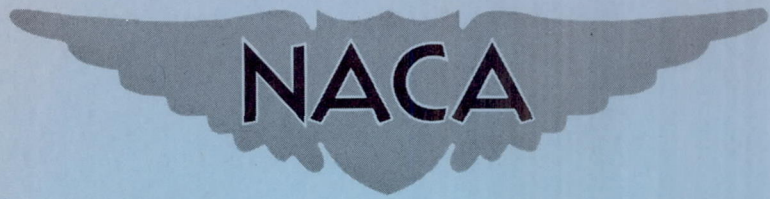RELEASE DATE

JUN 24 1958

CONFIDENTIAL

Copy 1
RM L58C17

NACA RM L58C17

NACA

RESEARCH MEMORANDUM

AERODYNAMIC CHARACTERISTICS OF A 45° SWEPT-WING

FIGHTER-AIRPLANE MODEL AND AERODYNAMIC LOADS

ON ADJACENT STORES AND MISSILES AT MACH

NUMBERS OF 1.57, 1.87, 2.16, AND 2.53

By Waldo I. Oehman and Kenneth L. Turner

Langley Aeronautical Laboratory
Langley Field, Va.

CLASSIFICATION CHANGE

To Unclassified _____ by H. Maines
By authority of _____ Date 4/15/71/51
Changed by M. Rudd _____ Date 4-123- /71

NATIONAL ADVISORY COMMITTEE
FOR AERONAUTICS
WASHINGTON
June 24, 1958

NATIONAL ADVISORY COMMITTEE FOR AERONAUTICS

RESEARCH MEMORANDUM

AERODYNAMIC CHARACTERISTICS OF A 45° SWEPT-WING

FIGHTER-AIRPLANE MODEL AND AERODYNAMIC LOADS

ON ADJACENT STORES AND MISSILES AT MACH

NUMBERS OF 1.57, 1.87, 2.16, AND 2.53

By Waldo I. Oehman and Kenneth L. Turner

SUMMARY

An investigation was performed in the Langley Unitary Plan wind tunnel to determine the aerodynamic characteristics of a model of a 45° swept-wing fighter airplane, and to determine the loads on attached stores and detached missiles in the presence of the model. Also included was a determination of aileron-spoiler effectiveness, aileron hinge moments, and the effects of wing modifications on model aerodynamic characteristics. Tests were performed at Mach numbers of 1.57, 1.87, 2.16, and 2.53. The Reynolds numbers for the tests, based on the mean aerodynamic chord of the wing, varied from about 0.9×10^6 to 5×10^6. The results are presented with minimum analysis.

INTRODUCTION

Aerodynamic loads on external stores and fired missiles, in the presence of an airplane, are of current interest to airplane manufacturers. Knowledge of the magnitude of the aerodynamic loads is necessary for an accurate determination of the flight path of a missile and efficient design of support structure for stores.

In consideration of the importance of the above problem, an investigation was made to provide pertinent data of this type. Wind-tunnel tests were made on a model of a fighter-type airplane with attached external stores and detached missiles near the model. The model, stores, and missiles were instrumented and test variables were controlled to provide the desired information. Other results obtained during the investigation include control effectiveness of aileron-spoiler combinations, aileron hinge-moment coefficients, the effect of Reynolds number on minimum drag coefficient, and the effect of fixed transition and two wing modifications

on the aerodynamic characteristics of the model. The wing modifica-
tions were proposed as a means to alleviate transonic pitch-up.

A $45°$ swept-wing model of a conventional fighter airplane was used
for the tests. The results were obtained at Mach numbers of 1.57, 1.87,
2.16, and 2.53 for angles of attack from about $-2°$ to $22°$ and for side-
slip angles from about $-9°$ to $9°$. The Reynolds numbers for the tests,
based on wing mean aerodynamic chord, varied from about 0.9×10^6 to
5×10^6. The results are presented with minimum analysis.

SYMBOLS

The symbols used in this report are listed below. Moment centers,
reference areas and lengths, and axes systems are defined in the section
entitled "Presentation of Results."

b wing span, in.

$\bar{c}$ mean aerodynamic chord of wing, in.

C_D' drag coefficient, $\dfrac{F_D}{q_\infty S}$

C_{D_b} base-drag coefficient, $\dfrac{\left(p_\infty - p_b\right)S_b}{q_\infty S}$

C_{D_c} chamber-drag coefficient, $\dfrac{\left(p_\infty - p_c\right)S_c}{q_\infty S}$

C_{D_i} duct internal-drag coefficient, $\dfrac{\text{Internal drag}}{q_\infty S}$

C_{D_e} net external-drag coefficient

$C_{D_{min}}$ minimum net external-drag coefficient

C_{h_a} aileron hinge-moment coefficient, $\dfrac{\text{Aileron hinge moment}}{2q_\infty M_a}$

C_L lift coefficient, $\dfrac{F_L}{q_\infty S}$

C_l rolling-moment coefficient, $\dfrac{\text{Rolling moment}}{q_\infty S b}$

C_m pitching-moment coefficient, $\dfrac{\text{Pitching moment}}{q_\infty S \bar{c}}$

C_N normal-force coefficient, $\dfrac{F_N}{q_\infty S}$

C_n yawing-moment coefficient, $\dfrac{\text{Yawing moment}}{q_\infty S b}$

C_Y side-force coefficient, $\dfrac{F_Y}{q_\infty S}$

d maximum diameter of store or missile, in.

F_D force along X stability axis, lb

F_L lift force, lb

F_N normal force, lb

F_Y side force, lb

l store or missile length, in.

M_a moment area of aileron, cu ft

M_∞ free-stream Mach number

p_b model base pressure, lb/sq ft

p_c model chamber pressure, lb/sq ft

p_∞ free-stream static pressure, lb/sq ft

q_∞ free-stream dynamic pressure, lb/sq ft

R Reynolds number

S   reference area (projected wing area for model and maximum
                   cross-sectional area for stores and missiles), sq ft

S_b model base area, sq ft

S_c model chamber area, sq ft

T   traverse position of missile nose along its X body axis
                   measured from firing position, in.

t   thickness of wing, in.

W_E mass flow at duct exit, slugs/sec

W_1 free-stream mass flow based on duct inlet area, slugs/sec

z   vertical distance between nose of missile and zero water
                   line of model, in.

α angle of attack of wing chord, deg

α_M angle of attack of missile center line, deg

β angle of sideslip of fuselage center line, deg

β_M angle of sideslip of missile center line, deg

δ_a aileron deflection angle (positive when trailing edge is
                   down), deg

δ_z spoiler deflection angle (positive when trailing edge is
                   down), deg

Subscripts:

C   center-line tank

L   left hand

M   missile

R   right hand

s   denotes coefficient referred to stability axis

T   center-line store

w   denotes coefficient referred either to wind axis or to stability axis

wt   wing tank

Note: Moment coefficients for missiles and stores are based on l rather than $\bar{c}$ or b.

APPARATUS AND TESTS

Tunnel

The tests were conducted in the low Mach number test section of the Langley Unitary Plan wind tunnel, which is a variable-pressure return-flow type. The test section is 4 feet square and approximately 7 feet long. The nozzle leading to the test section is of the asymmetric sliding-block type which permits a continuous variation of Mach number from approximately 1.57 to 2.80.

Model Support

The airplane model was mounted on a six-component, internal strain-gage balance which, in turn, was supported by a sting. The external stores were mounted on individual four-component internal strain-gage balances that were supported by pylons extending from the model. For the detached missile tests, the missile was fastened to an internally mounted four-component strain-gage balance that was supported by a motor-driven sting. This sting was clamped to the model sting.

Model and Test Conditions

A three-view drawing of the 1/20-scale model of a 45° swept-wing supersonic fighter airplane is presented in figure 1. Model geometric characteristics are presented in table I. The model configurations tested are listed in table II with the ranges of test variables for each. Drawings and photographs of the configurations are shown in figures 2 and 3. All missiles were attached to the model in a retracted position for all airplane model tests. When the forward missile was moved through the interference field of the model, the rearward missiles were considered to have been fired and were removed from the model. When the rearward missile was moved through the interference field of

the model, the forward missiles and the other rearward missile were attached to the model in a retracted position. All model configurations, with one exception, were tested with the all-movable horizontal tail set at an incidence of 0° and with the inlets and ducts open.

The tests were performed at a stagnation pressure of approximately 6.0 pounds per square inch absolute and a stagnation temperature of approximately 125° F. However, a few tests were performed at higher stagnation pressures that corresponded to balance load capability. The dewpoint, measured at stagnation pressure, was maintained below -30° F to assure negligible condensation effects.

Test Procedure

For the missile tests, each missile was traversed in a straight path and its attitude was dependent on its preset angle, the model sting attitude, and the deflection of the missile balance and sting under load. The model was set at angles of attack and sideslip of 0° and test positions for the missile were selected by traversing the missile forward from its launching position to positions such that maximum or minimum pitching moments were experienced by the missile. Traversing was continued until the missile was completely out of the interference field of the model. These same positions were used for all other model attitudes at a given Mach number. New traverse positions were obtained for each change in Mach number.

In order to determine the minimum drag coefficient of the basic model with a fully turbulent boundary layer, a few tests were performed with a transition strip fixed around the nose, 1 inch rearward of the tip, and also on the 10-percent chord of the wing (top and bottom, full span). Two sizes of grain for the transition strips were used: No. 60 carborundum (nominal height, 0.012 inch) and No. F carborundum (nominal height, 0.0015 inch). Past experience on tests of this size model in this Mach number range has shown that No. 60 carborundum is sufficiently large to effect boundary-layer transition. The F carborundum was used in order to afford some idea of the added wave drag that might be caused by the transition strips. The transition strips were $\frac{1}{4}$ inch wide with the carborundum grain imbedded in shellac. When the No. 60 carborundum was used there were about 250 grains per square inch, and when the F carborundum was used there were about 1,500 grains per square inch. The tests performed at high stagnation pressure were made in order to determine the effect of Reynolds number on external drag.

Schlieren photographs were taken of each of the model configurations at various attitudes and Mach numbers.

MEASUREMENTS

Accuracy

The accuracy of the individual measured quantities, based on balance calibration and repeatability of data, is estimated to be within the following limits:

C_L . . . . ±0.002

C_D' . . . . ±0.001

C_{D_b} . . . . ±0.0002

C_{D_c} . . . . ±0.0002

C_{D_i} . . . . ±0.0001

C_m . . . . ±0.001

C_l . . . . ±0.0002

C_n . . . . ±0.0005

C_Y . . . . ±0.0015

$C_{N,M}$ . . . . ±0.150

$C_{m,M}$ . . . . ±0.040

$C_{n,M}$ . . . . ±0.040

$C_{Y,M}$ . . . . ±0.150

$C_{N,wt}$ . . . . ±0.030

$C_{m,wt}$ . . . . ±0.005

$C_{n,wt}$ . . . . ±0.004

$C_{Y,wt}$ . . . . ±0.010

$C_{N,C}$ . . . . ±0.030

$C_{m,C}$ . . . . ±0.005

$C_{n,C}$ . . . . ±0.004

$C_{Y,C}$ . . . . ±0.010

$C_{N,T}$ . . . . ±0.030

$C_{m,T}$ . . . . ±0.003

$C_{n,T}$ . . . . ±0.003

$C_{Y,T}$ . . . . ±0.030

M_∞ . . . . ±0.015

For the missile separation tests, the quoted accuracies apply only to the individual test points. The large changes in the flow field along the missile path may lead to larger deviations from the faired curves between test points.

Corrections

Calibration of the tunnel test section has not been completed; however, measured pressure gradients are sufficiently small to insure negligible buoyancy corrections for the model. Any flow angularity that might exist in the test section has not been determined.

The drag coefficients presented in the characteristic plots have not been adjusted for chamber, base, and internal drag. The net external-drag coefficient may be obtained, therefore, by subtracting these values from the drag coefficient shown on the characteristic plots at the same model attitude and Mach number; that is,

$$C_{D_e} = C_D' - C_{D_i} - C_{D_c} - C_{D_b}$$

PRESENTATION OF RESULTS

The coefficients of the forces and moments acting on the model are referred to the stability axes system (fig. 4) and the coefficients of the forces and moments acting on the missiles and stores are referred to the body axes system (fig. 5). All aerodynamic moments for the model were taken about a center of gravity located longitudinally at 33 percent of the wing mean aerodynamic chord and at a station 1.55 inches above the zero water line of the model (fig. 1). Aerodynamic coefficients for the model are based on mean aerodynamic chord, projected wing area, and wing span. Aerodynamic moments of the missiles and stores were taken about their respective centers of gravity (fig. 2). Aerodynamic coefficients for the missiles and stores are based on their respective maximum cross-sectional area and body length.

The results of the investigation are shown in the following figures:

RESULTS

The results of this investigation are presented without analysis.
It is pertinent, however, to make several observations with regard to
what is shown by the data.

The aerodynamic forces acting on the missile as it passed through
the interference field of the model were very erratic. The magnitude
of the force coefficients appears to be independent of Mach number.

The basic model was longitudinally stable at all test Mach numbers and in the angle-of-attack range for the tests; furthermore, the model stability was not changed by a wing notch at the wing-fuselage juncture.

The center-line tank and the center-line store were neutrally stable, longitudinally, and had very little effect on the longitudinal stability of the basic model. The wing tanks, which were unstable longitudinally, decreased the model longitudinal stability.

The center-line tank was directionally unstable at all Mach numbers. The wing tanks were directionally unstable and the center-line store was directionally stable at a Mach number of 1.57. At Mach numbers of 1.87 and 2.16, the wing tanks and the center-line tank were neutrally stable. The model was directionally stable at all Mach numbers with either of the external stores attached. At a Mach number of 1.57, the model was more stable with either the wing tanks or the center-line store than with the center-line tank. The directional stability of the model was the same with either of the external stores attached at Mach numbers of 1.87 and 2.16.

The minimum external-drag coefficients of the basic model are 0.040, 0.039, 0.037, and 0.037 for Mach numbers of 1.57, 1.87, 2.16, and 2.53, respectively; and the corresponding Reynolds numbers are 1.3×10^6, 1.2×10^6, 1.1×10^6, and 0.9×10^6. An increase in Reynolds number resulted in a slight decrease in the minimum external-drag coefficients, and the decrease is approximately the same as predicted by the minimum theoretical correction as given in reference 1. However, in consideration of the limited number of test points, the accuracy of measurement, and the departure of the model from a slender body of revolution, no conclusions can be made regarding extrapolation of the model data to full-scale Reynolds number.

Langley Aeronautical Laboratory,
    National Advisory Committee for Aeronautics,
        Langley Field, Va., February 26, 1958.

REFERENCE

1. Chapman, Dean R., and Kester, Robert H.: Turbulent Boundary-Layer and Skin-Friction Measurements in Axial Flow Along Cylinders at Mach Numbers Between 0.5 and 3.6. NACA TN 3097, 1954.

TABLE I.- GEOMETRIC CHARACTERISTICS OF THE SUPERSONIC FIGHTER AIRPLANE MODEL

[Fuselage station 0.00 is 0.40 inch behind nose]

Model scale, percent 5
Center-of-gravity location, percent of mean aerodynamic chord 33

Wing:
  Area, sq ft -
    Exposed 0.886
    Projected 1.325
  Span, in. 23.2
  Aspect ratio 2.821
  Taper ratio 0.167
  Sweep angle of quarter-chord line, deg 45
  Dihedral, deg . . . . 0 inboard, 12 outboard
  Incidence, deg 1
  Geometric twist, deg 0
  Airfoil -
    Root . . . . NACA 0006.4-64 (modified)
    Body line (B.L.) 8.00 . . . . NACA 0004.0-64 (modified)
    Tip . . . . NACA 0003.0-64 (modified)
  Root chord, in. 14.10
  Tip chord, in. 2.35
  Root-chord location -
    Longitudinal (leading edge) . . . . Fuselage station (F.S.) 7.518
    Vertical . . . . Water line (W.L.) 0.574
  Mean aerodynamic chord, in. 9.63
  Mean-aerodynamic-chord location -
    Longitudinal (leading edge) . . . . F.S. 13.054
    Lateral . . . . B.L. 4.42

Fuselage:
  Length, in. 33.60
  Width (maximum), in. 3.375
  Depth (maximum), in. 3.730
  Overall fineness ratio 8.40
  Base area, sq ft 0

Horizontal tail:
  Area (theoretical), sq ft 0.237
  Span, in. 10.626
  Aspect ratio 3.310
  Taper ratio 0.200
  Root chord, in. 5.35
  Tip chord, in. 1.07
  Mean aerodynamic chord, in. 3.686
  Mean-aerodynamic-chord location:
    Longitudinal (leading edge) . . . . F.S. 29.16
    Lateral . . . . B.L. 2.065
  Tail length (distance from quarter-chord point of mean aerodynamic chord of wing to
    quarter-chord point of mean aerodynamic chord of horizontal tail), in. 14.619
  Sweep angle of quarter-chord line, deg 35.5
  Dihedral, deg . . . . -15
  Geometric twist, deg 0
  Airfoil -
    Root . . . . NACA 0003.7-64 (modified)
    Tip . . . . NACA 0003.0-64 (modified)

Vertical tail:
  Area (theoretical), sq ft 0.197
  Span, in. 3.825
  Aspect ratio 0.5976
  Root chord length, in. 10.35
  Tip chord length, in. 2.355
  Mean aerodynamic chord, in. 7.192
  Mean-aerodynamic-chord location:
    Longitudinal (leading edge) . . . . F.S. 26.11
    Vertical (leading edge) . . . . W.L. 4.836
  Tail length (distance from quarter-chord point of mean aerodynamic chord of wing to
    quarter-chord point of mean aerodynamic chord of vertical tail), in. 11.507
  Airfoil -
    Root . . . . NACA 0003.2-64 (modified)
    Tip . . . . NACA 0002.5-64 (modified)

Duct with double compression ramp (5° to 8°) -
  Capture area, per side, sq ft 0.011944
  Exit, per side, sq ft 0.007906

TABLE II.- MODEL CONFIGURATIONS AND TEST VARIABLES

Model configuration	Mach numbers	Angle-of-attack range, deg	Sideslip-angle range, deg
Basic model	1.57, 1.87, 2.16, and 2.53	-2 to 22	0
Model with center-line tank	1.57, 1.87, and 2.16	-2 to 17	-3 to 9
Model with wing tanks	1.57, 1.87, and 2.16	-2 to 17	-9 to 9
Model with center-line store	1.57, 1.87, and 2.16	-2 to 17	-3 to 9
Model with notched wing	1.57, 1.87, and 2.16	-2 to 17	0
Model with a notched wing, leading-edge cuff, and a 25° negative-dihedral horizontal tail	1.57, 1.87, and 2.16	-2 to 17	0
Rearward missile moved through interference field of model	1.57, 1.87, and 2.16	0 to 18	-9 to 9
Forward missile moved through interference field of model	1.57, 1.87, and 2.16	0 to 18	-9 to 9
Basic model with transition strips	1.57, 1.87, 2.16, and 2.53	-2 to 22	0
Model with aileron and spoiler deflected . .	1.57, 1.87, and 2.16	-2 to 22	0

Note: The angle of attack was 0° for the sideslip-angle range and the sideslip angle was 0° for the angle-of-attack range.
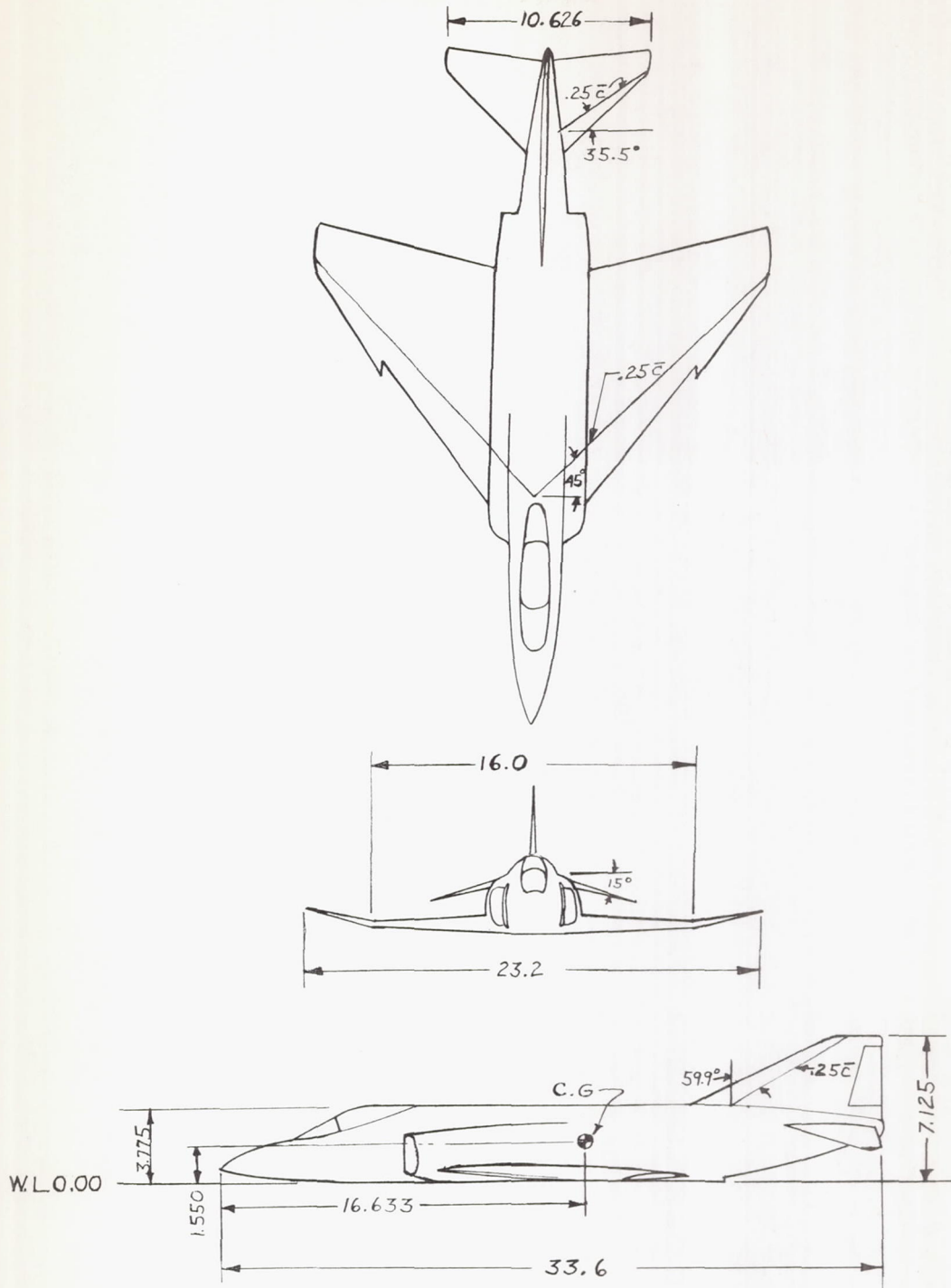
Figure 1.- Three-view drawing of a 1/20-scale model of a supersonic fighter airplane. (All dimensions in inches.)

F.S. −.40

W.L. 0.00

A

3°

A

F.S. 16.51

B.L. 0.00

F.S. 23.24
W.L. −.675
B.L. 0.00

6.27

13.00

B.L. 0.00

W.L. 0.00

SECTION A-A
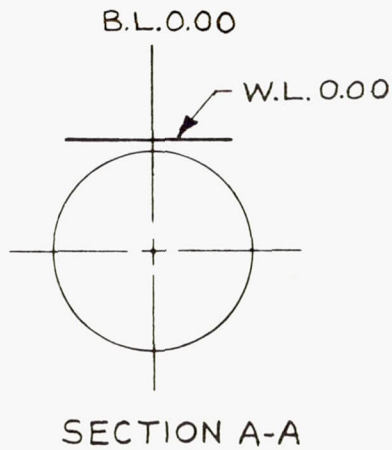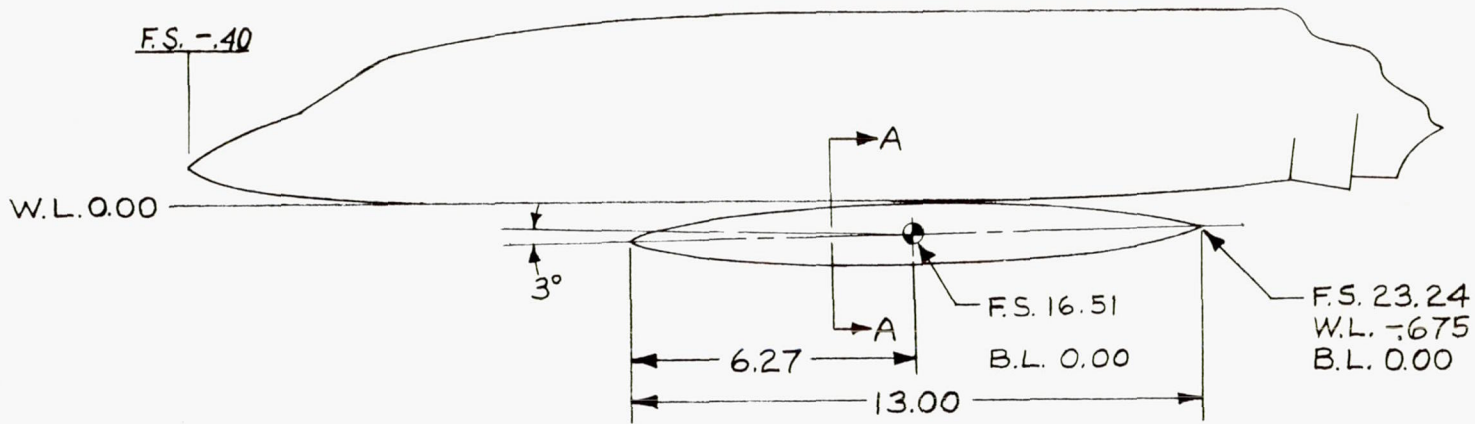
(a) Center-line tank.

Figure 2.- Test configurations.

F.S. -.40

W.L. 0.00

A

A

STORE C.G
F.S. 16.696
W.L.-0.55

3.73

T.S. 0.00

2°

Ȼ

Ȼ

SECTION A-A
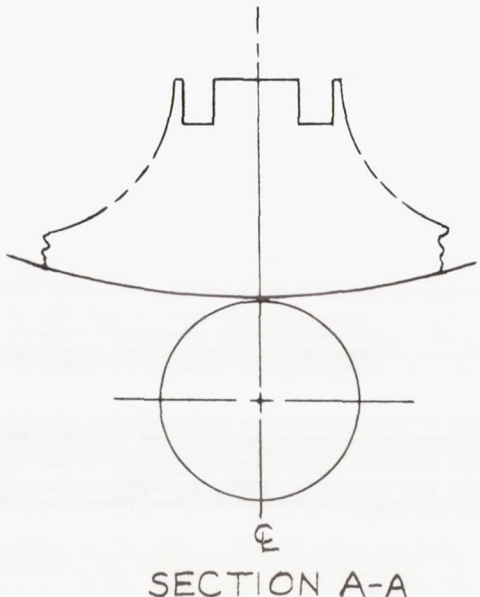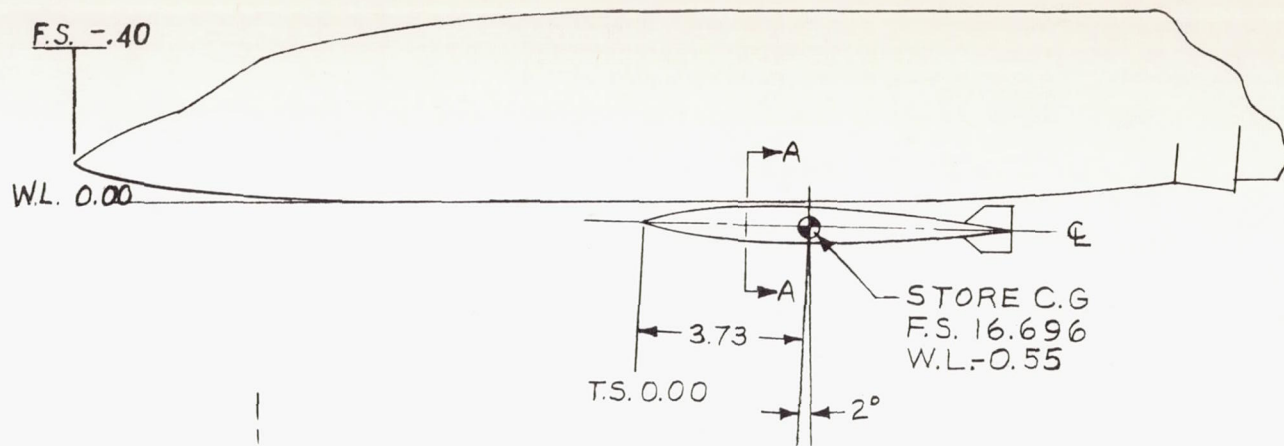
(b) Center-line store.

Figure 2.- Continued.

W. L. -0.984

0° 30'

F.S. 11.042

C_L STORE

F.S. 17.000
B.L. 6.450
W. L. -0.984

B.L. 0.00

B. L. 6.450

C_L
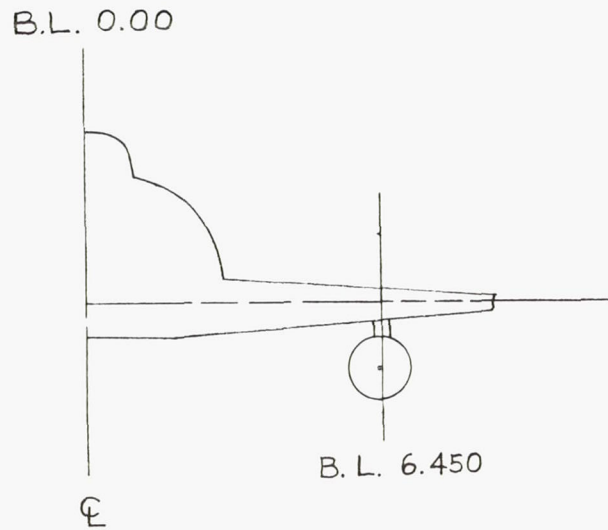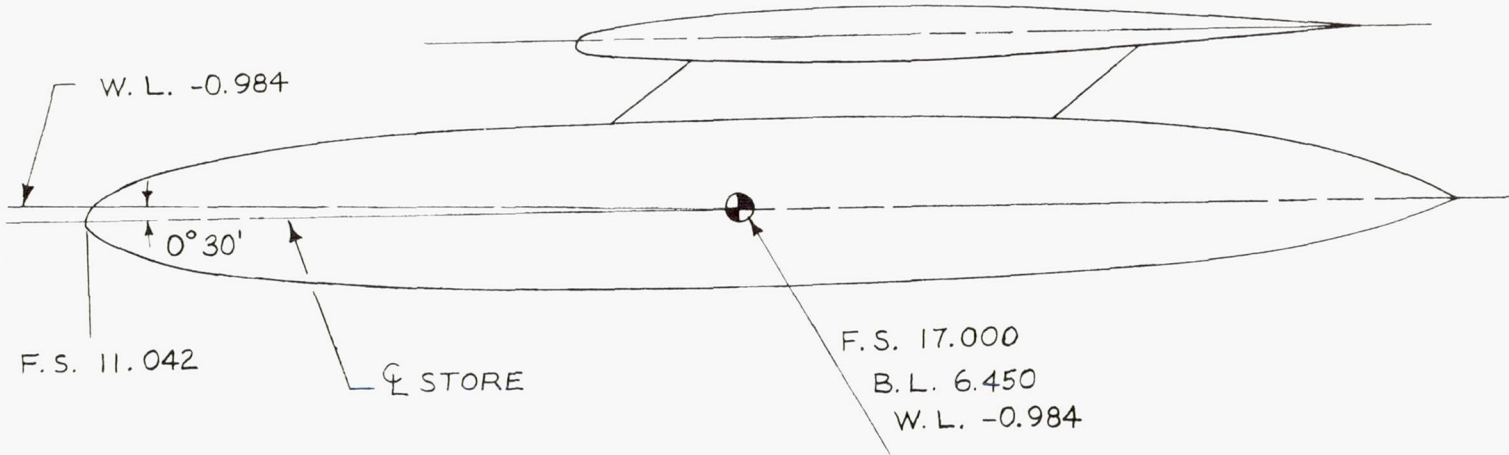
(c) Wing tank.

Figure 2.- Continued.
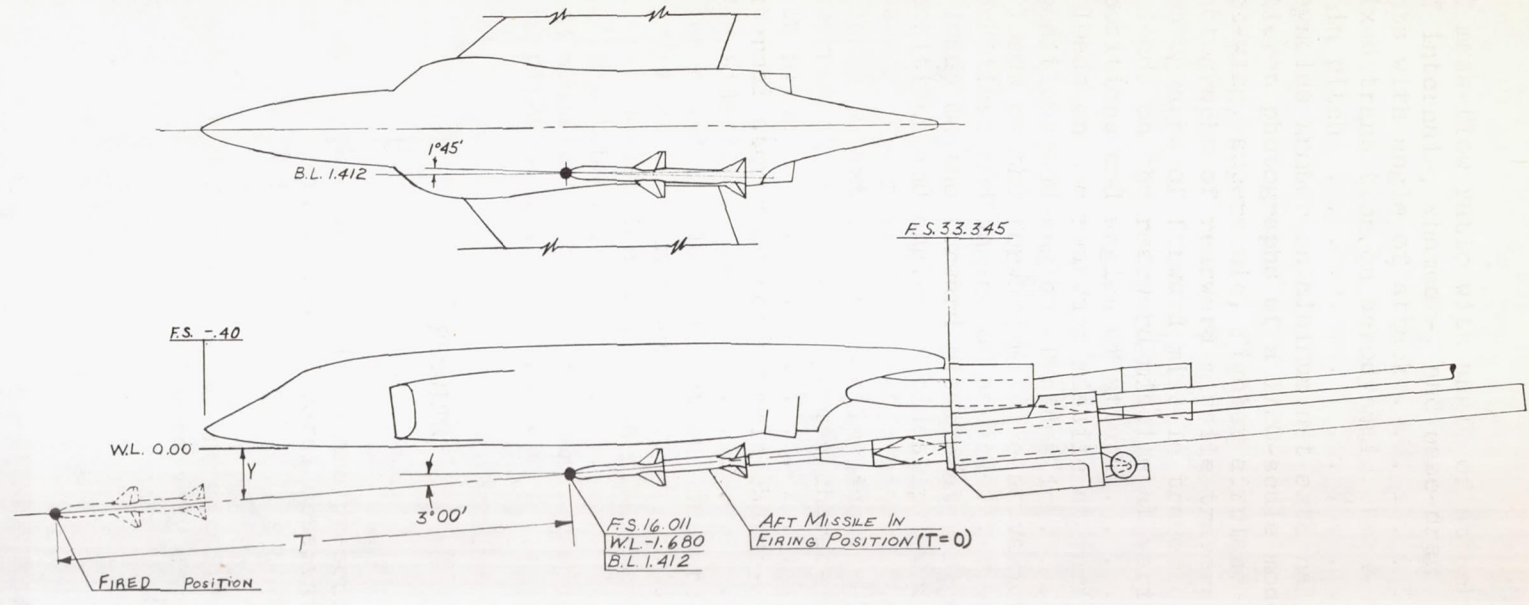
(d) Rearward missile.

Figure 2.- Continued.
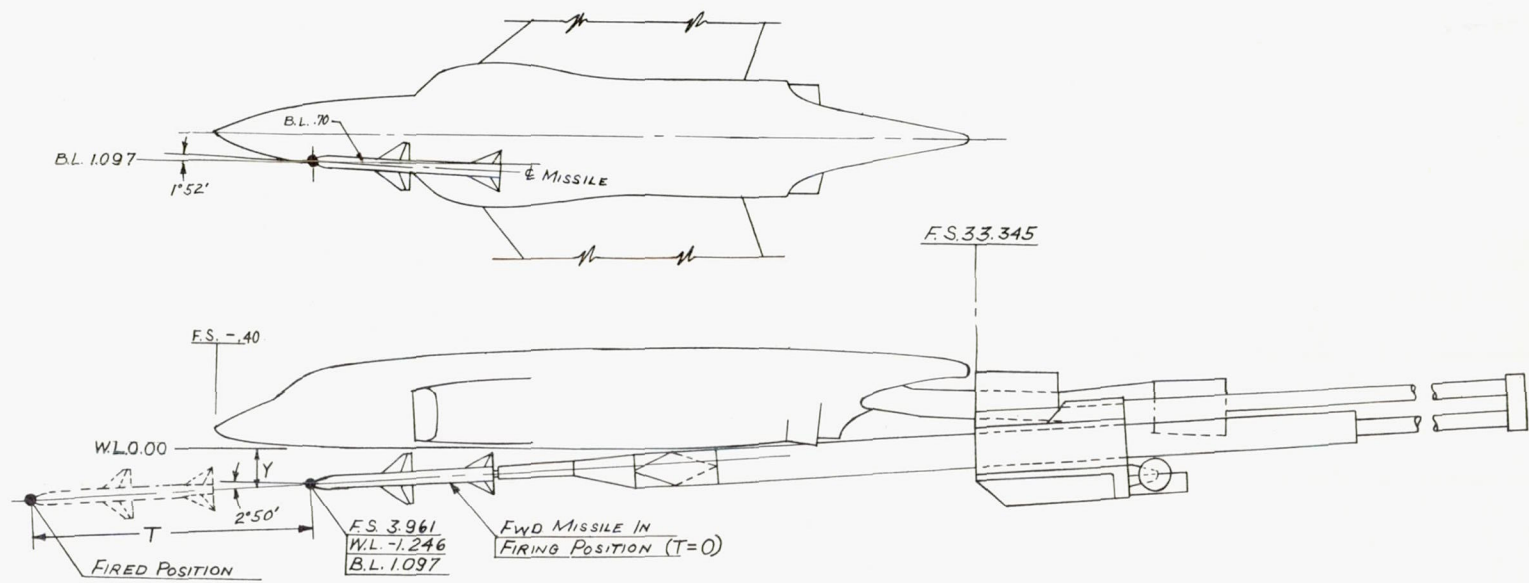
(e) Forward missile.

Figure 2.- Continued.
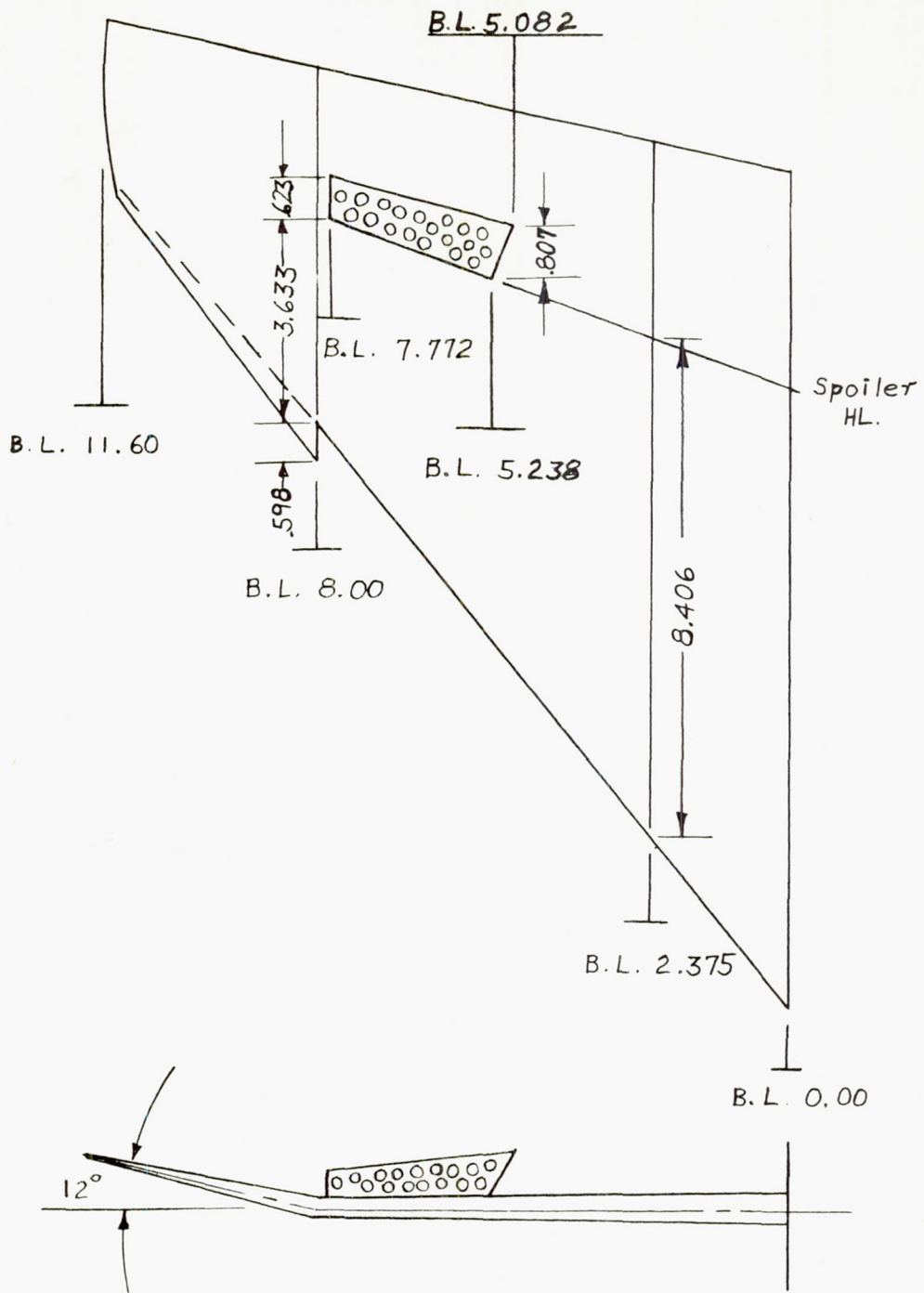
(f) Spoiler (20-percent porosity).

Figure 2.- Continued.
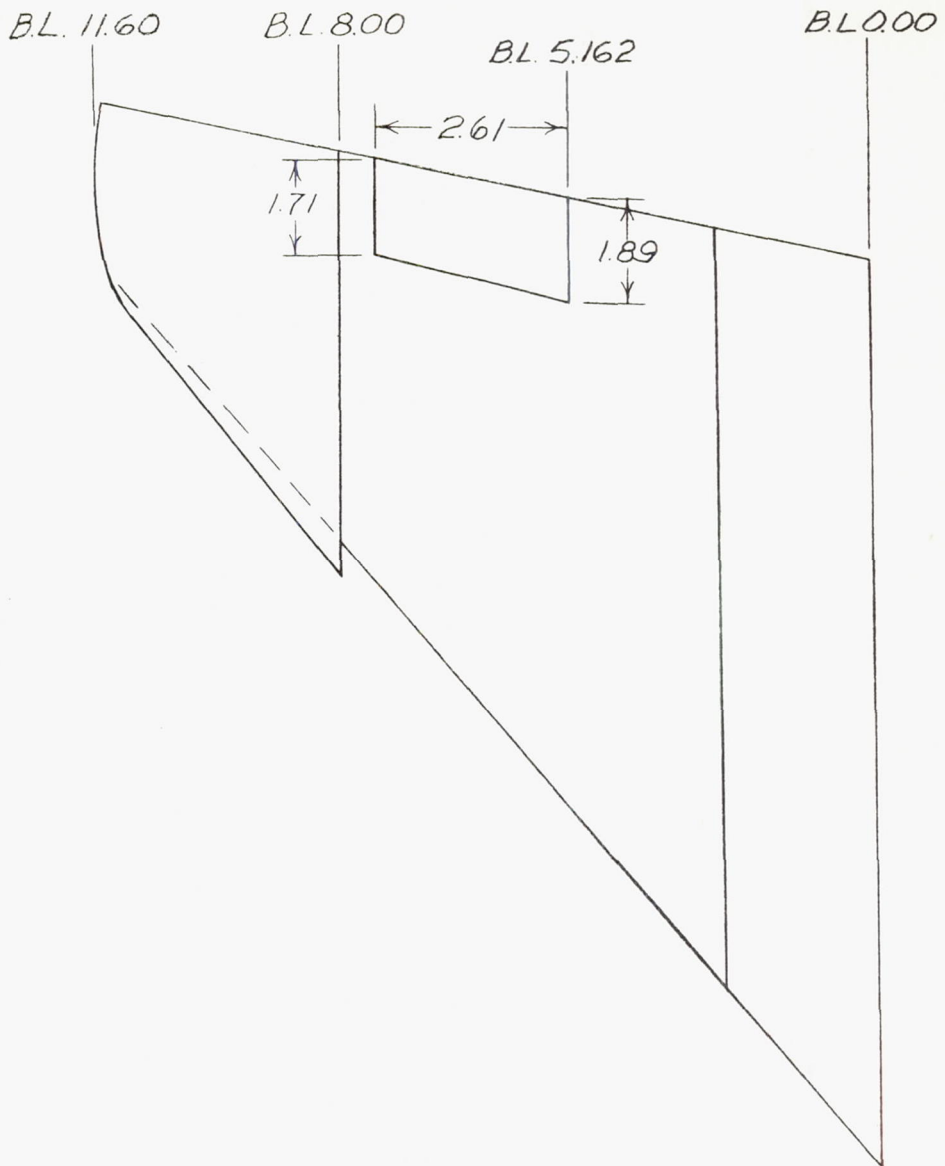
(g) Aileron.

Figure 2.- Continued.
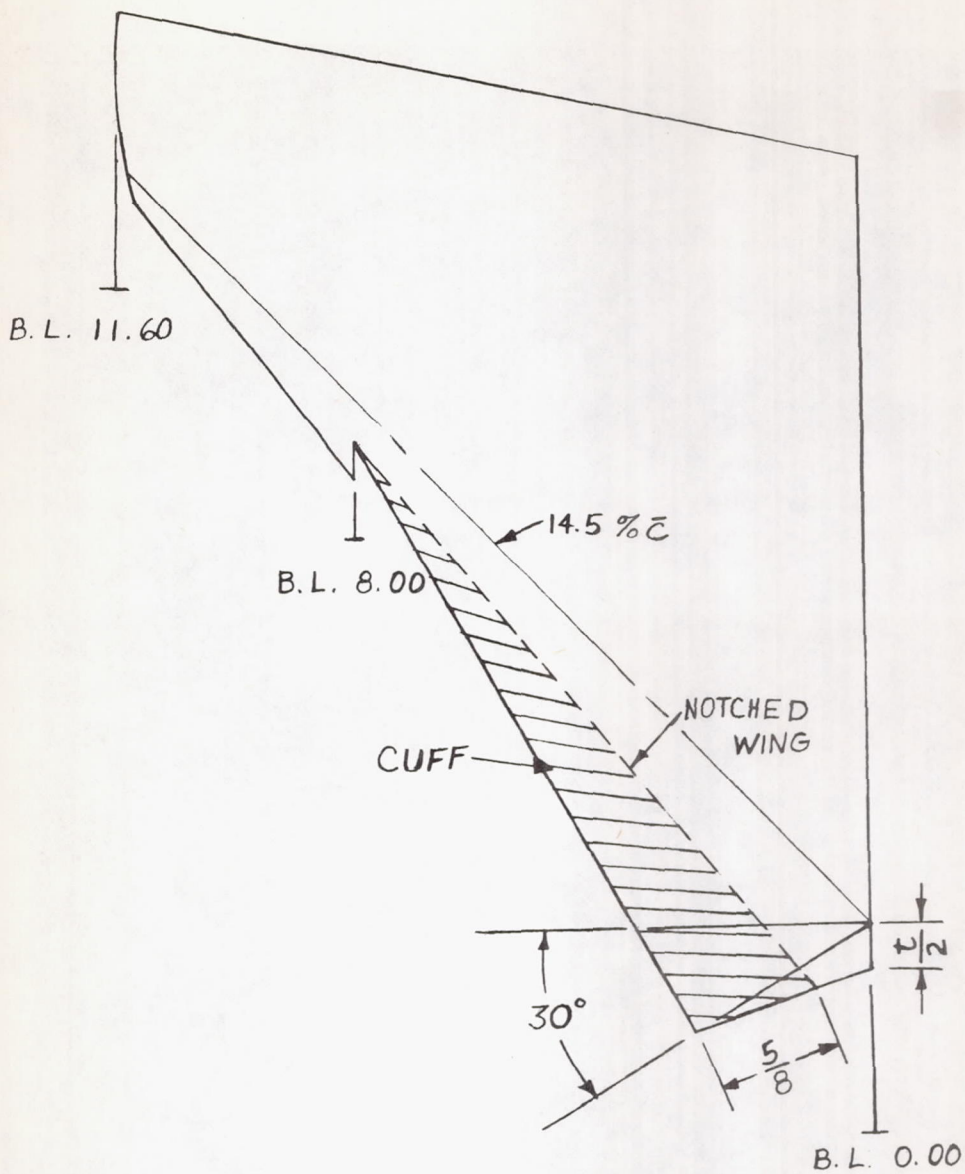
(h) Notched wing and cuff.

Figure 2.- Concluded.
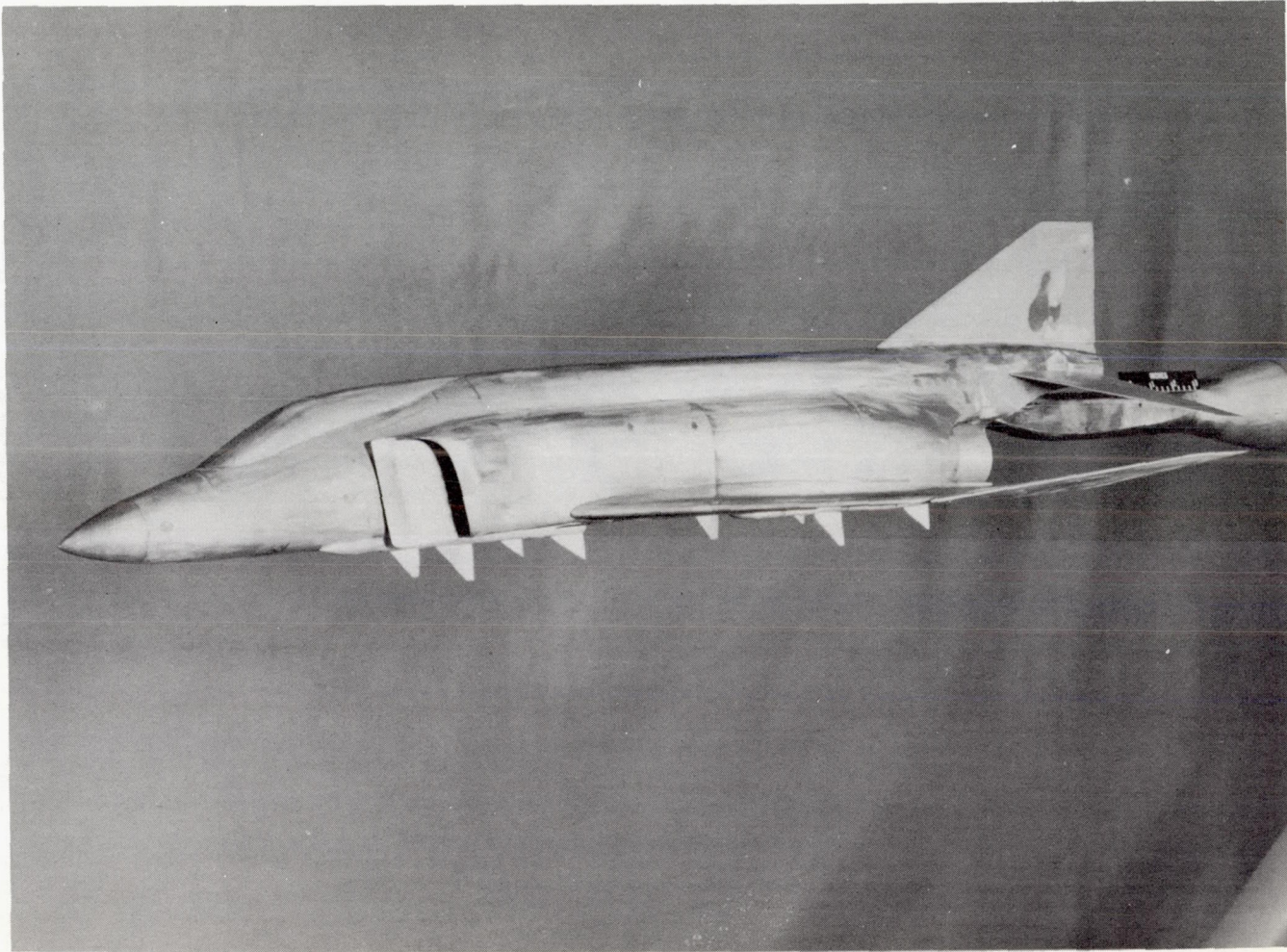
(a) Three-quarter front view.   L-57-472

Figure 3.- Photographs of a 1/20-scale model of a supersonic fighter airplane.
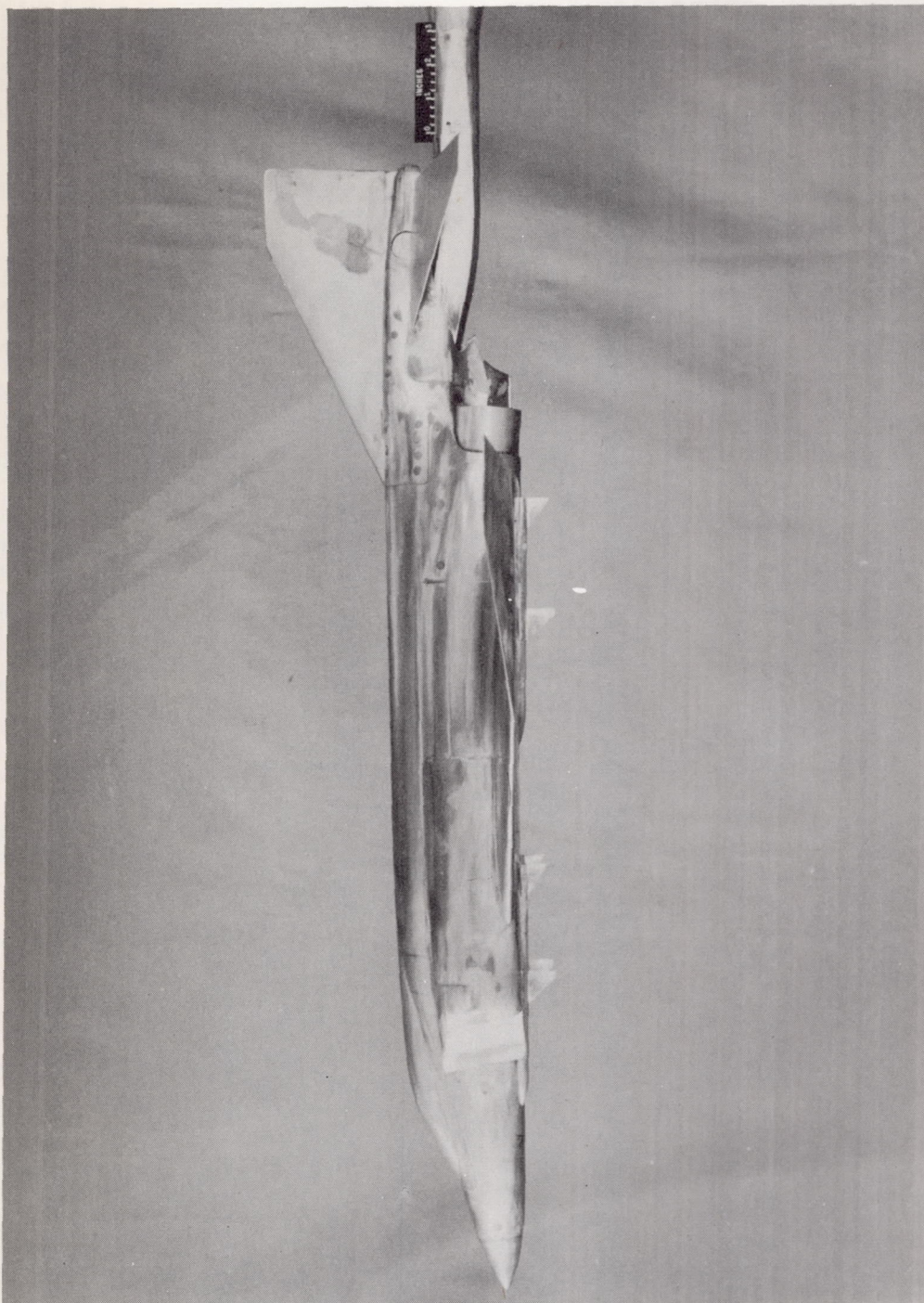
L-57-478

(b) Side view.

Figure 3.- Continued.
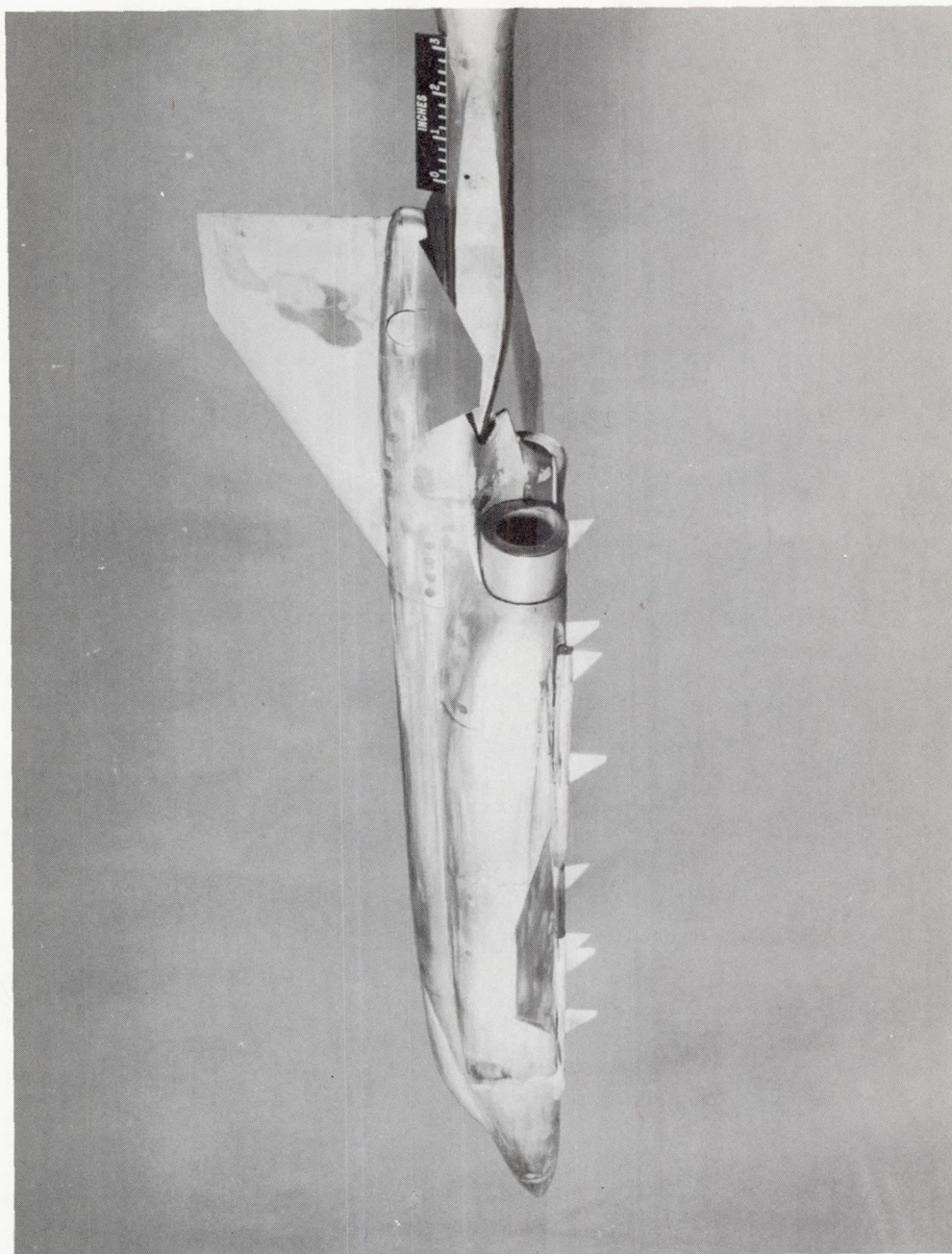
(c) Three-quarter rear view.   L-57-473

Figure 3.- Continued.
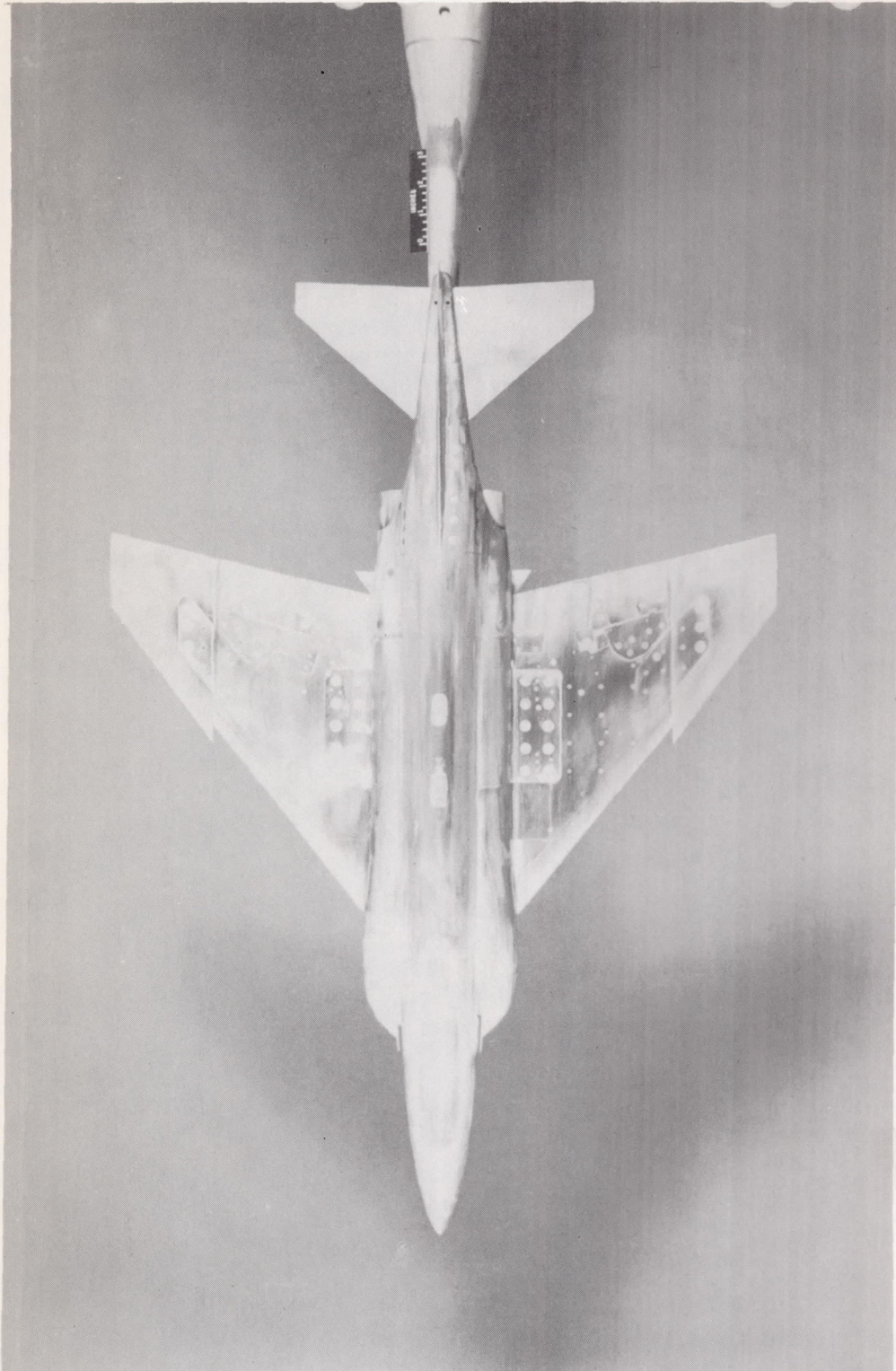
(d) Top view.   L-57-469
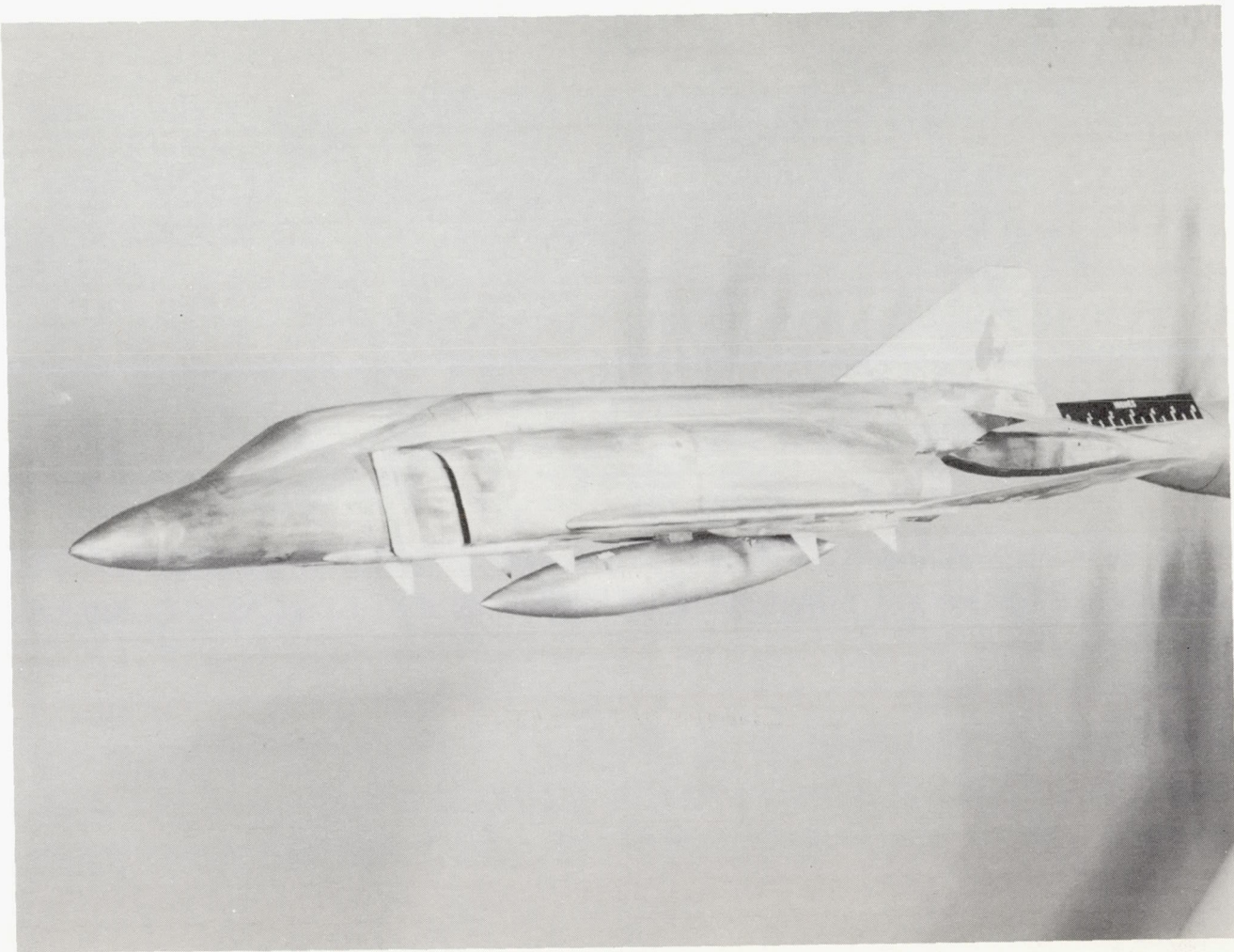
Figure 3.- Continued.

(e) Three-quarter front view with center-line tank.   L-57-474

Figure 3.- Continued.
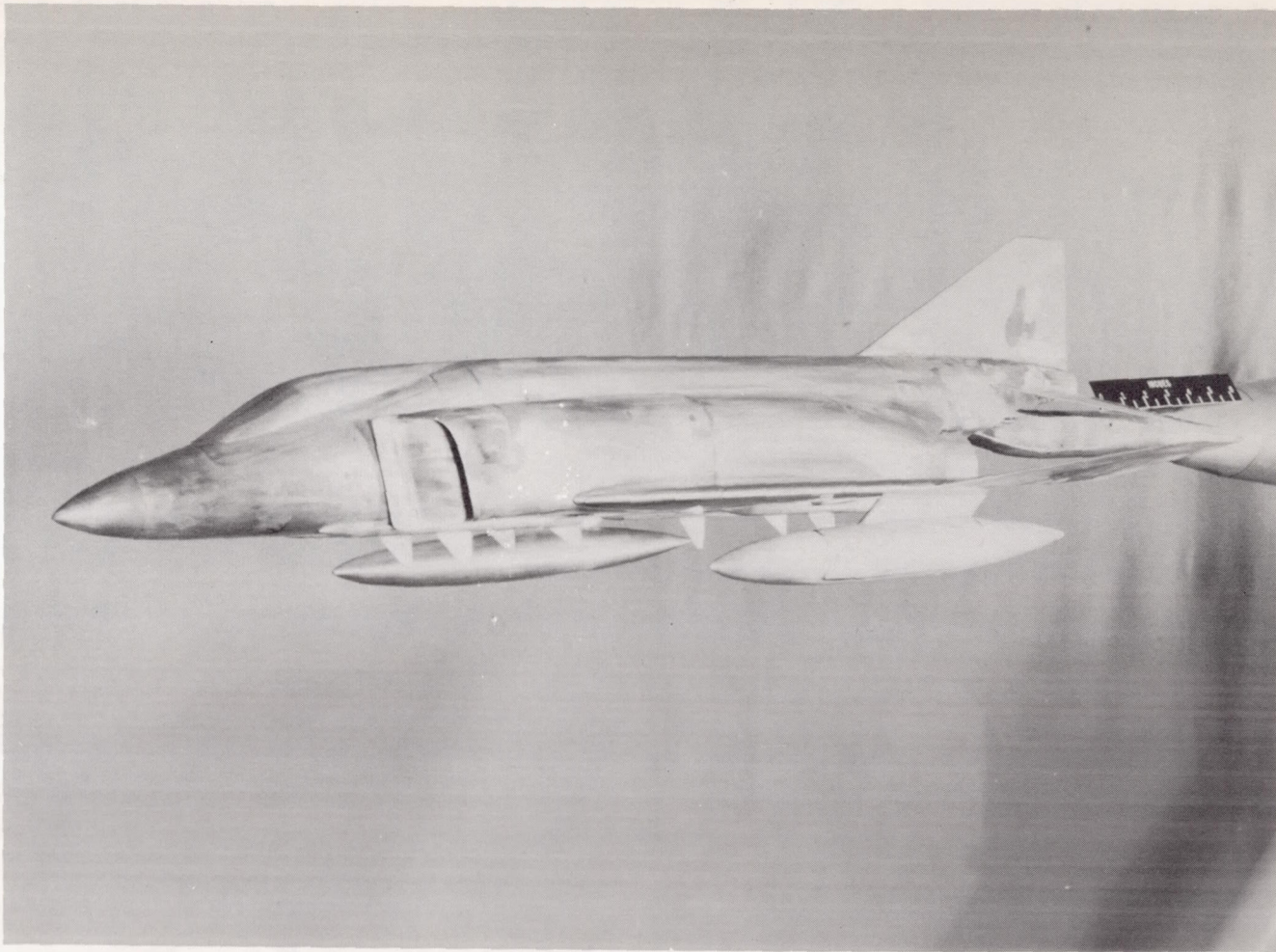
(f) Three-quarter front view with wing tanks.   L-57-470

Figure 3.- Continued.
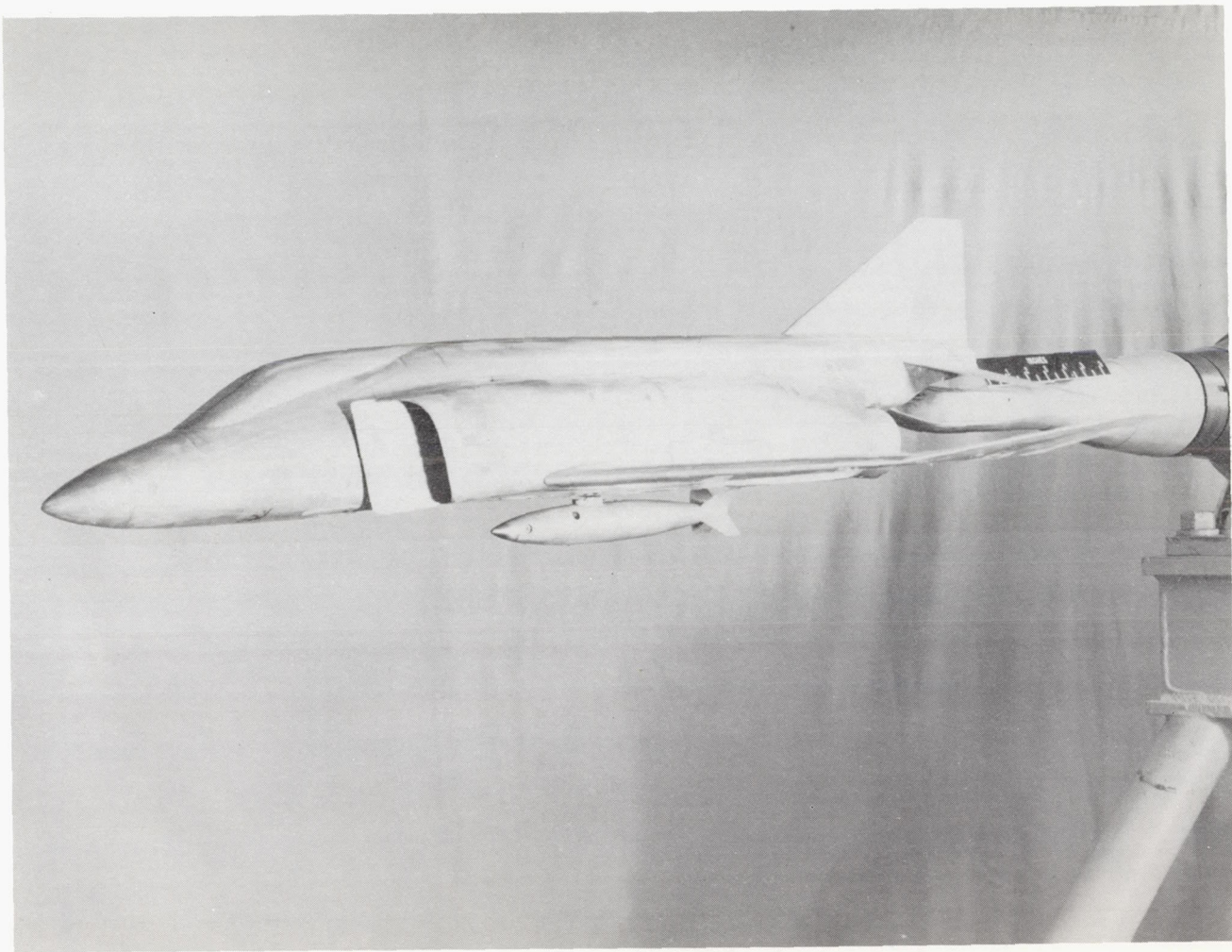
(g) Three-quarter front view with center-line store. L-57-476

Figure 3.- Continued.
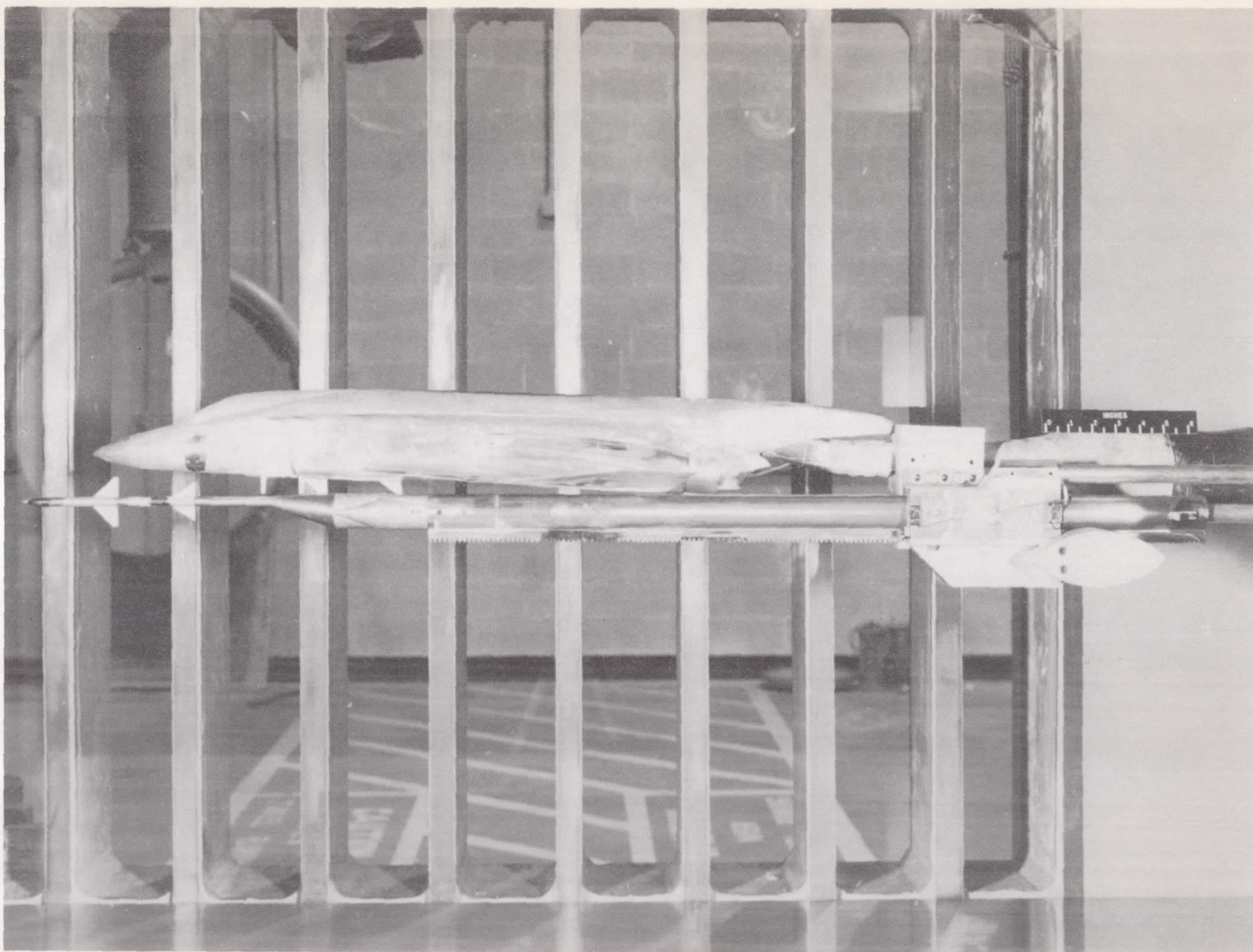
(h) Side view showing missile support system.   L-57-297

Figure 3.- Concluded.
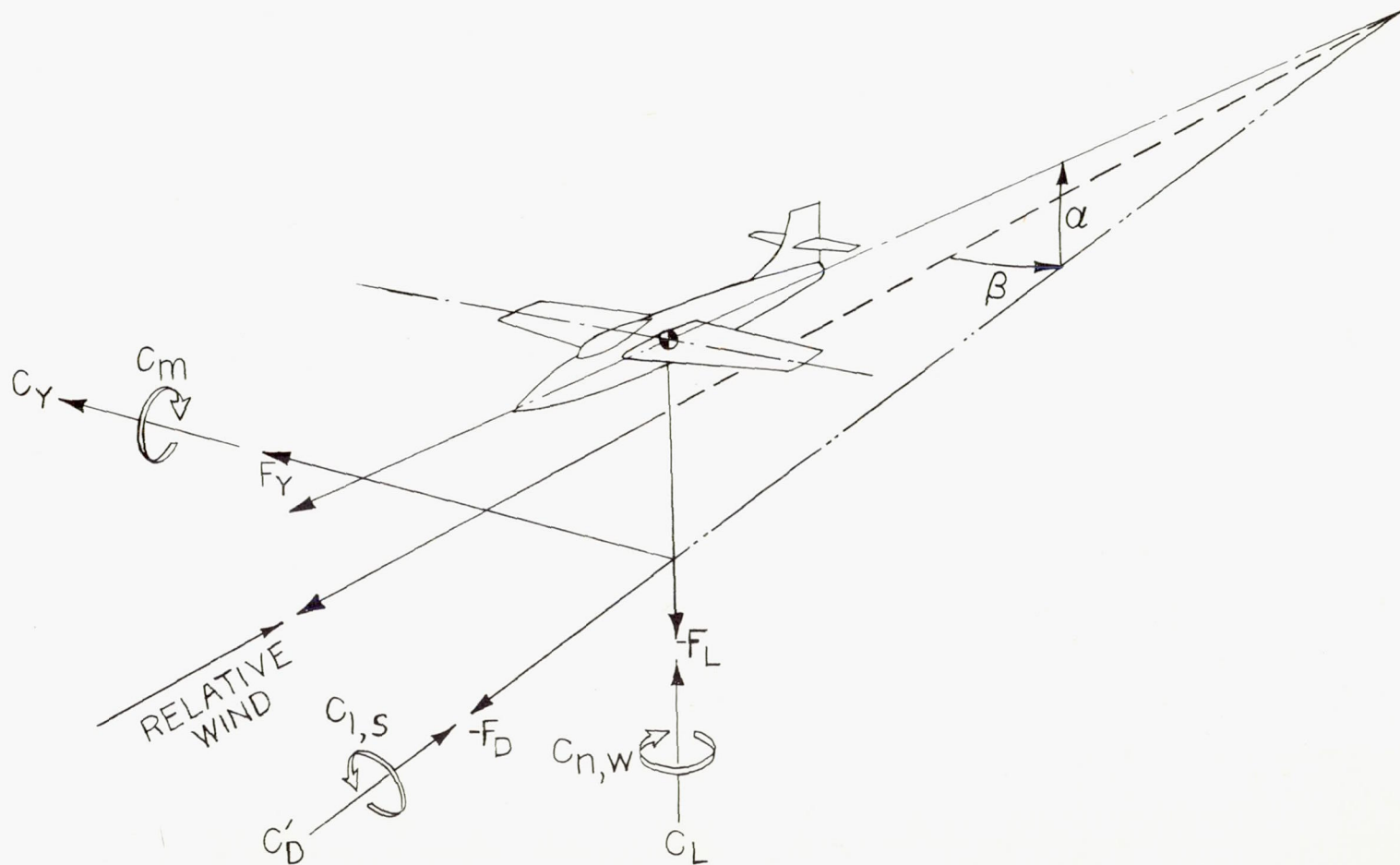
Figure 4.- Stability axes system. (Arrows indicate positive directions, except where noted by a minus sign.)
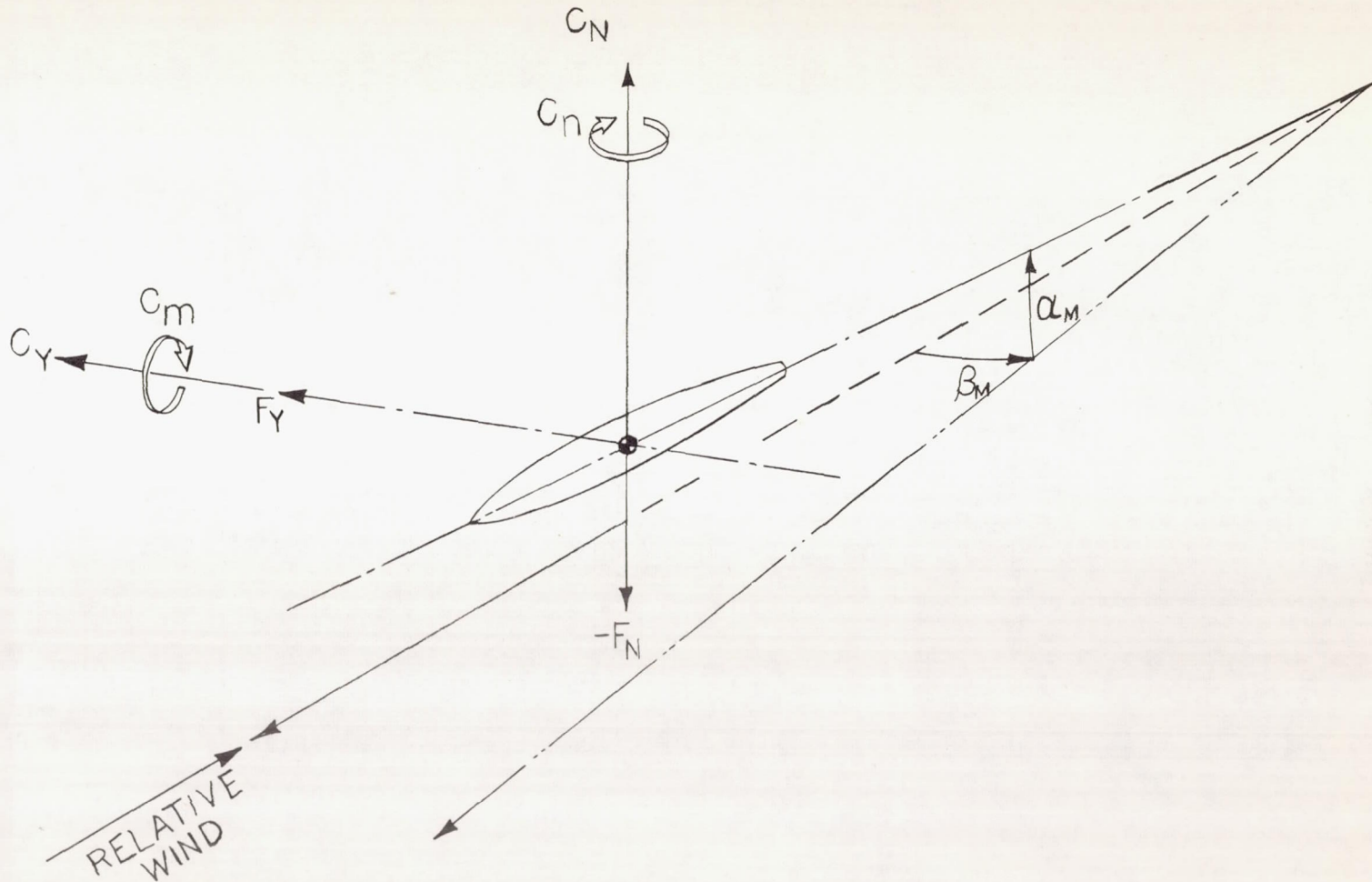
Figure 5.- Body axes system. (Arrows indicate positive directions, except where noted by a minus sign.)
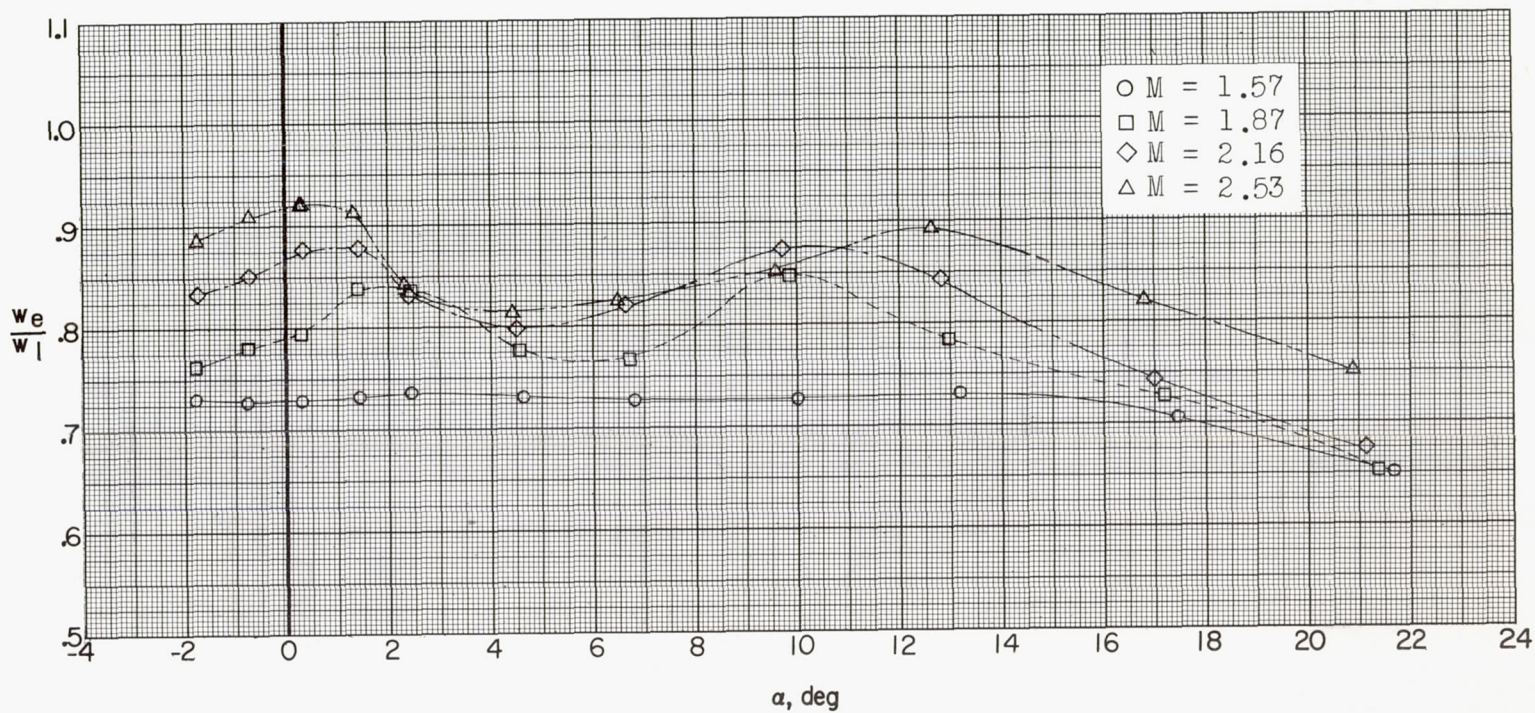
Figure 6.- Variation of mass-flow ratio with angle of attack.
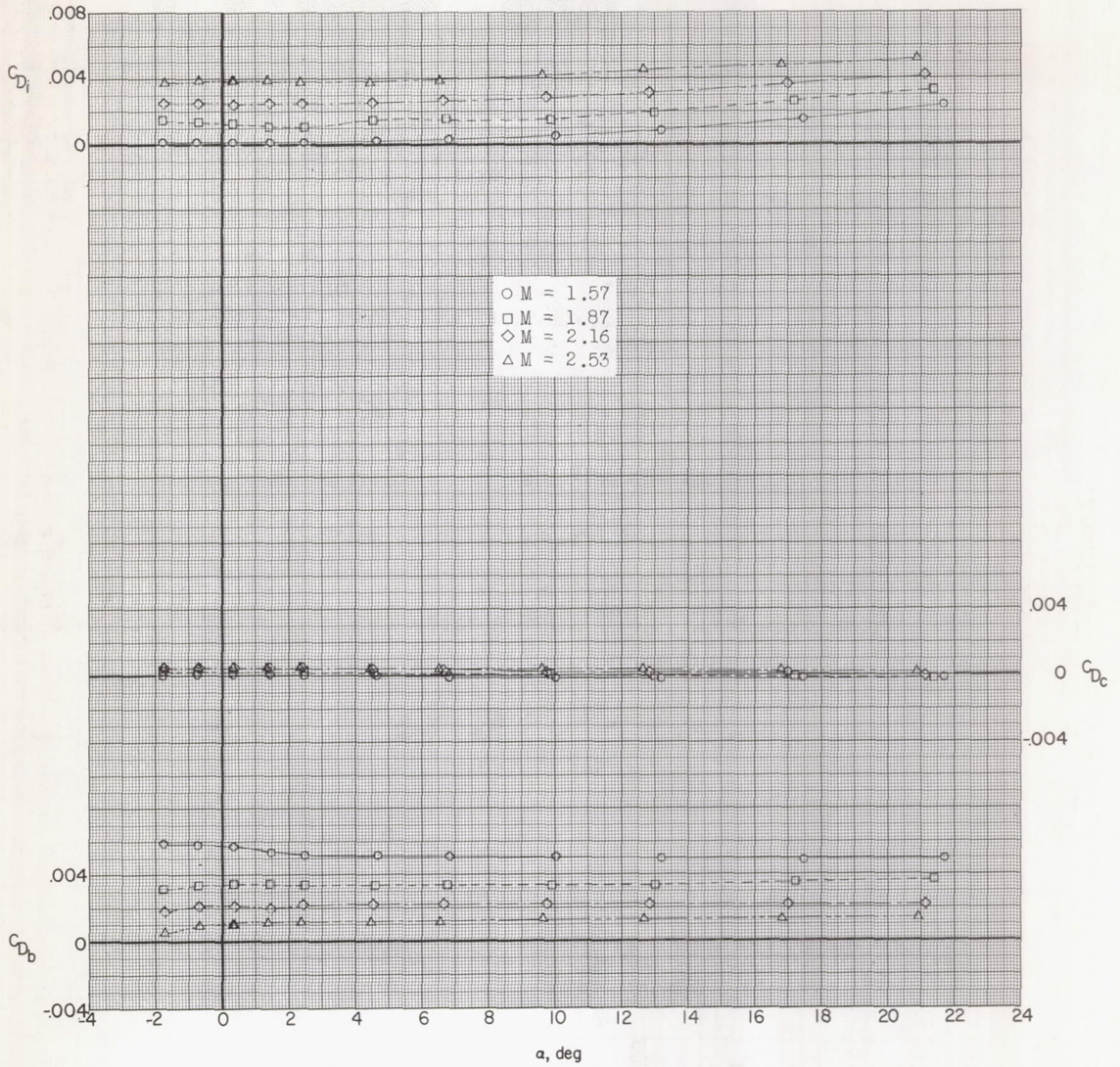
Figure 7.- Variation of internal-, chamber-, and base-drag coefficients with angle of attack.
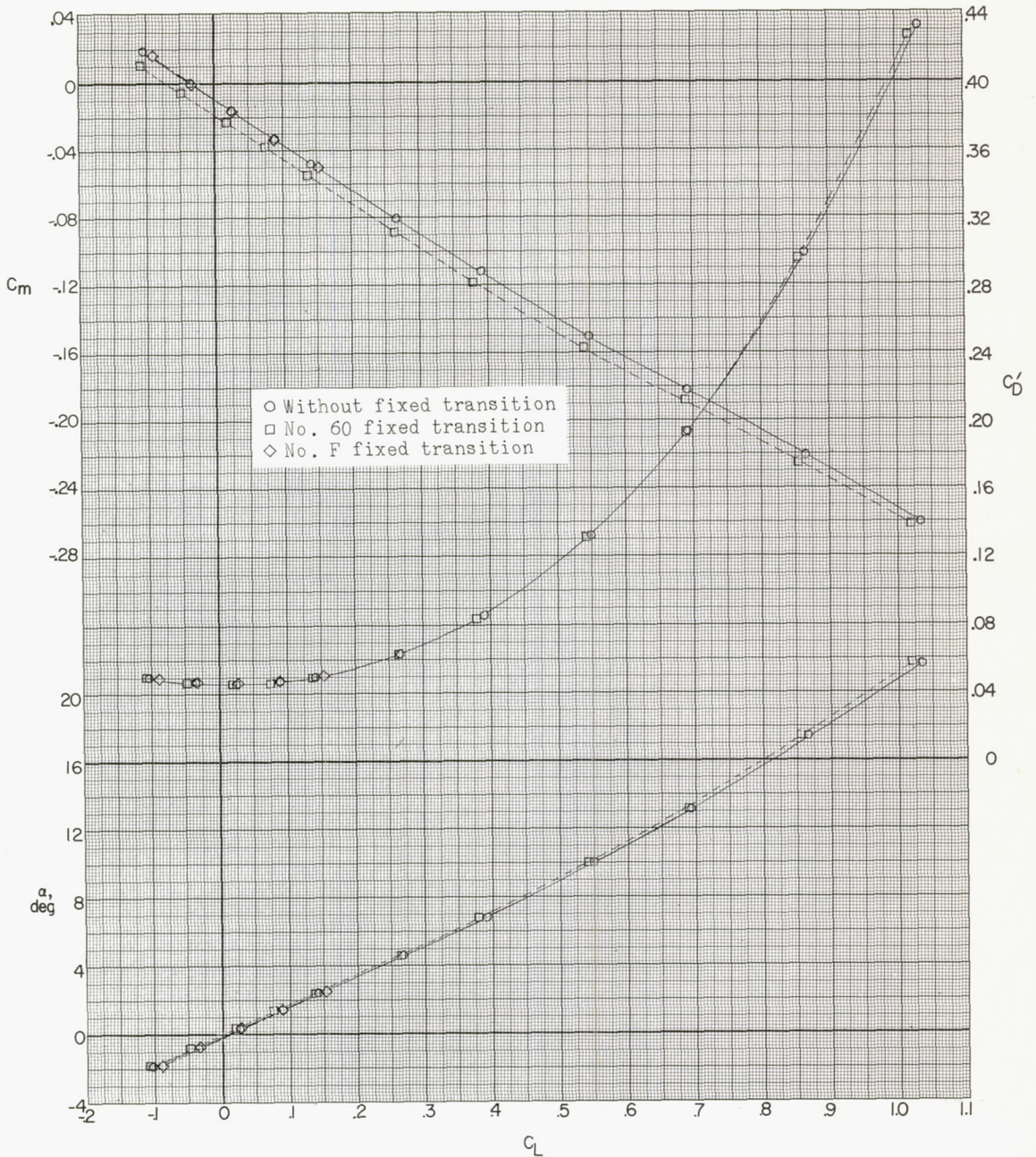
(a)   M = 1.57; R ≈ 1.3 × 10^6.

Figure 8.- Effect of fixed transition on aerodynamic characteristics in pitch.
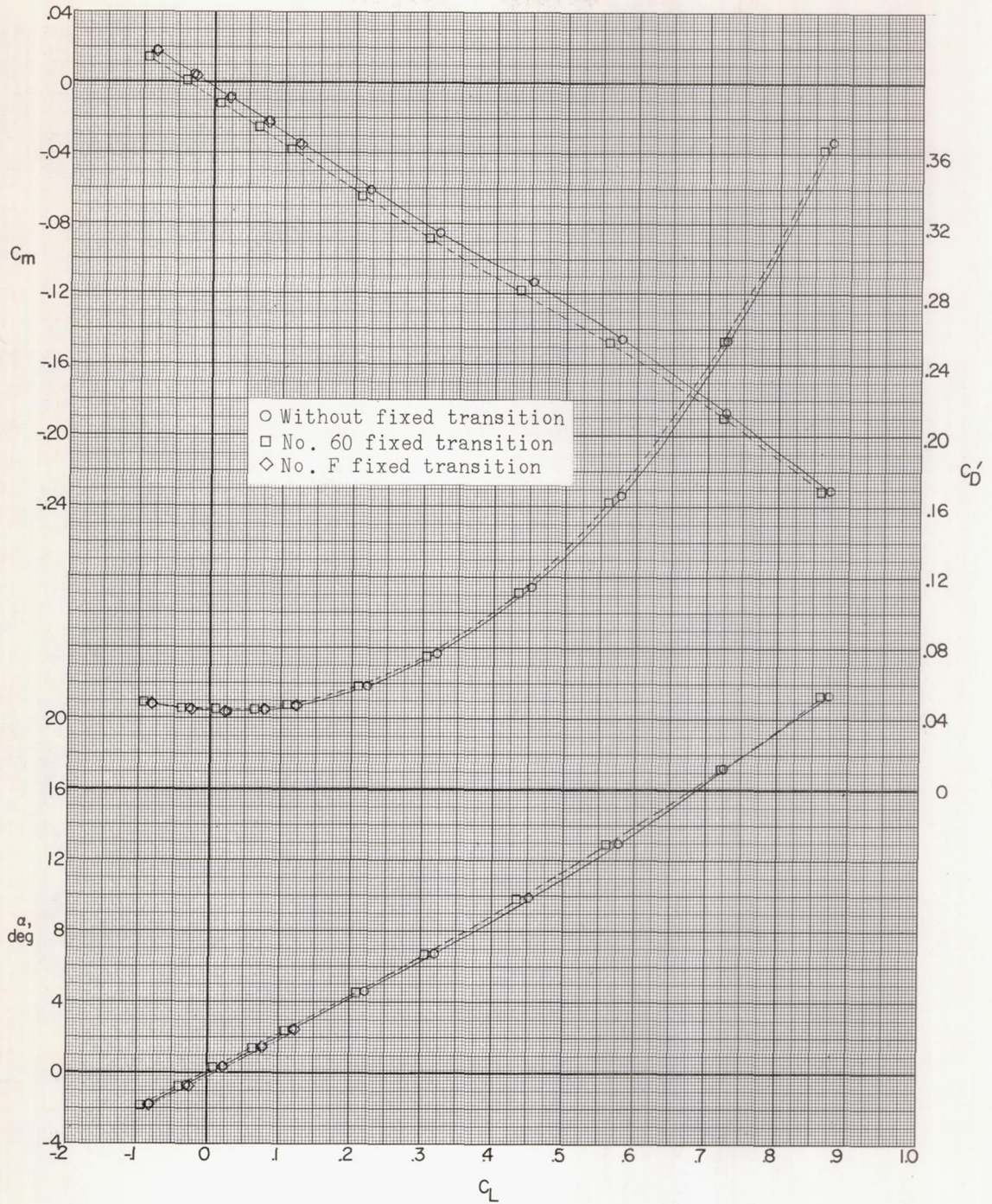
(b)   M = 1.87; R ≈ 1.2 × 10^6.

Figure 8.- Continued.
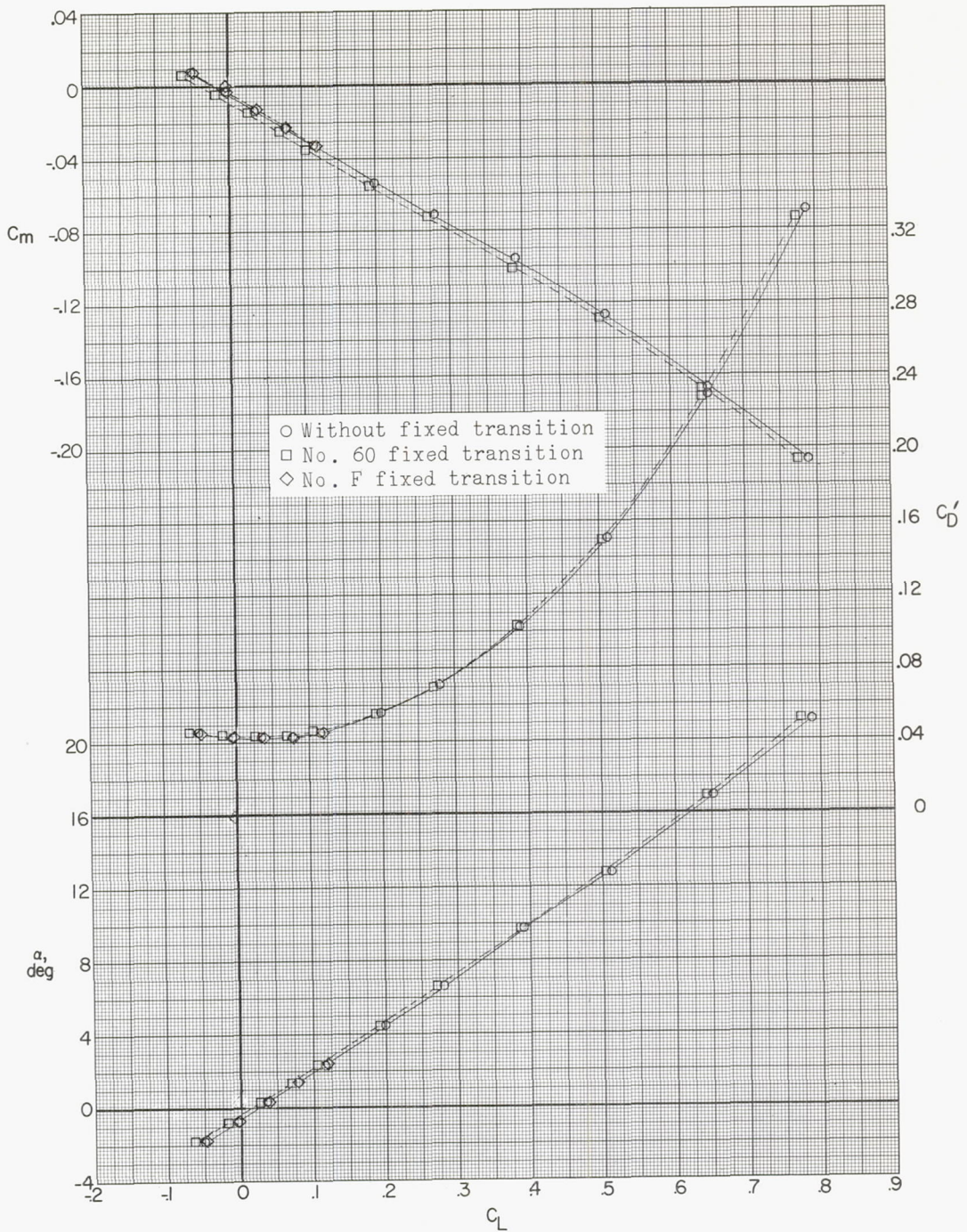
(c)   M = 2.16; R ≈ 1.1 × 10^6.

Figure 8.- Continued.
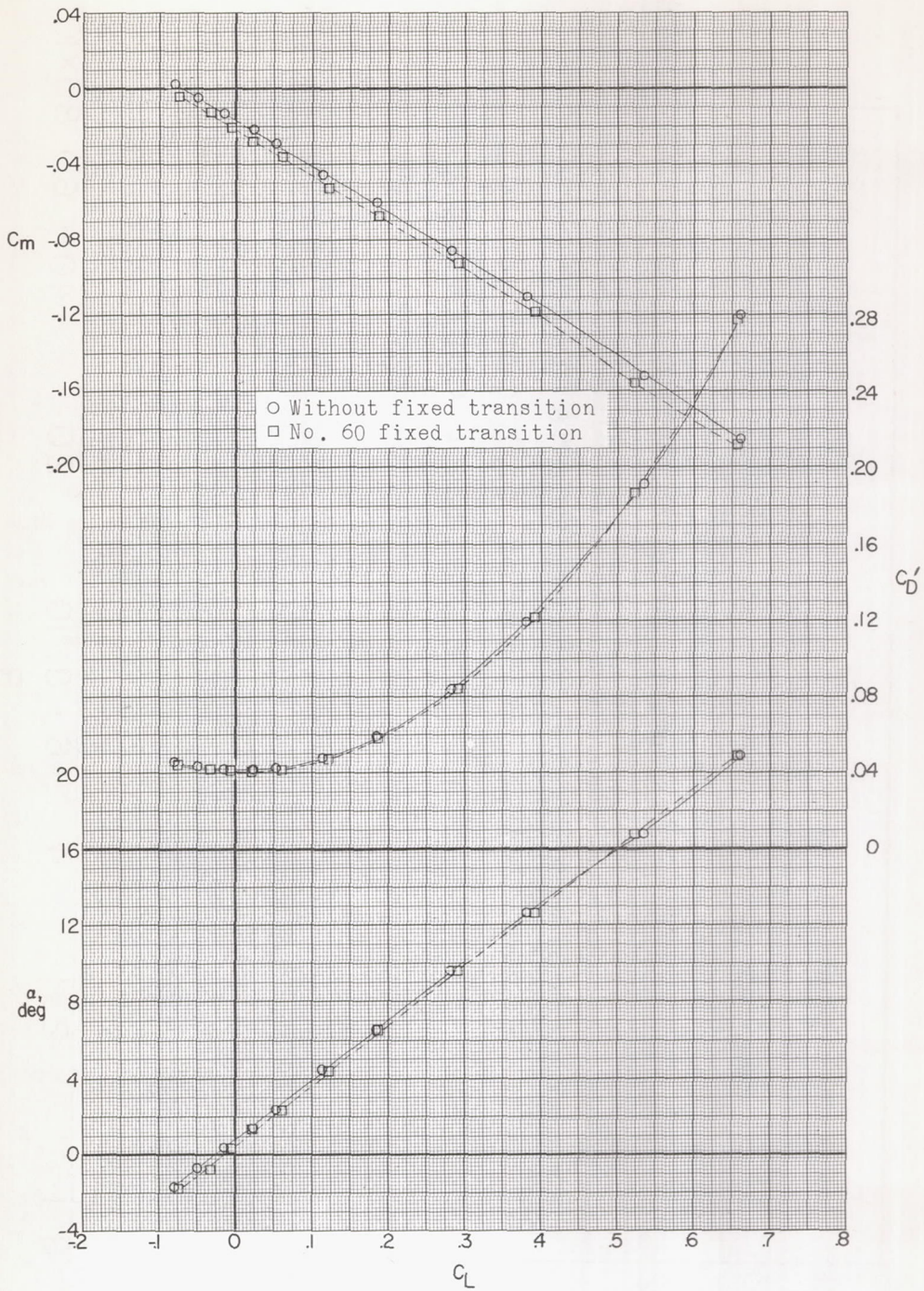
(d) $M = 2.53$; $R \approx 0.9 \times 10^6$.

Figure 8.- Concluded.
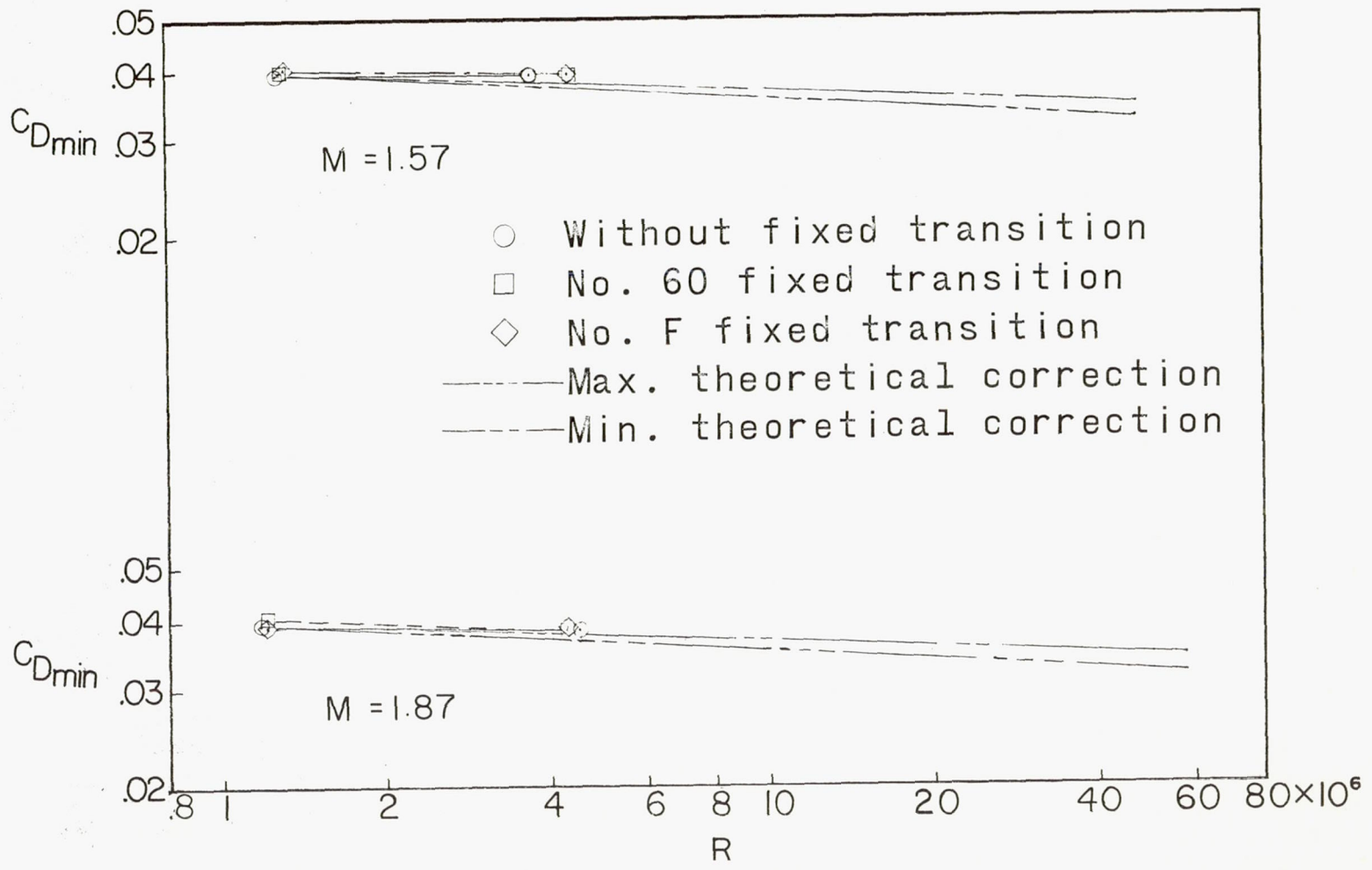
Figure 9.- Effect of Reynolds number on minimum net external drag.
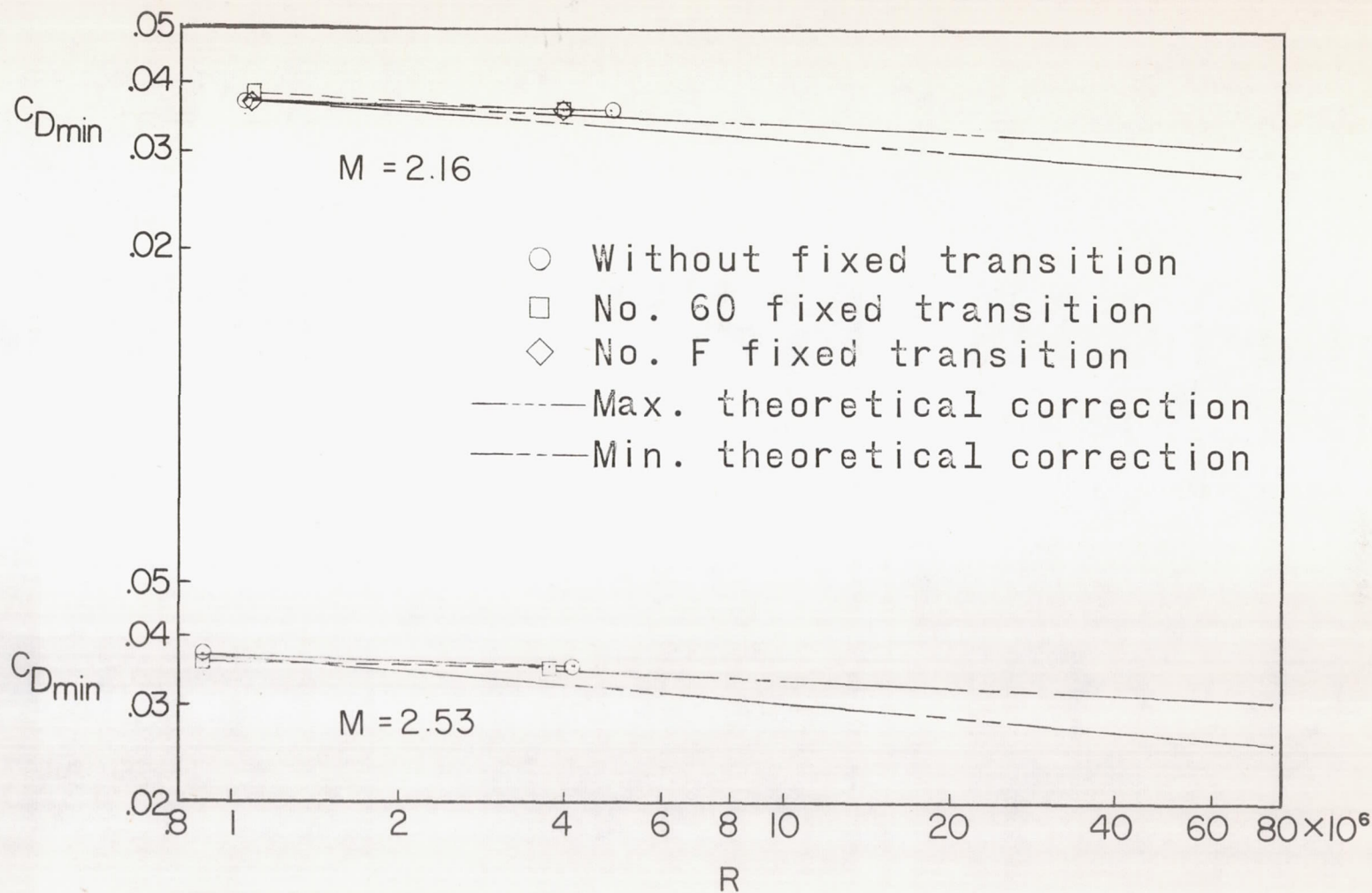
Figure 9.- Concluded.

$\alpha = -1.8°$ $\alpha = 0.4°$ $\alpha = 13.0°$

M = 1.57

$\alpha = -1.9°$ $\alpha = 0.4°$ $\alpha = 13.2°$
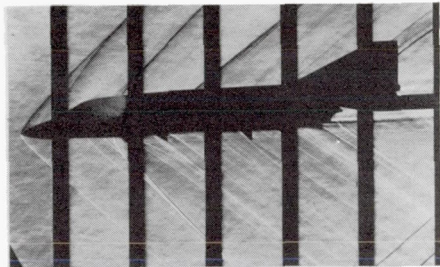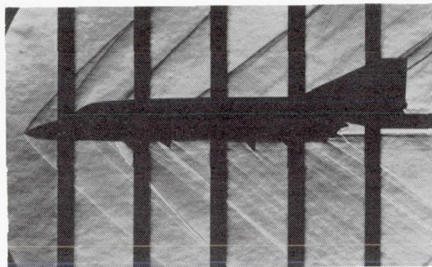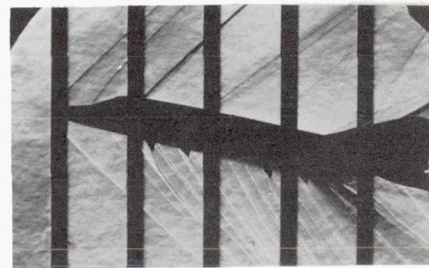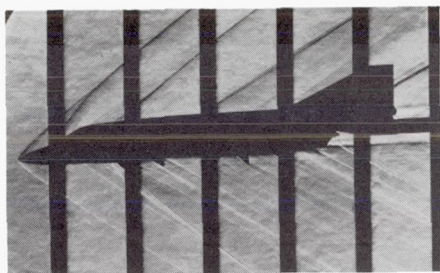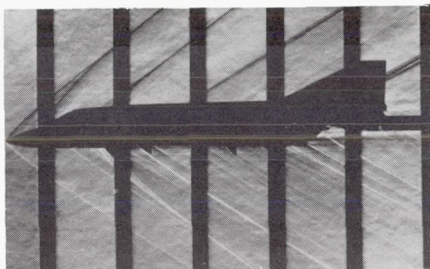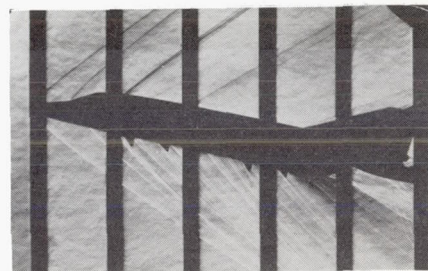
M = 1.87

(a) Basic model.   L-58-139

Figure 10.- Typical schlieren photographs of a 1/20-scale model of a 45° swept-wing, supersonic, fighter airplane.
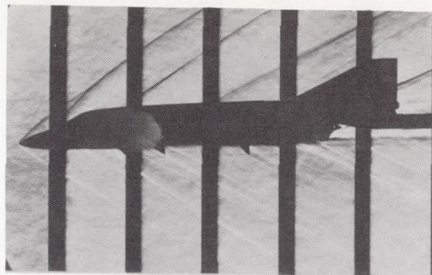
$\alpha = -1.7°$
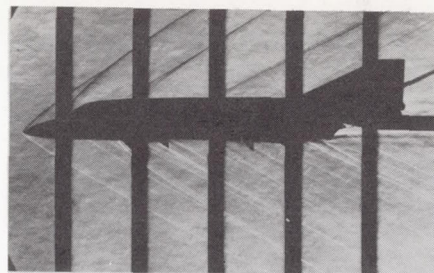
$\alpha = 0.4°$

M = 2.16

$\alpha = 12.8°$

$\alpha = -1.7°$

$\alpha = 0.3°$

M = 2.53

$\alpha = 12.7°$
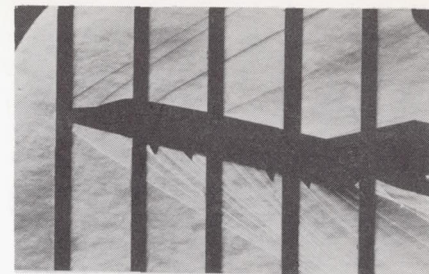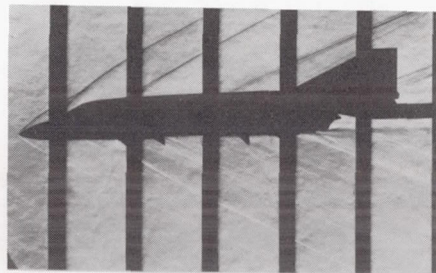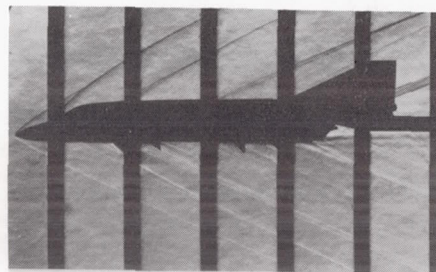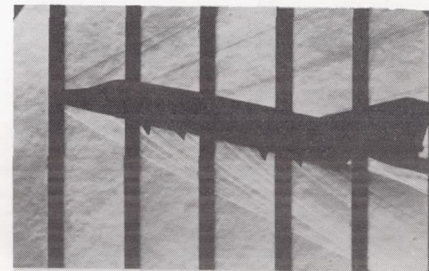
(a) Concluded.   L-58-140

Figure 10.- Continued.
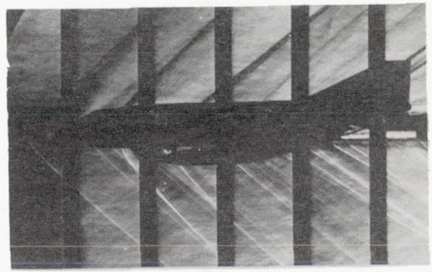
M = 1.57
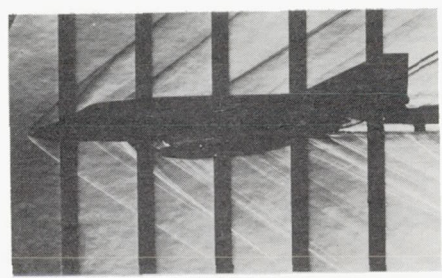
M = 1.87
$\alpha=0.4°$ $\beta=0°$
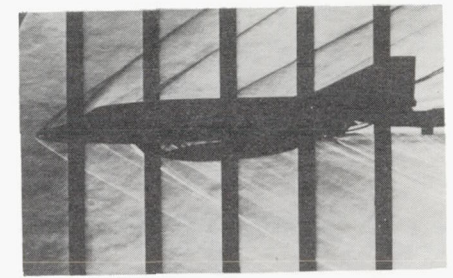
M = 2.16

(b) Center-line tank.
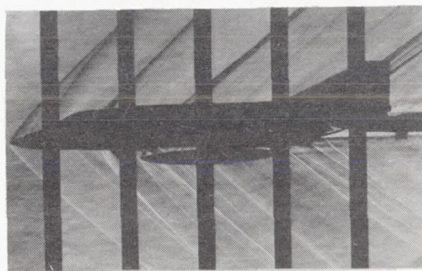
M = 1.57
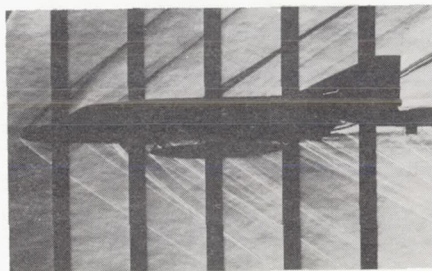
M = 1.87
$\alpha=0.4°$ $\beta=0°$
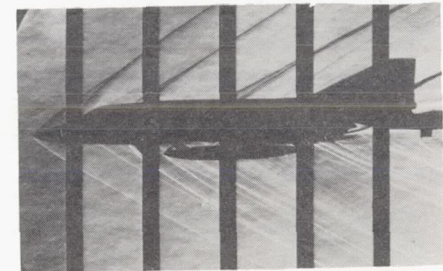
M = 2.16

(c) Wing tank.

L-58-141

Figure 10.- Continued.

α =0.4°

M =1.57

α =6.8°

α =0.4°

M =1.87

α =6.7°

α =0.4°

M =2.16

α =6.6°
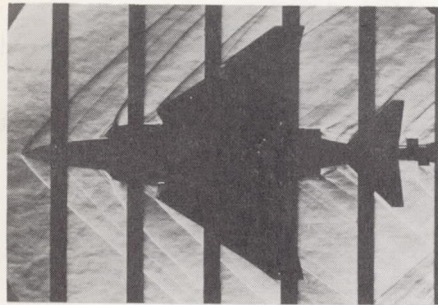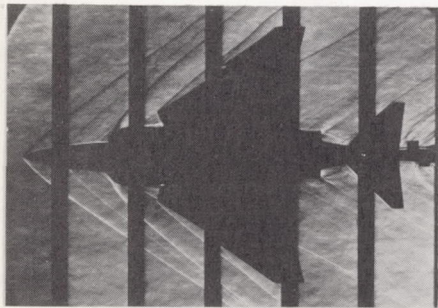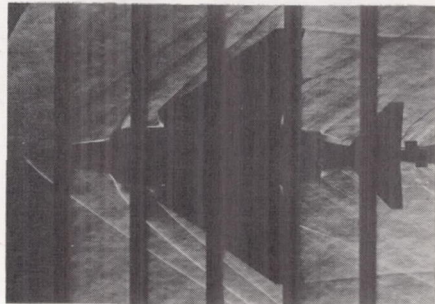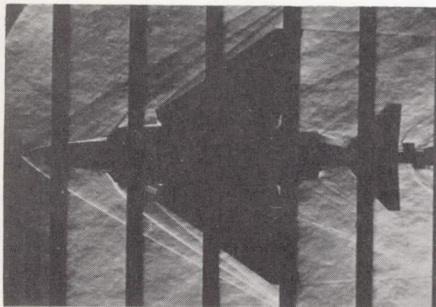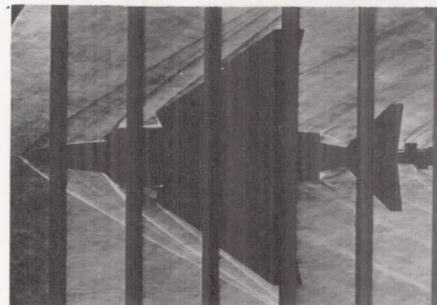
L-58-142

(d) Notched wing with leading-edge cuff and a 25° negative-dihedral horizontal tail.
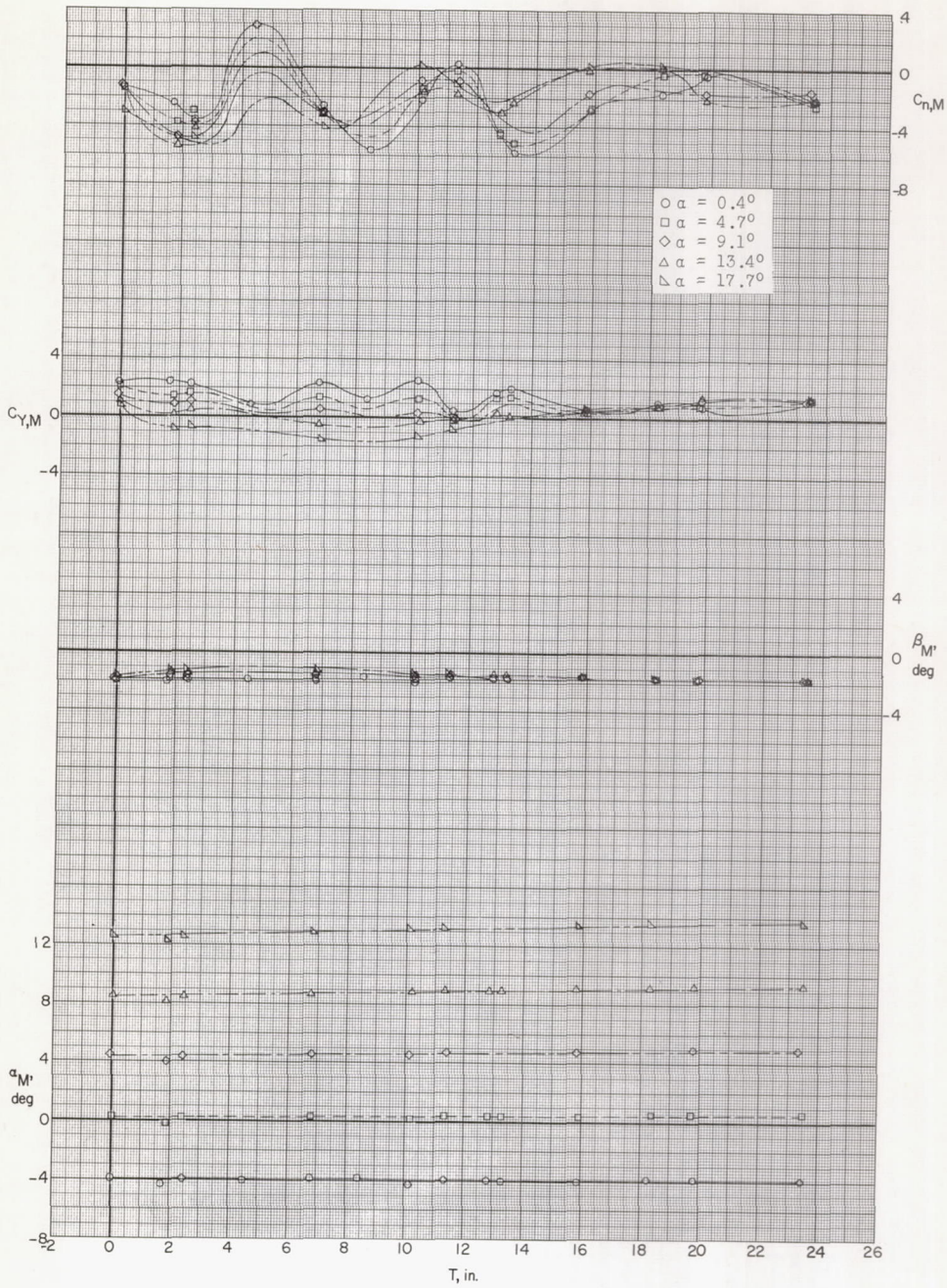
Figure 10.- Concluded.
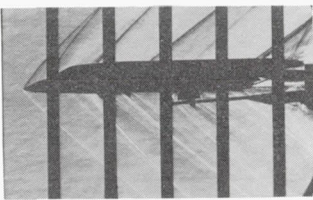
T=0 in.
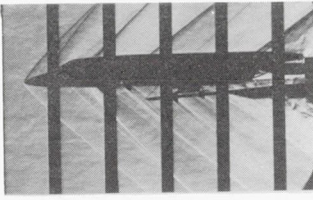
T=1.7 in.
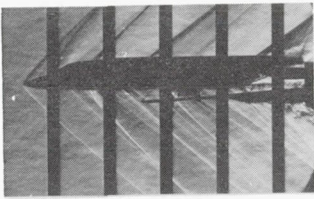
T=2.4 in.
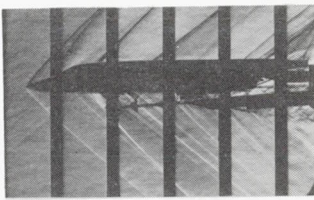
T=6.8 in.
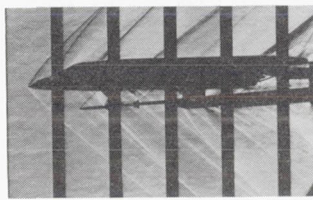
T=10.1 in.
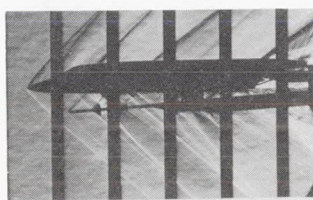
T=11.3 in.

T=12.8 in.

T=13.3 in.

T=15.8 in.

T=18.3 in.

T=19.8 in.

T=23.4 in.

α = 0.4°

(a) M = 1.57.   L-58-143

Figure 11.- Schlieren photographs of rearward missile traverse.
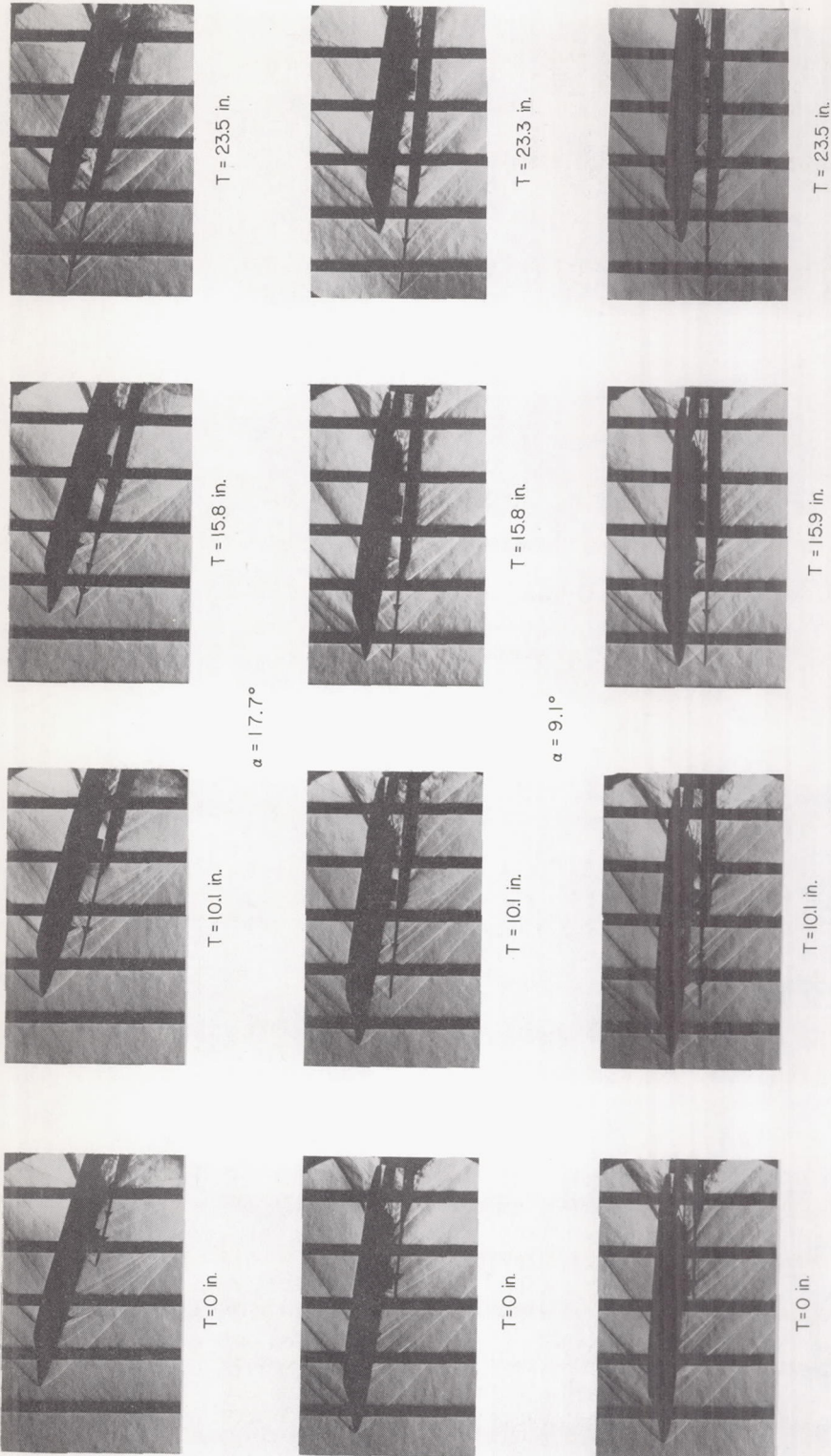
(a) Continued.

L-58-144

Figure 11.- Continued.
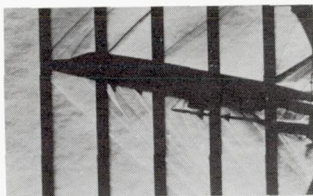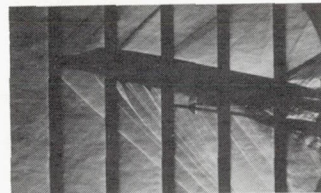
T=0 in.

T=1.8 in.
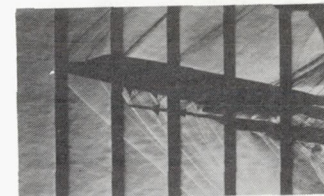
T=6.8 in.
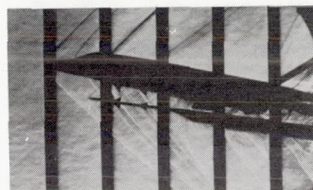
T=10.2 in.

T=11.3 in.

T=12.8 in.

T=13.2 in.

T=15.8 in.

T=18.3 in.
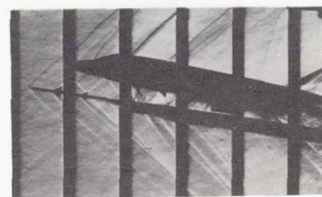
T=19.8 in.
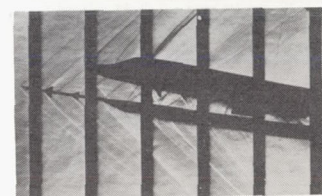
T=23.5 in.

$\alpha = 13.4°$

(a) Concluded.

L-58-145

Figure 11.- Continued.
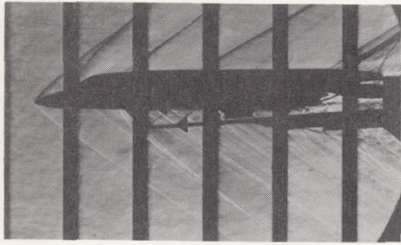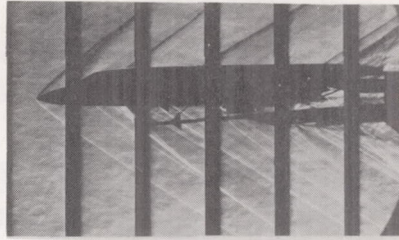
T=5.4in.   T=6.3in.
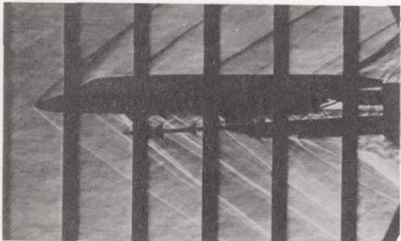
T=7.7in.   T=9.7in.
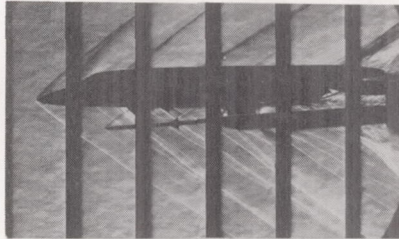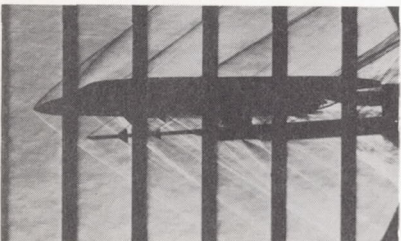
T=11.0in.   T=13.1in.
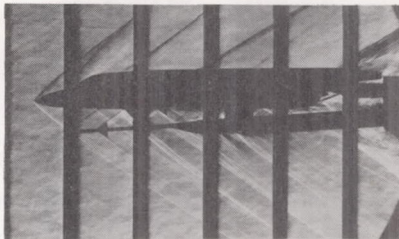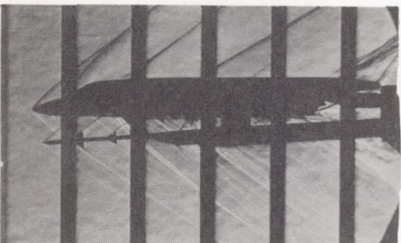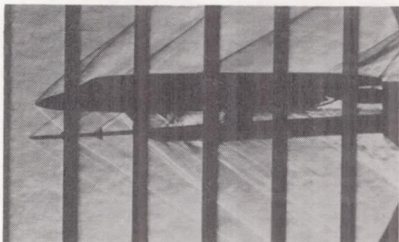
T=15.2in.   T=16.8in.

α = 0.4°

(b)   M = 1.87.   L-58-146

Figure 11.- Continued.

NACA RM L58C17
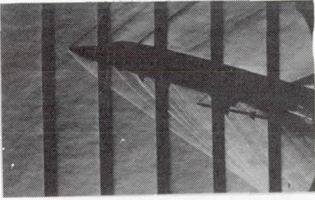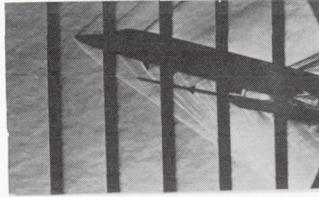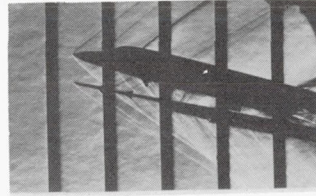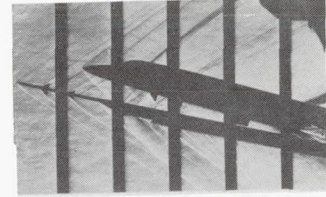
T=0 in. T=7.8 in. T=15.2 in. T=23.5 in.

α = 17.4°

T=0 in. T=7.8 in. T=15.2 in. T=23.5 in.

α = 8.9 in.
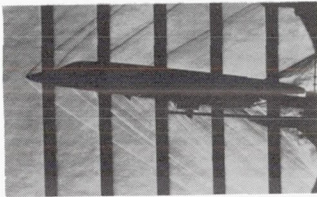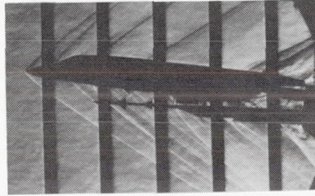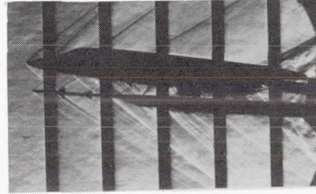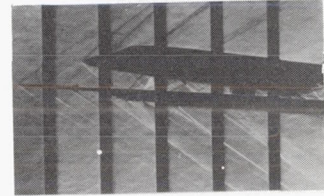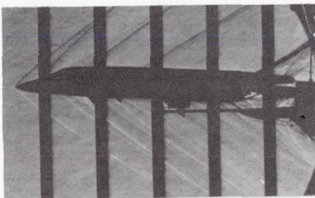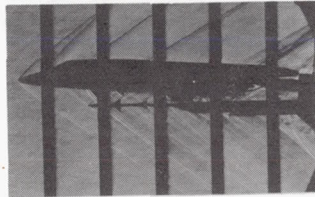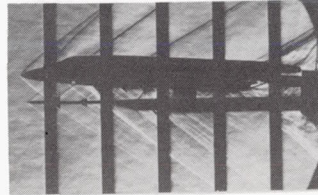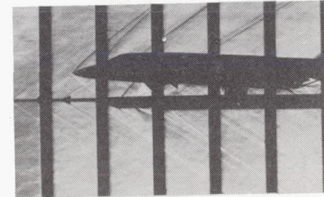
T=0 in. T=7.8 in. T=15.2 in. T=23.5 in.

α = 4.6°

(b) Continued. L-58-147

Figure 11.- Continued.
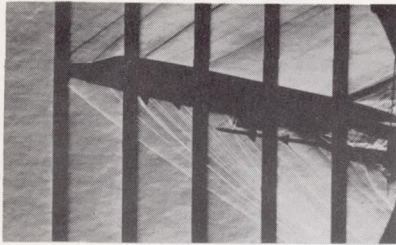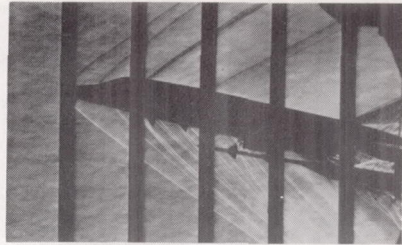
T=0 in.

T=2.4 in.
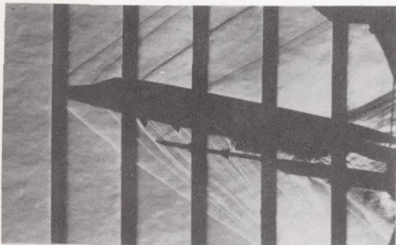
T=5.5 in.
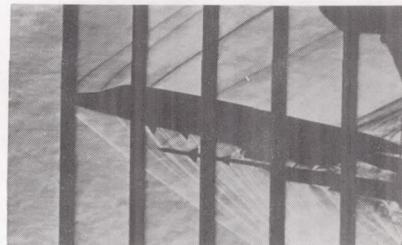
T=6.2 in.

T=7.7 in.
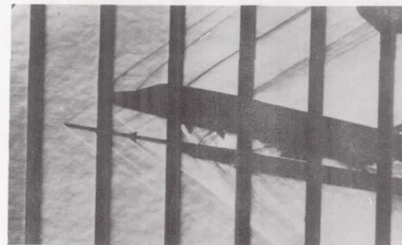
T=18.8 in.
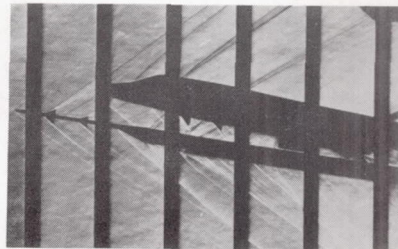
T=23.5 in.

$\alpha = 13.1°$

(b) Concluded.   L-58-148

Figure 11.- Continued.
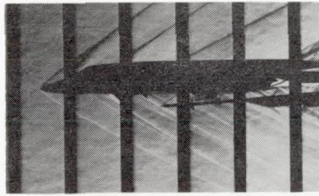
T=0 in.

T=2.0 in.

T=4.6 in.
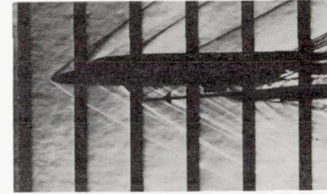
T=5.8 in.
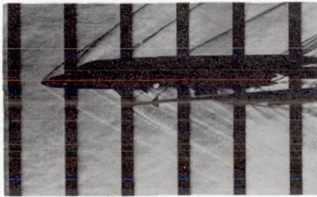
T=6.2 in.
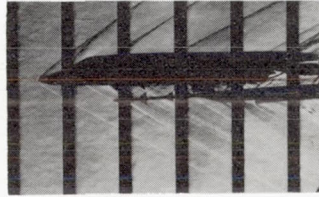
T=7.3 in.

T=9.1 in.
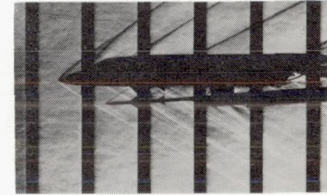
T=10.6 in.
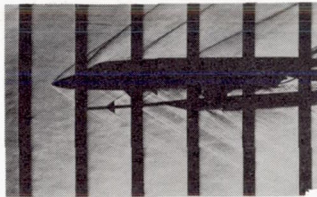
T=12.5 in.
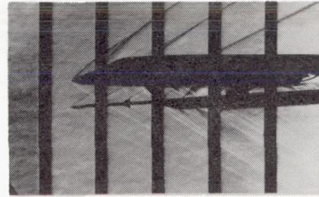
T=16.3 in.
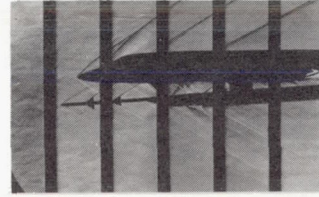
T=18.1 in.
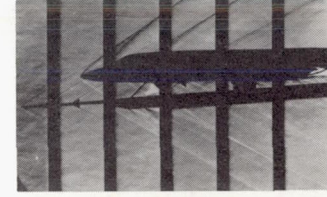
T=23.5 in.

$\alpha = 0.4°$

(c) M = 2.16.   L-58-149

Figure 11.- Continued.
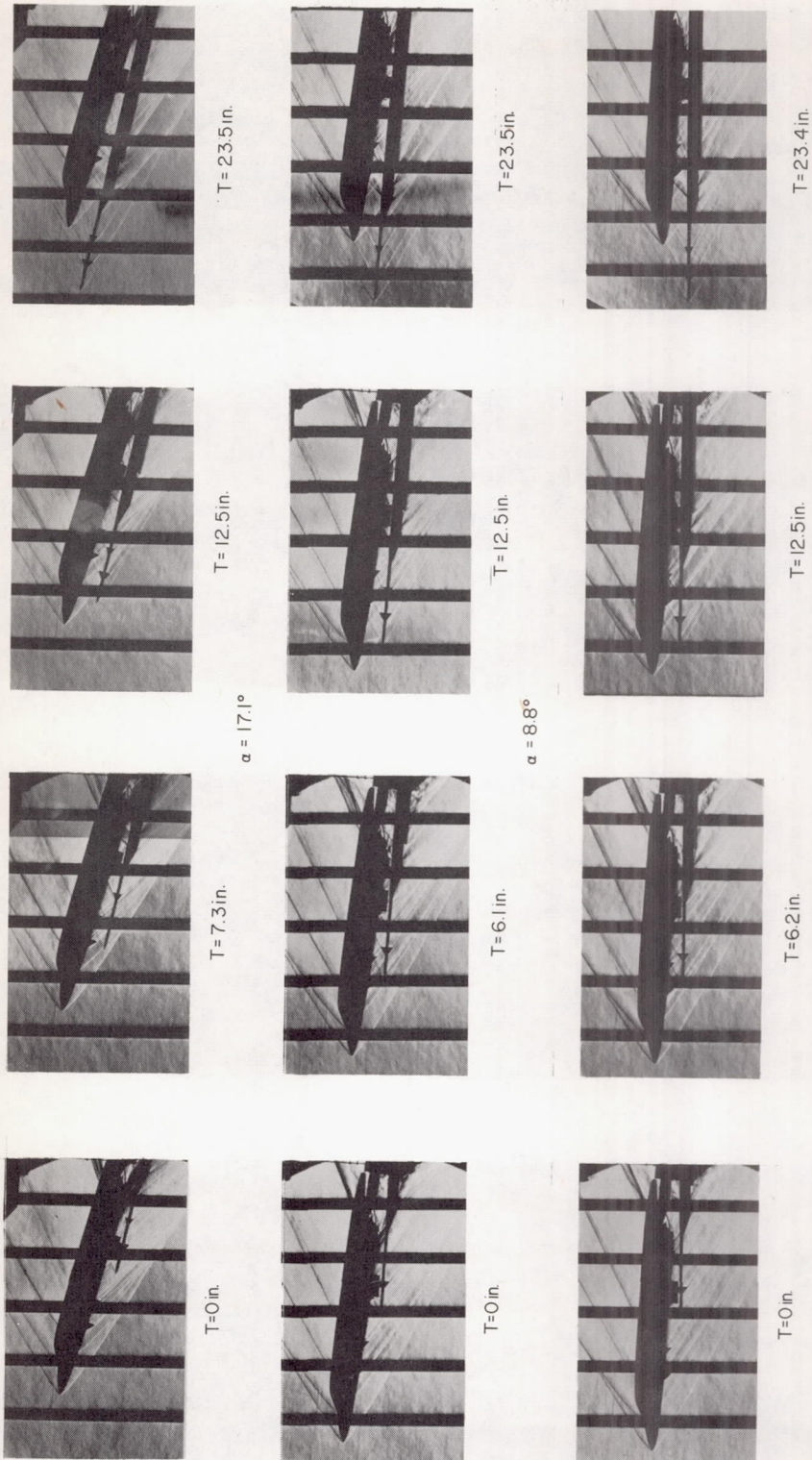
(c) Continued.   L-58-150

Figure 11.- Continued.

T=0 in.

T=2.0 in.
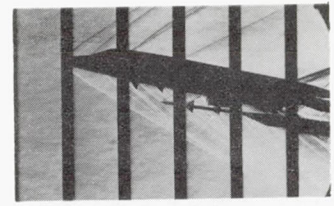
T=3.5 in.
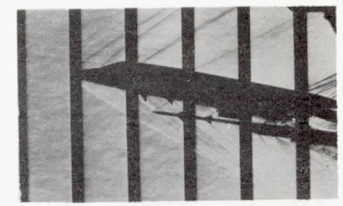
T=5.7 in.
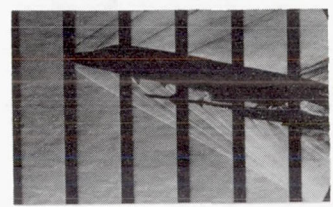
T=6.2 in.

T=7.3 in.
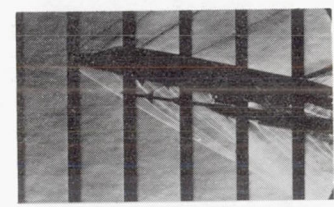
T=9.1 in.
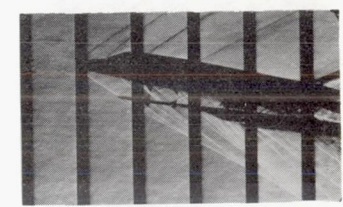
T=10.5 in.

T=12.5 in.

T=16.2 in.

T=18.0 in.

T=23.5 in.

$\alpha = 12.9°$
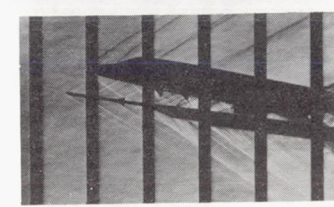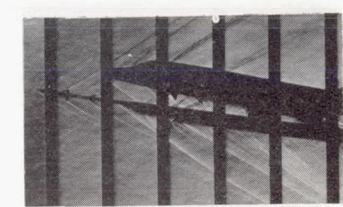
(c) Concluded.

L-58-151

Figure 11.- Concluded.
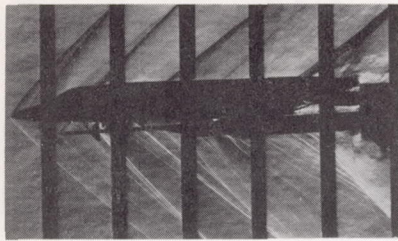
T=0 in.
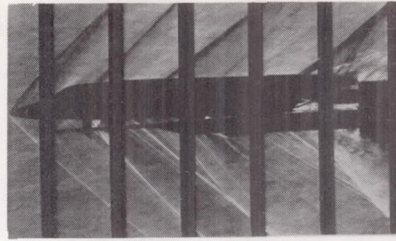
T=0.6 in.
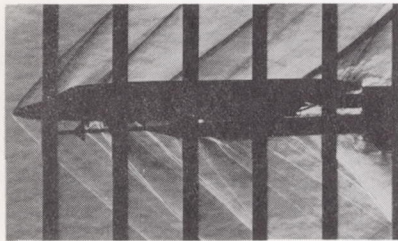
T=1.6 in.
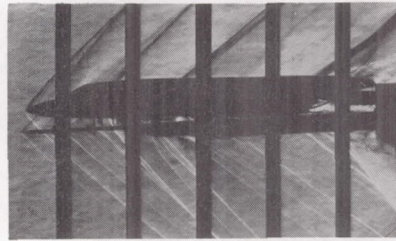
T=5.0 in.
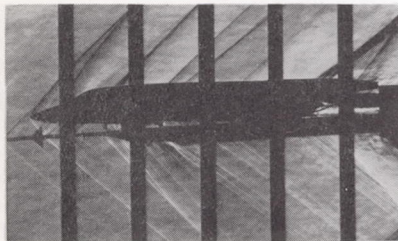
T=7.3 in.
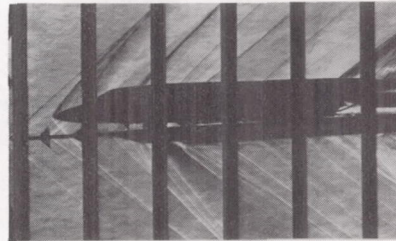
T=8.9 in.

T=11.8 in.

$\alpha = 0.4°$

(a) M = 1.57.   L-58-152

Figure 12.- Schlieren photographs of forward missile traverse.
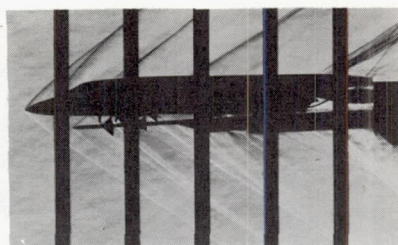
T=0 in.
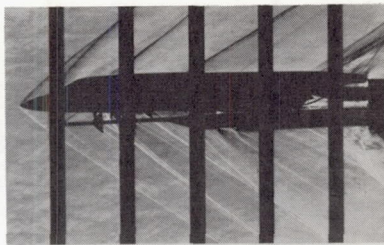
T=0.5 in.
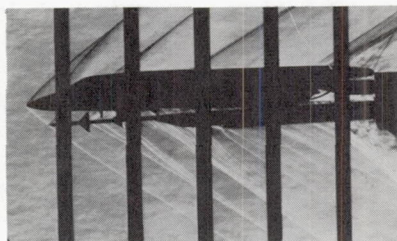
T=2.5 in.
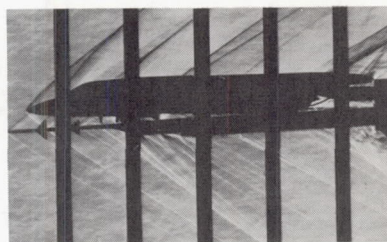
T=6.5 in.

T=8.2 in.
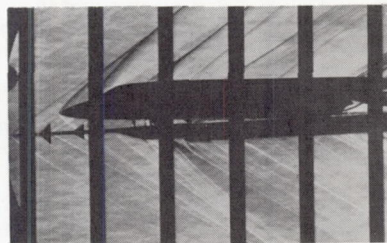
T=9.4 in.

T=11.8 in.

$\alpha = 0.4°$

(b)   M = 1.87.   L-58-153

Figure 12.- Continued.
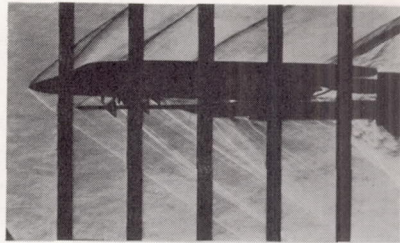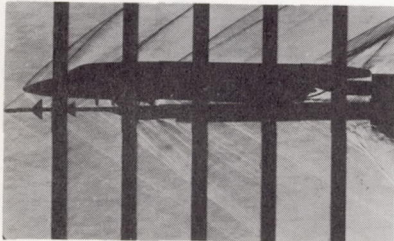
T=0 in.
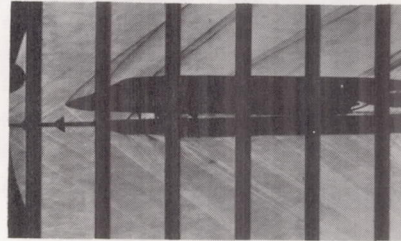
T=6.5in.   T=11.8in.

$\alpha = 1.8°$
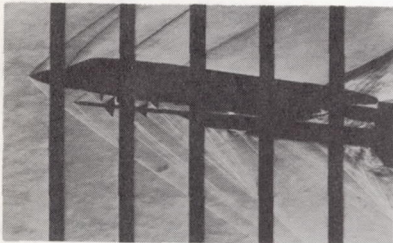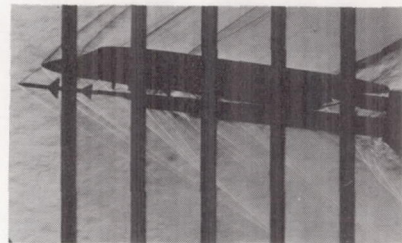
T=0 in.   T=6.6°

$\alpha = 8.9°$
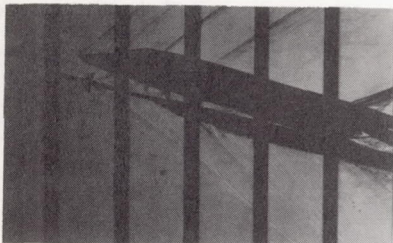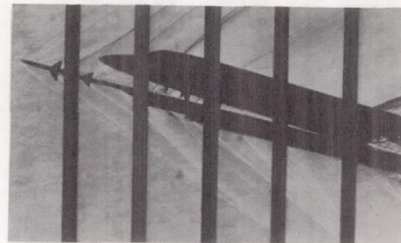
T=6.6in.   T=11.8in.

$\alpha \doteq 17.3°$

(b) Continued.   L-58-154

Figure 12.- Continued.
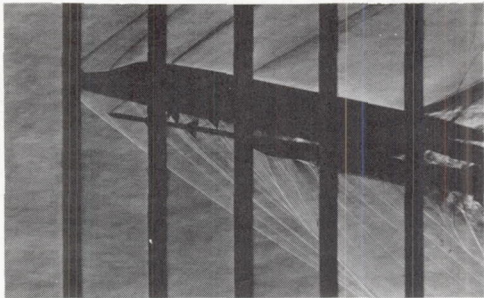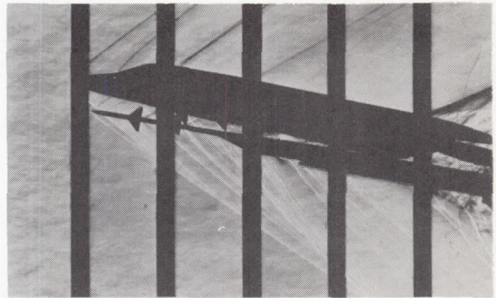
T = 0.5 in.   T = 2.5 in.
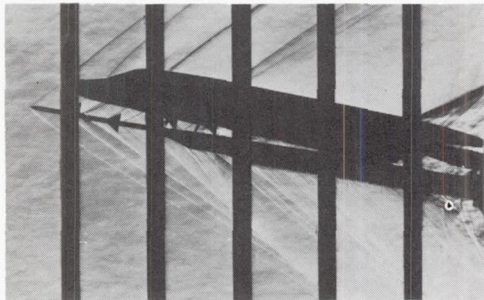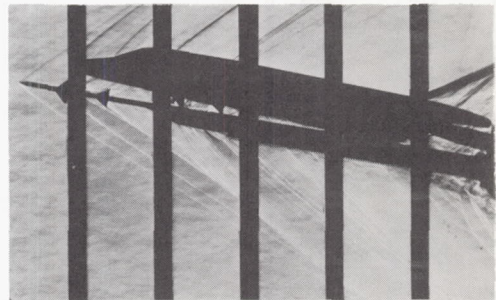
T = 6.5 in.   T = 8.0 in.
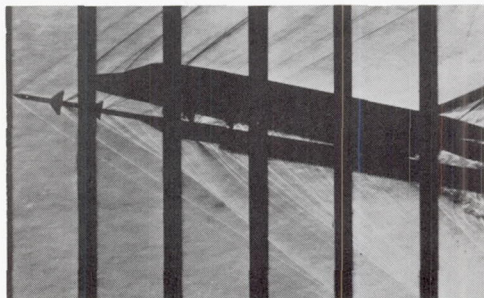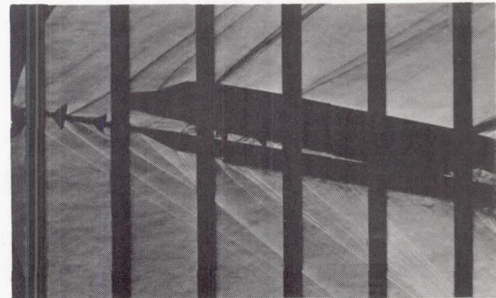
T = 9.4 in.   T = 11.8 in.

$\alpha = 13.1°$

(b) Concluded.   L-58-155

Figure 12.- Continued.
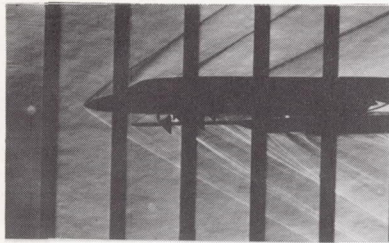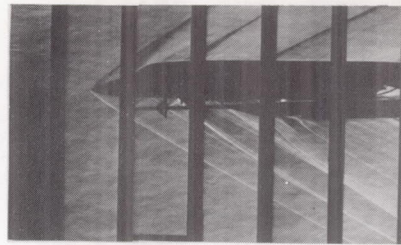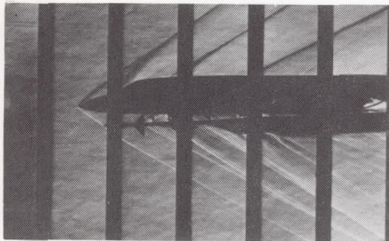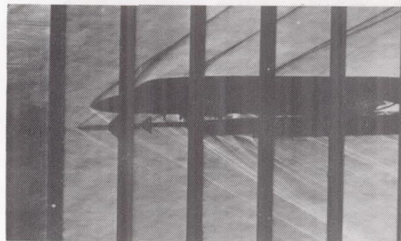
T=0 in.
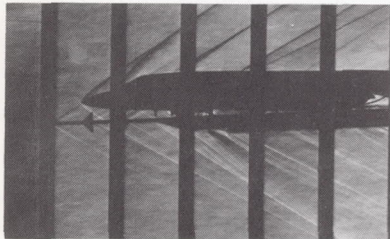
T=1.2 in.
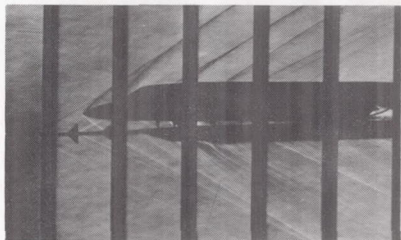
T=2.1 in.
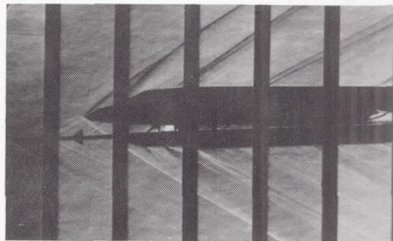
T=5.7 in.

T=7.4 in.

T=9.0 in.

T=11.9 in.

$\alpha = 0.4°$

(c) M = 2.16.   L-58-156

Figure 12.- Continued.
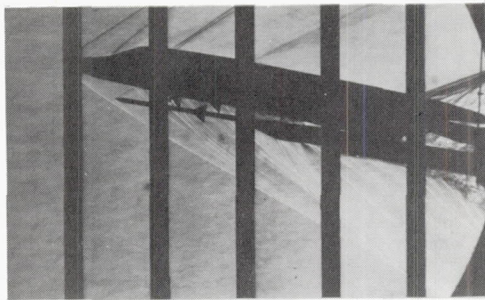
T=0 in.   T=1.2 in.
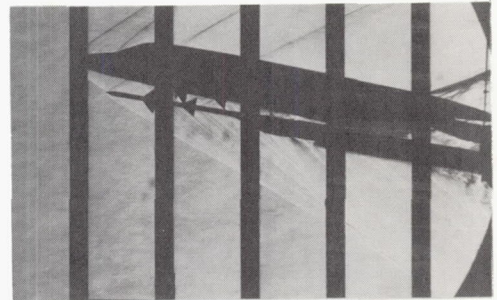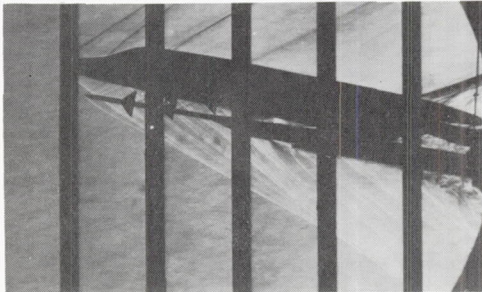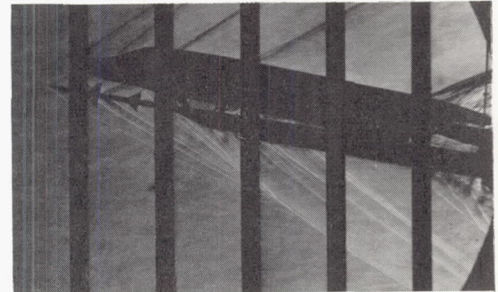
T=2.1 in.   T=5.7 in.
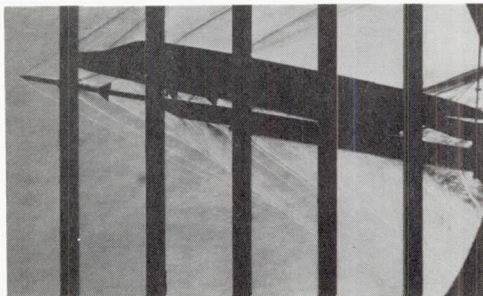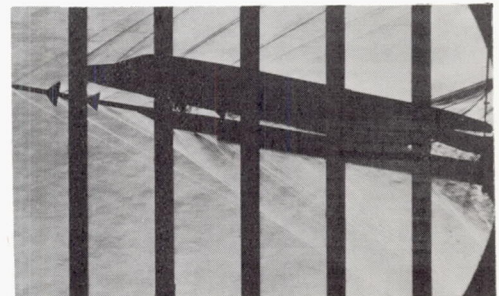
T=7.4 in.   T=9.0in.

$\alpha = 12.9°$

(c) Concluded.   L-58-157

Figure 12.- Concluded.

(a) M = 1.57; β = 0°.

Figure 13.- Aerodynamic loads on the rearward missile at various
traverse positions and angles of attack.
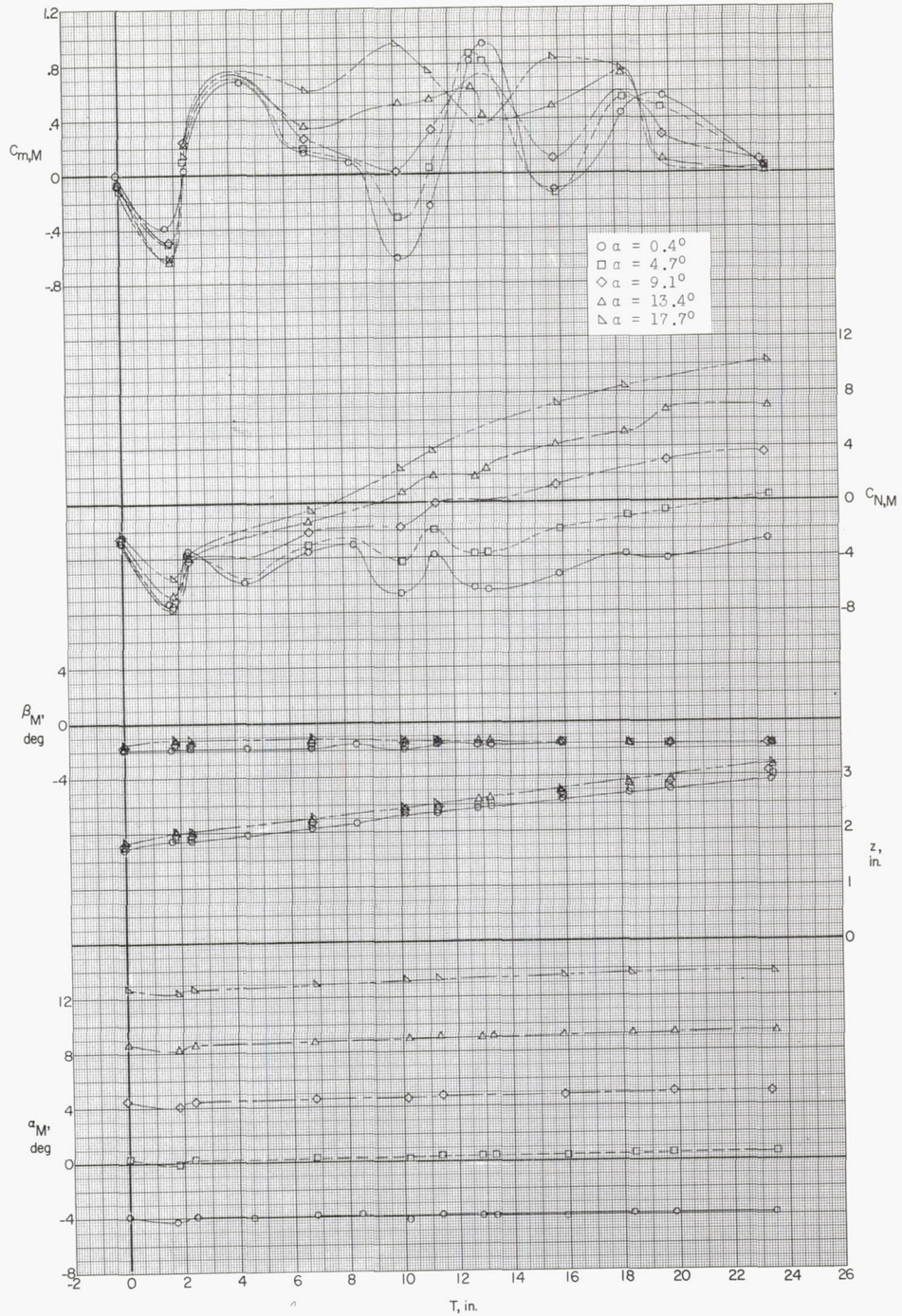
(a) Concluded.

Figure 13.- Continued.

(b)　M = 1.87; β = 0°.
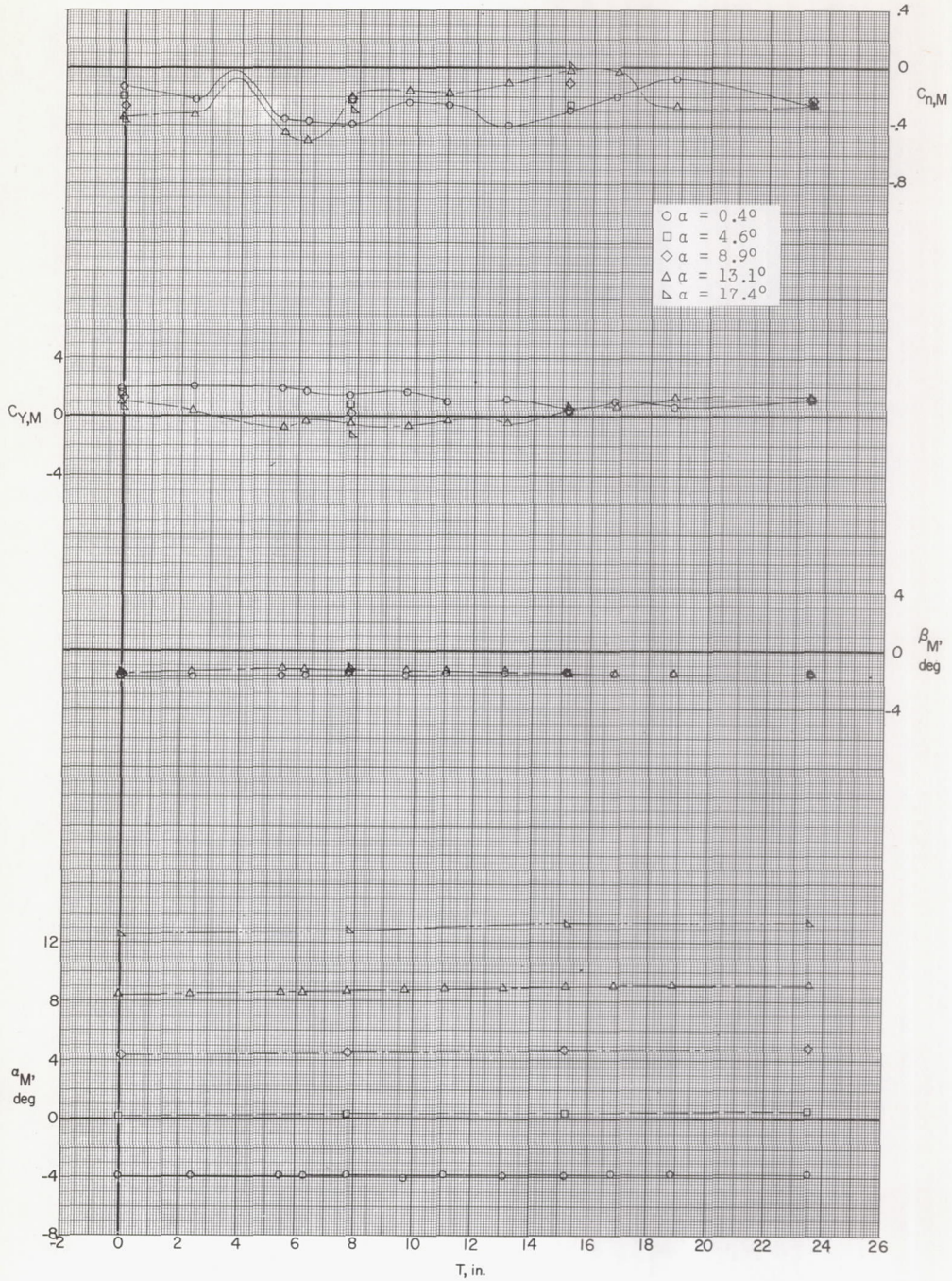
Figure 13.- Continued.
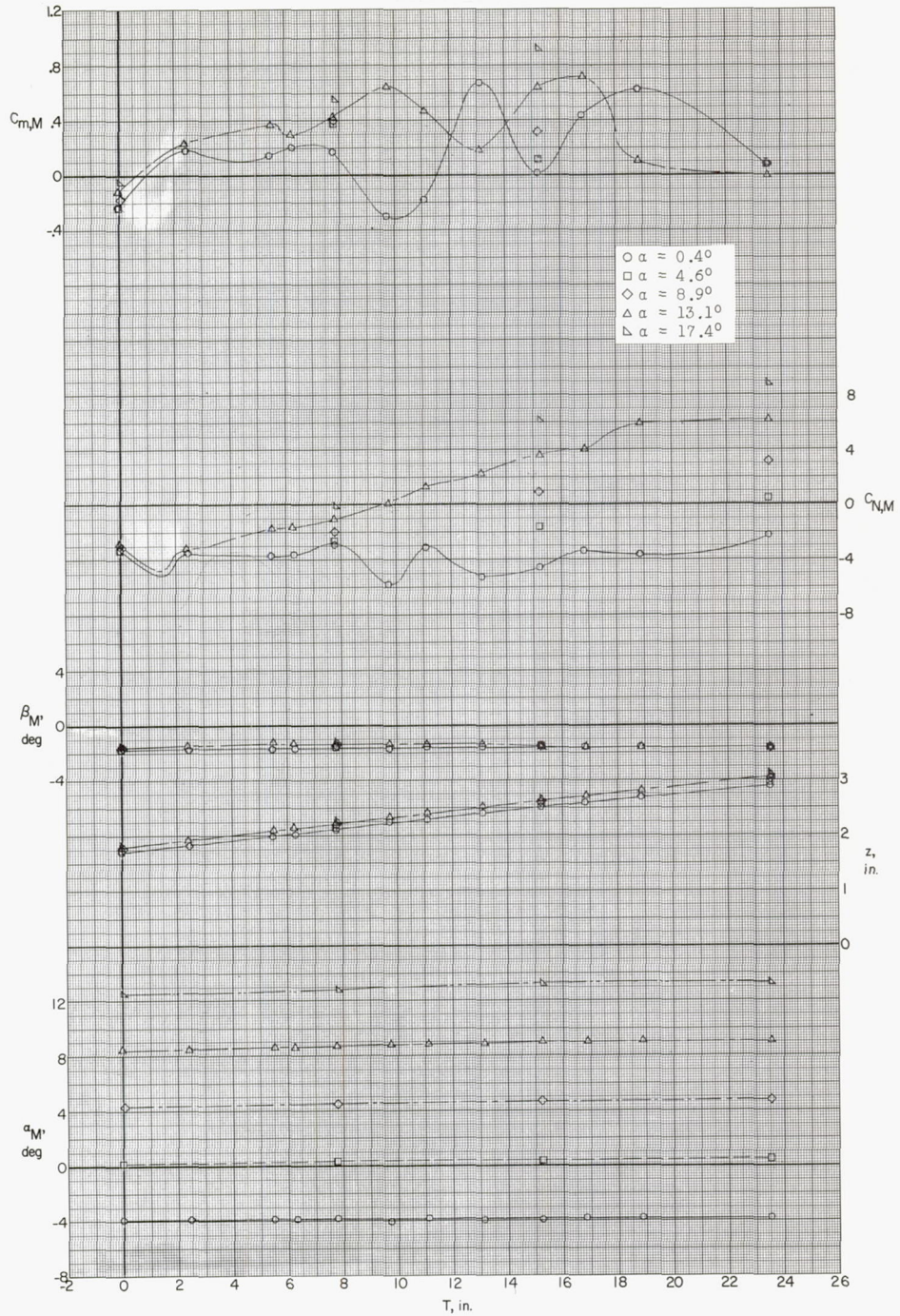
(b) Concluded.

Figure 13.- Continued.
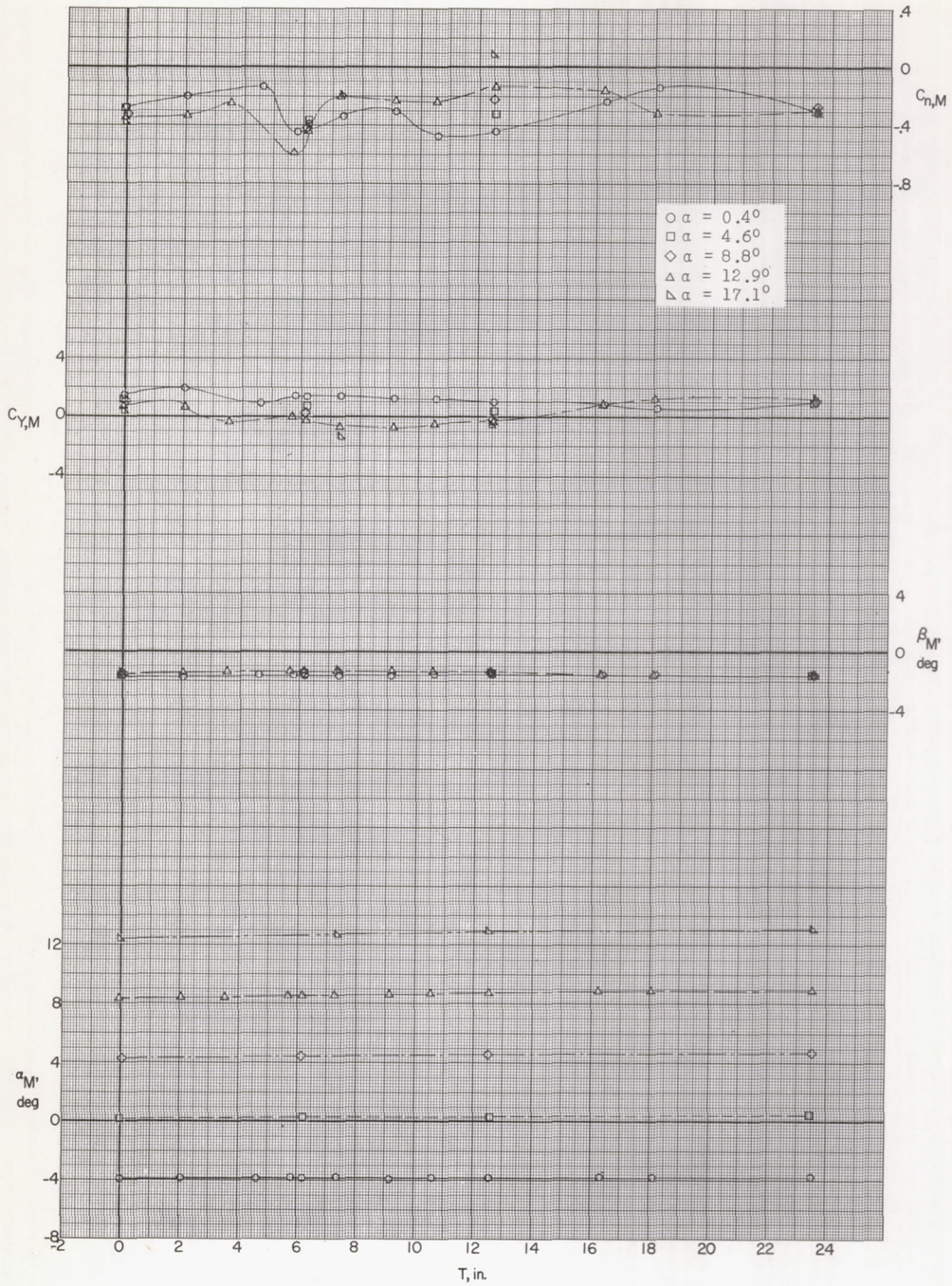
(c)　$M = 2.16$; $\beta = 0^{\circ}$.

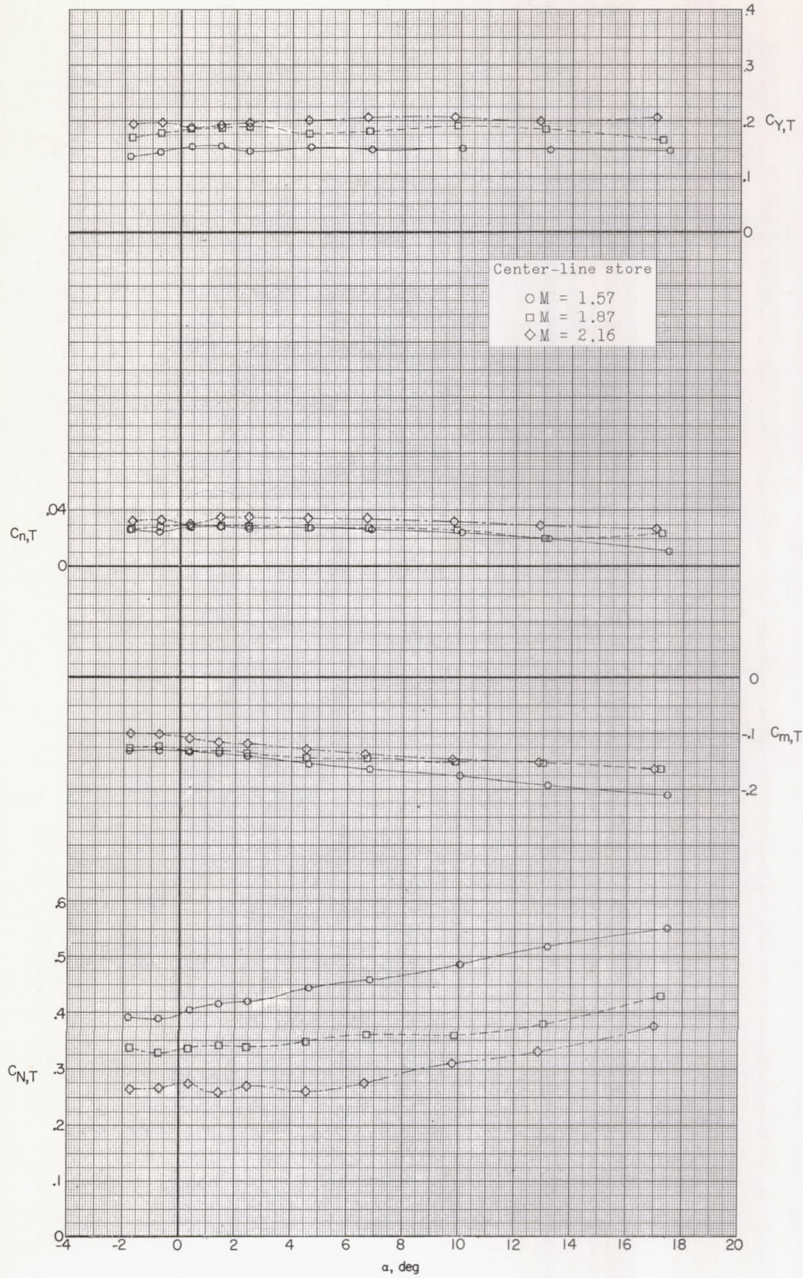Figure 13.- Continued.
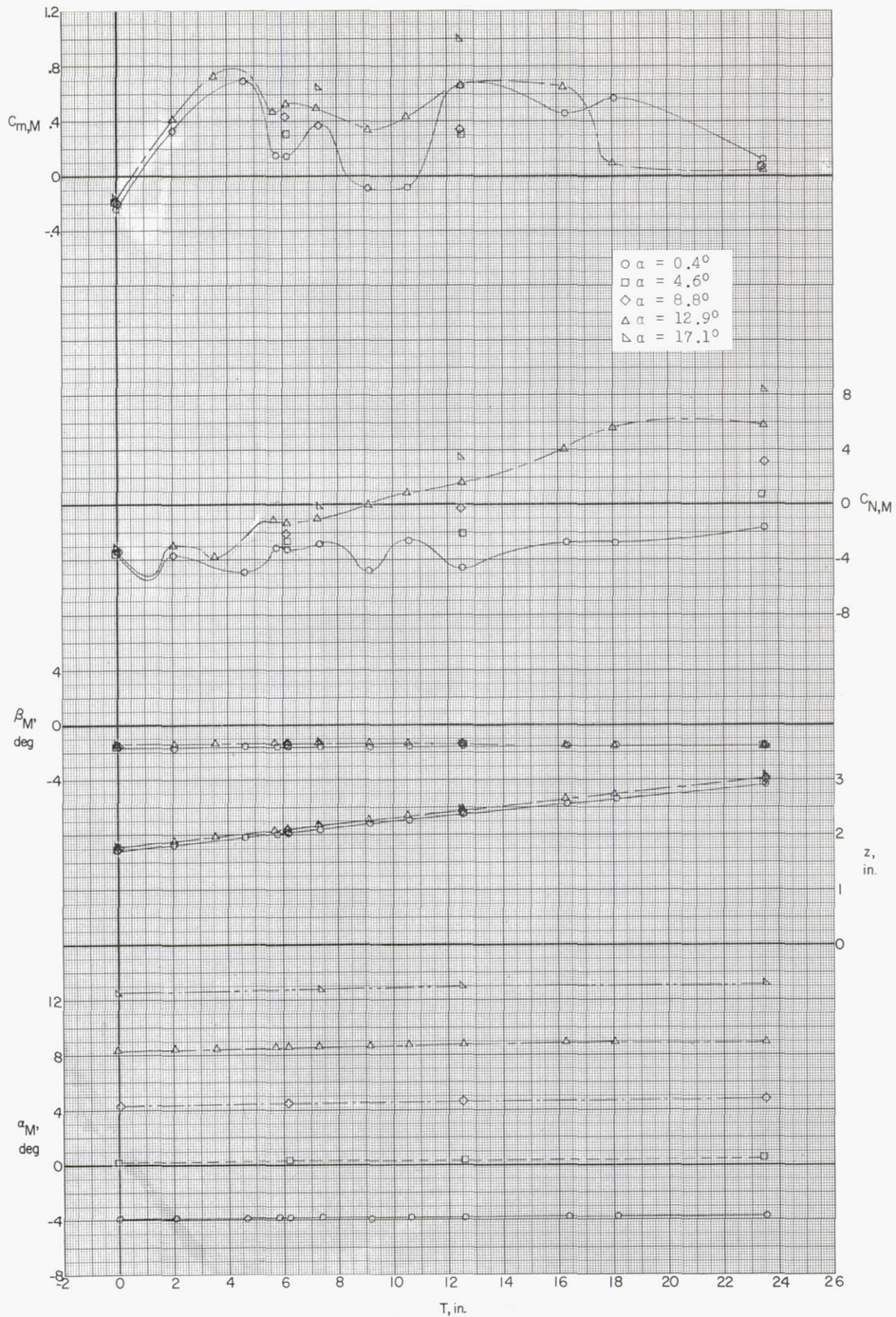
(c) Concluded.

Figure 13.- Concluded.
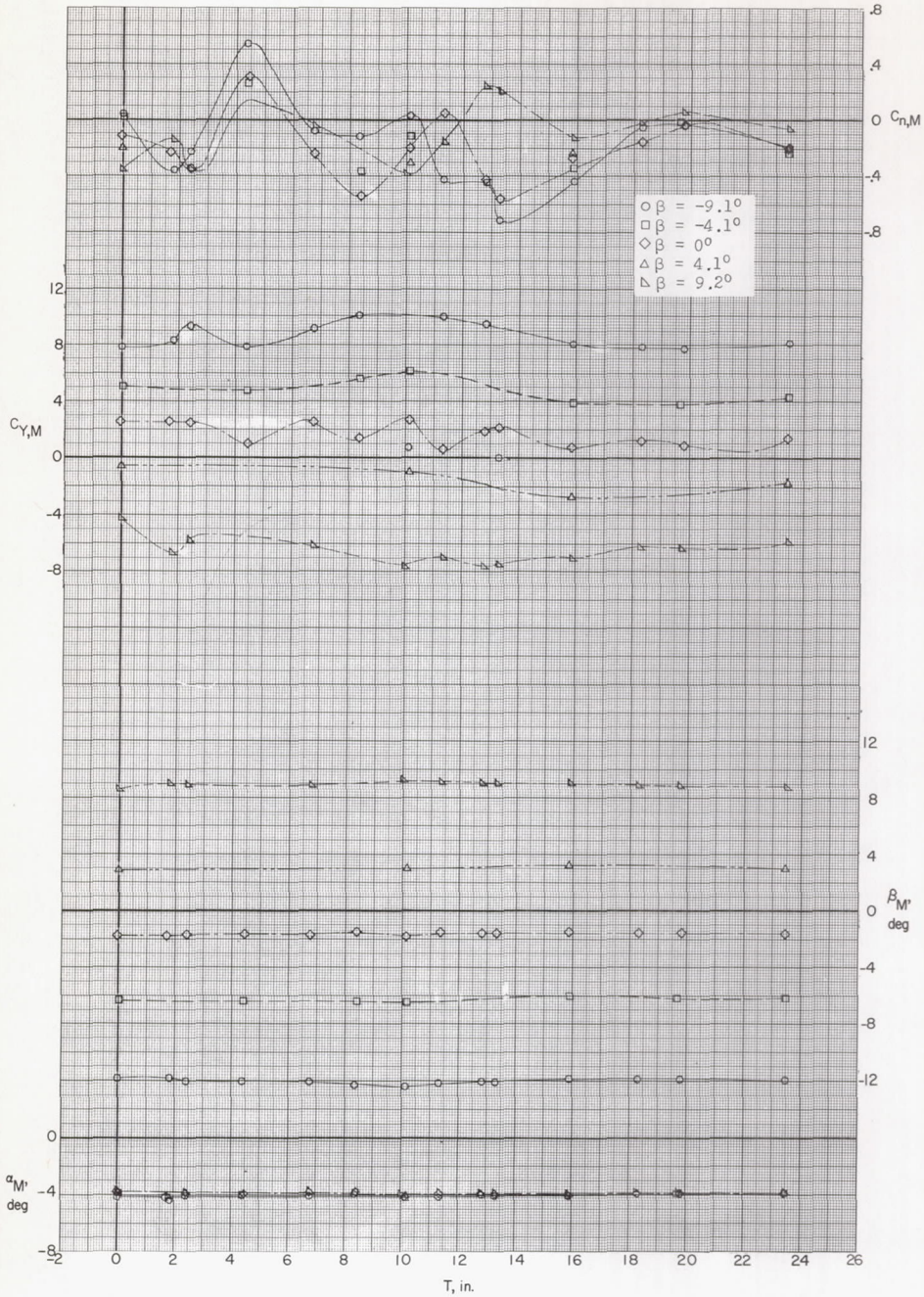
(a) $M = 1.57$; $\alpha = 0°$.

Figure 14.- Aerodynamic loads on the rearward missile at various
traverse positions and angles of sideslip.
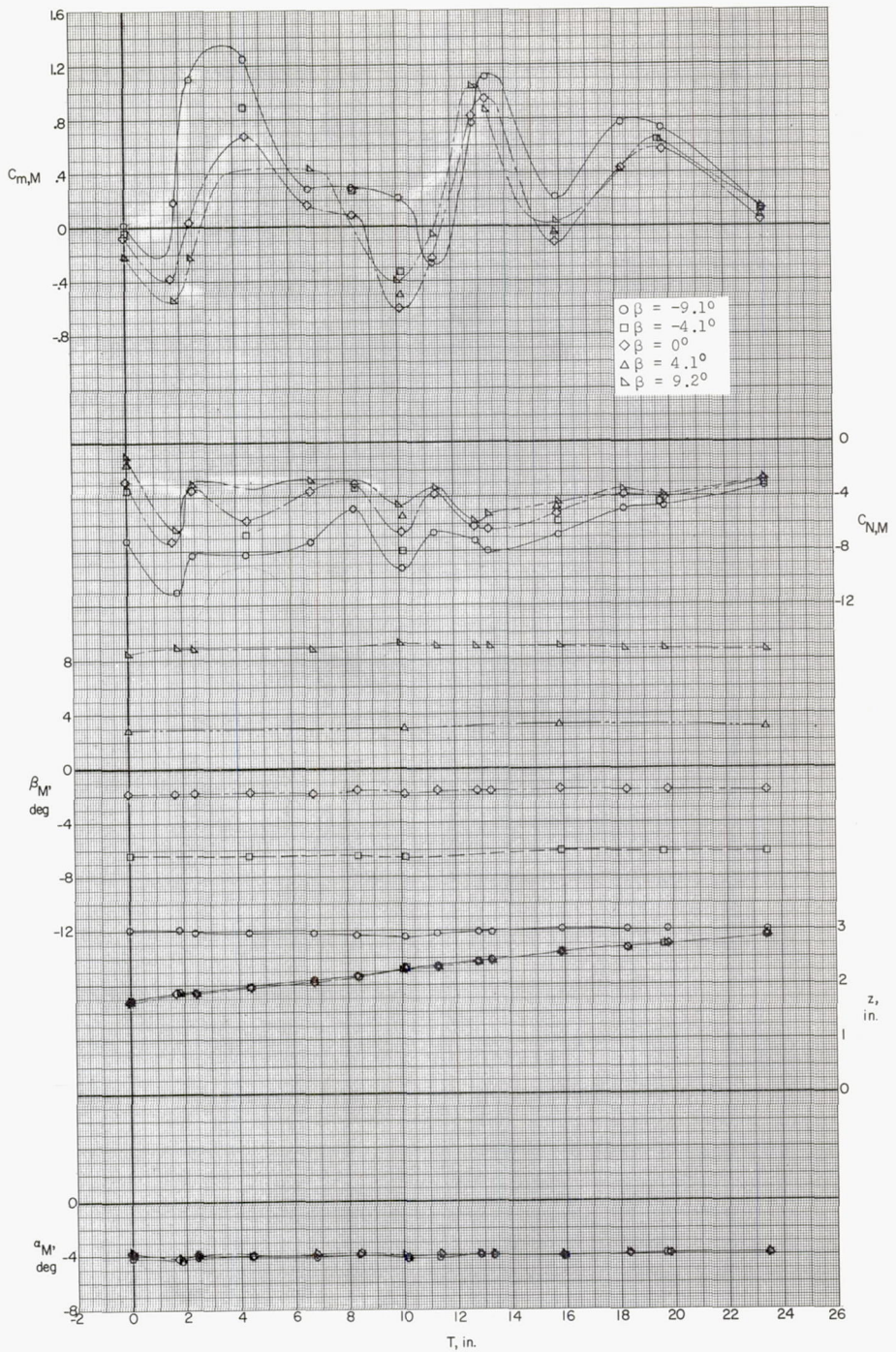
(a) Concluded.

Figure 14.- Continued.

(b) M = 1.87; α = 0°.
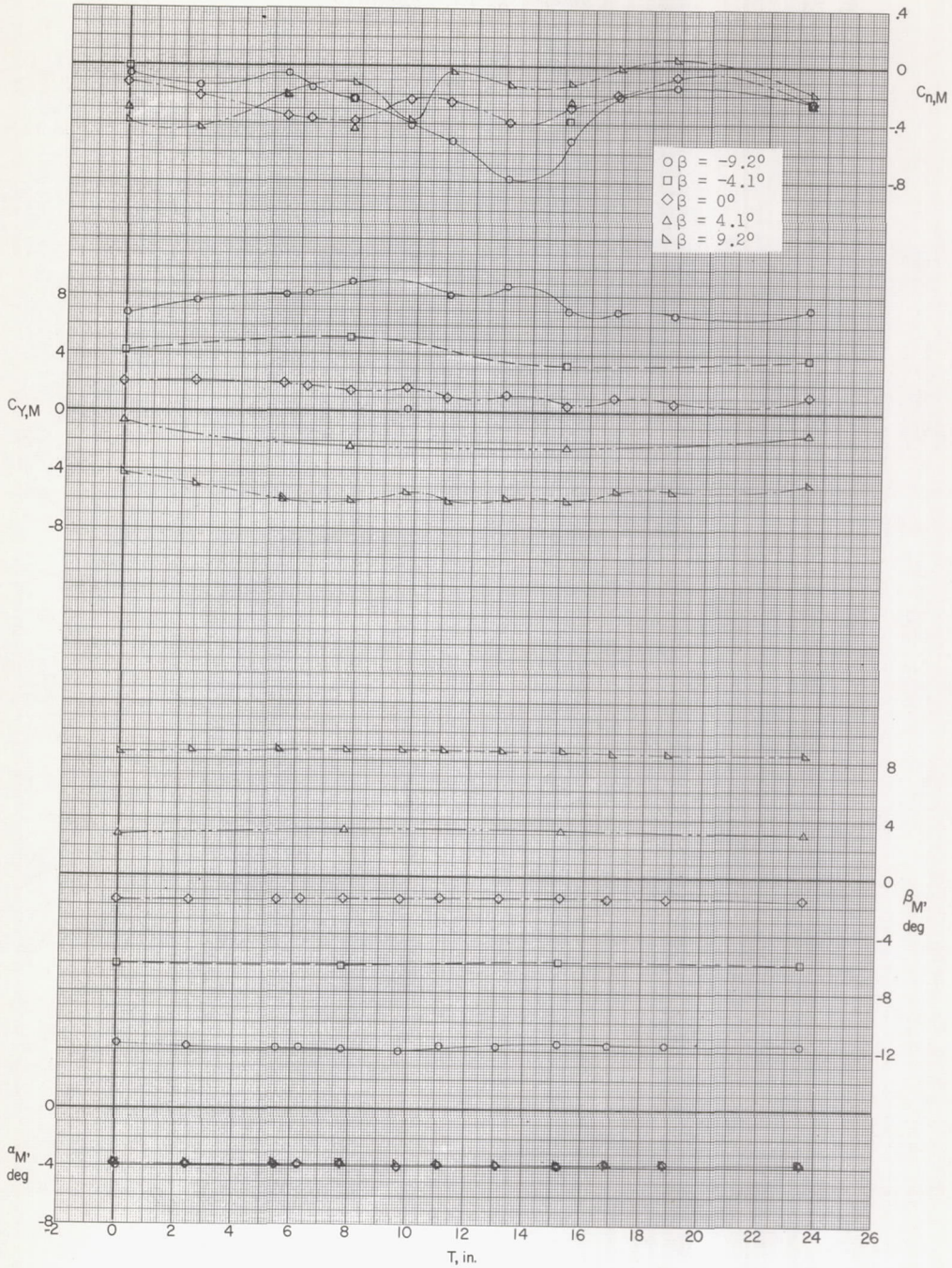
Figure 14.- Continued.
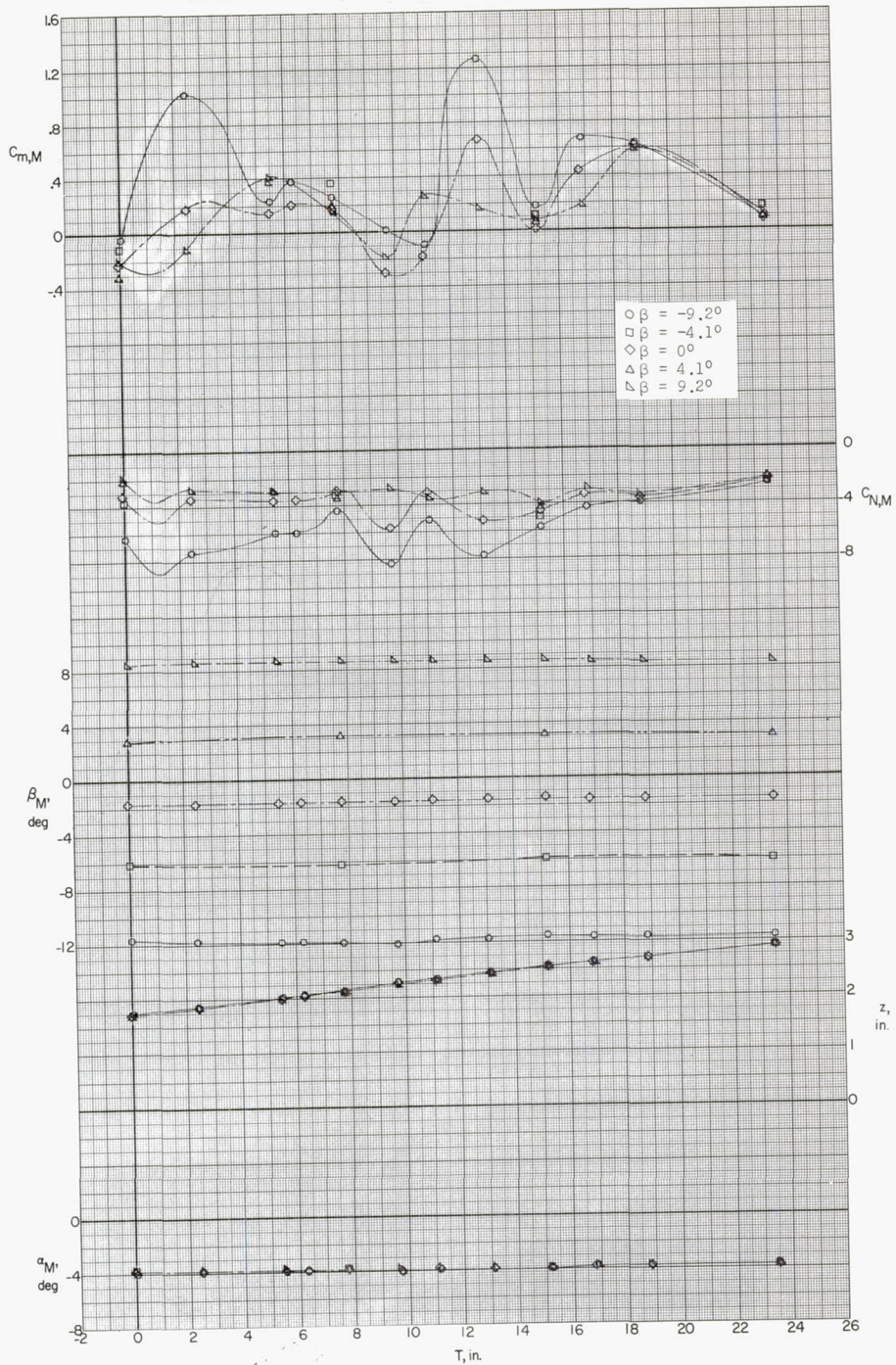
(b) Concluded.

Figure 14.- Continued.

(c) M = 2.16; α = 0°.
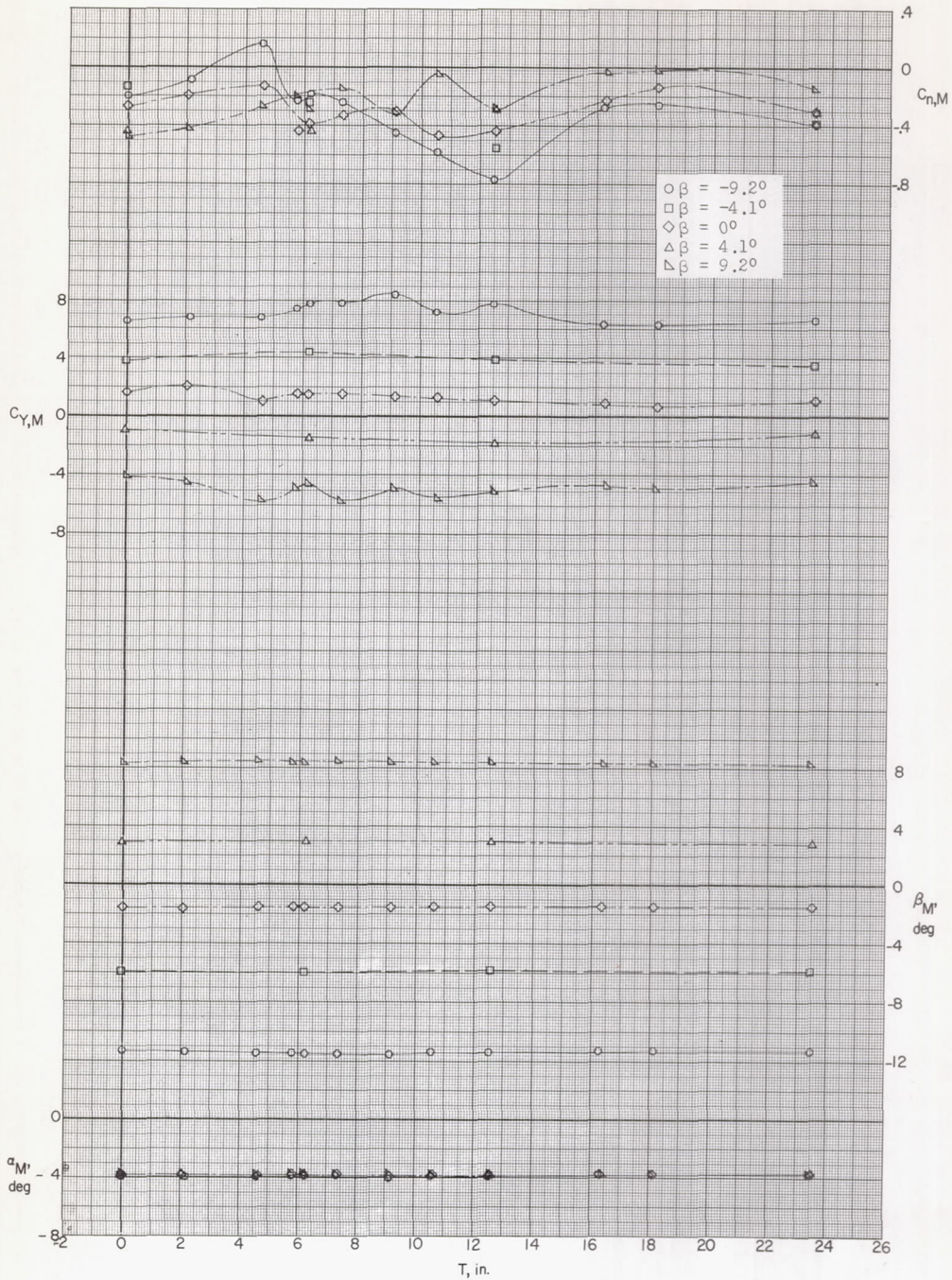
Figure 14.- Continued.
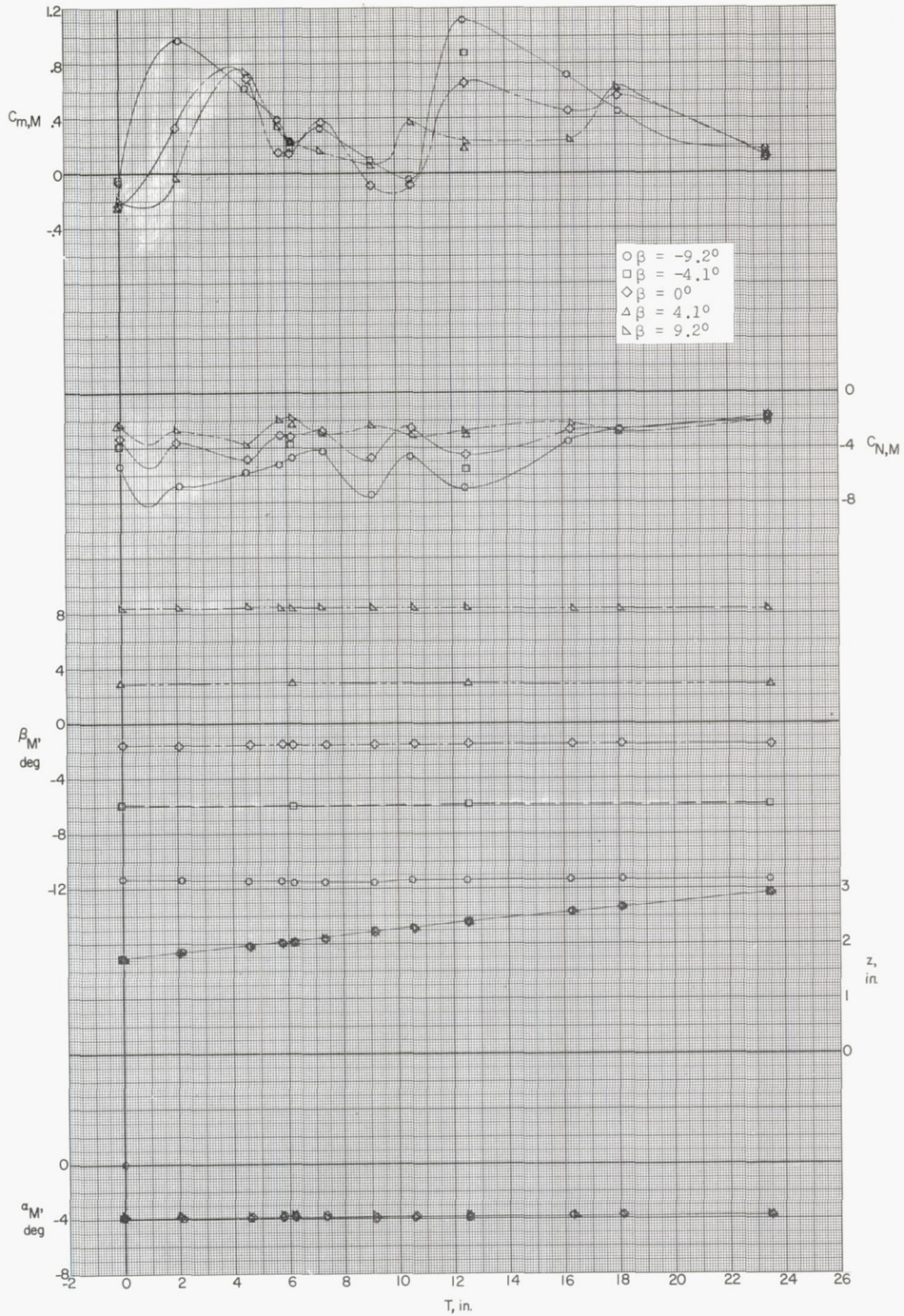
(c) Concluded.

Figure 14.- Concluded.
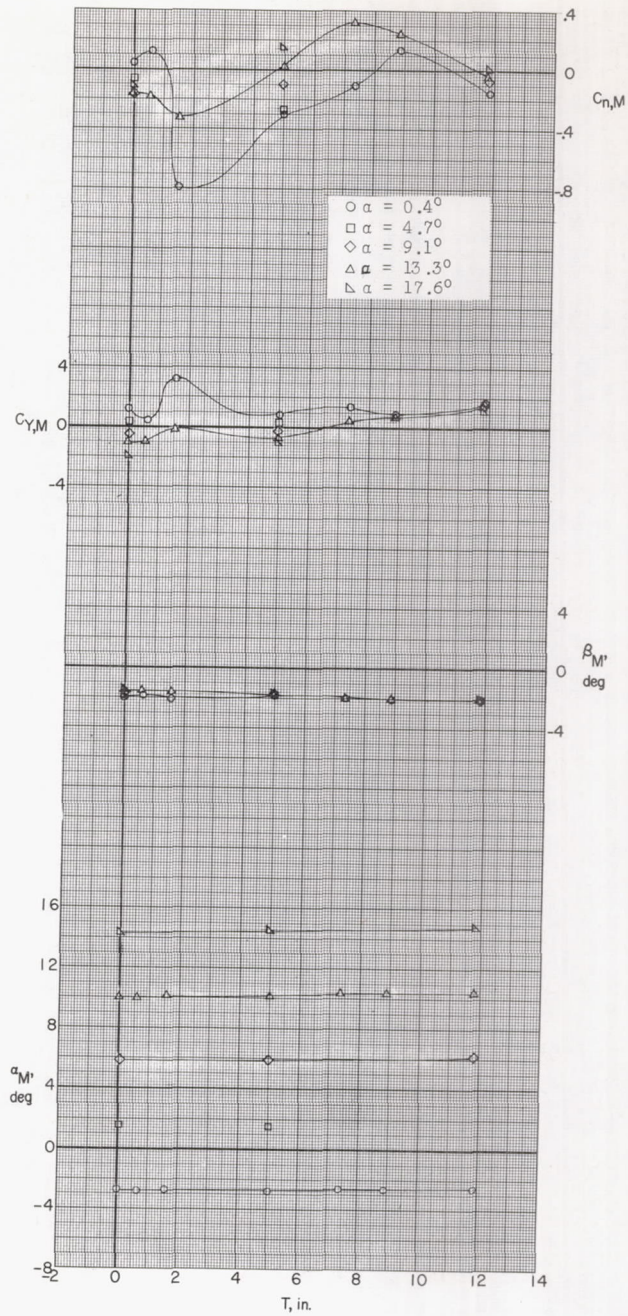
(a)   M = 1.57; β = 0°.

Figure 15.- Aerodynamic loads on the forward missile at various
traverse positions and angles of attack.
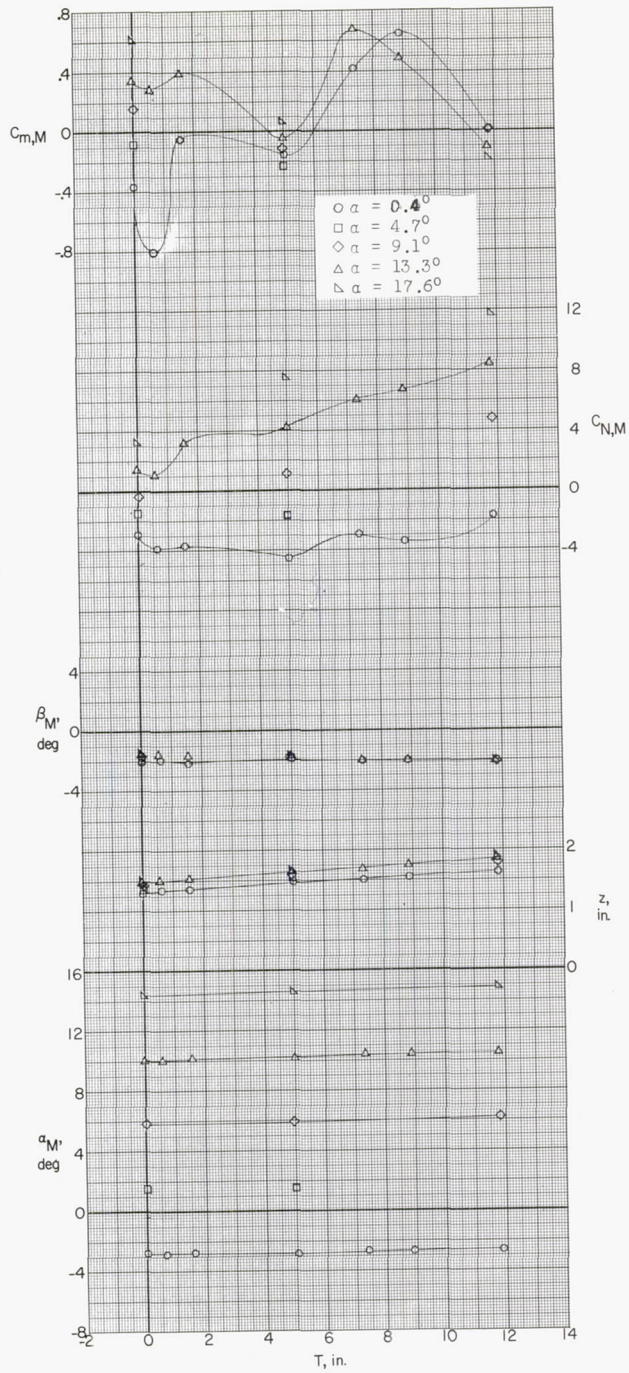
(a) Concluded.

Figure 15.- Continued.

(b)   M = 1.87; β = 0°.
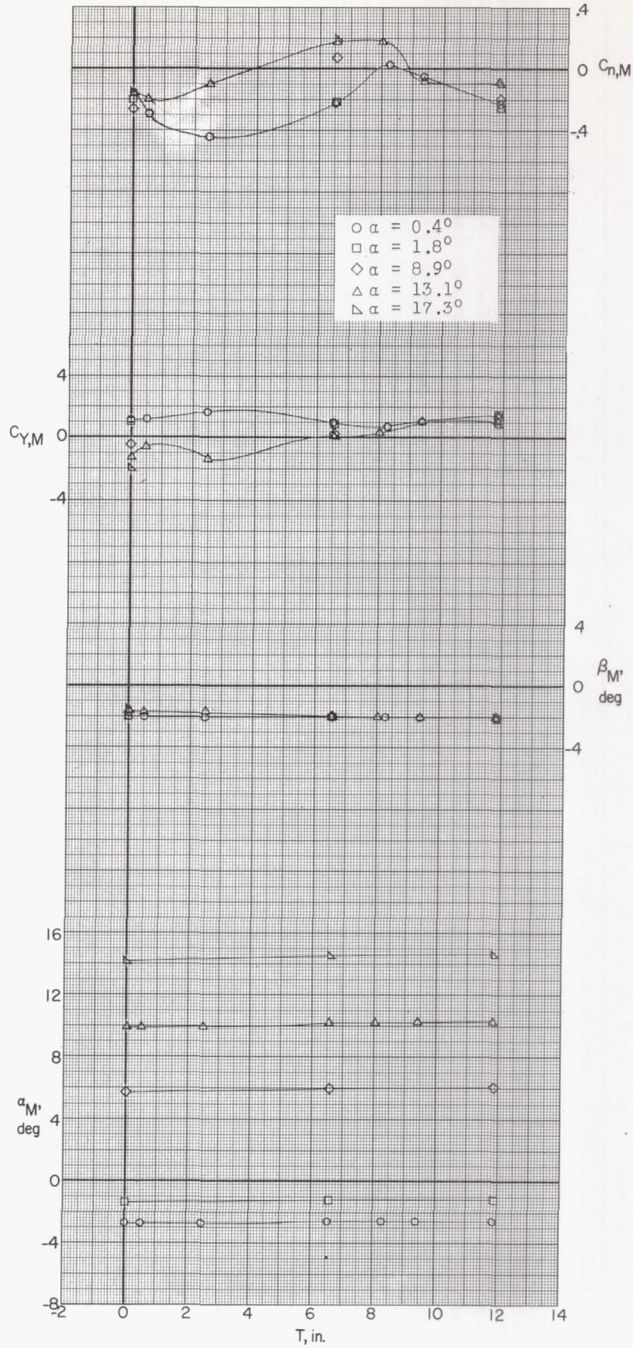
Figure 15.- Continued.
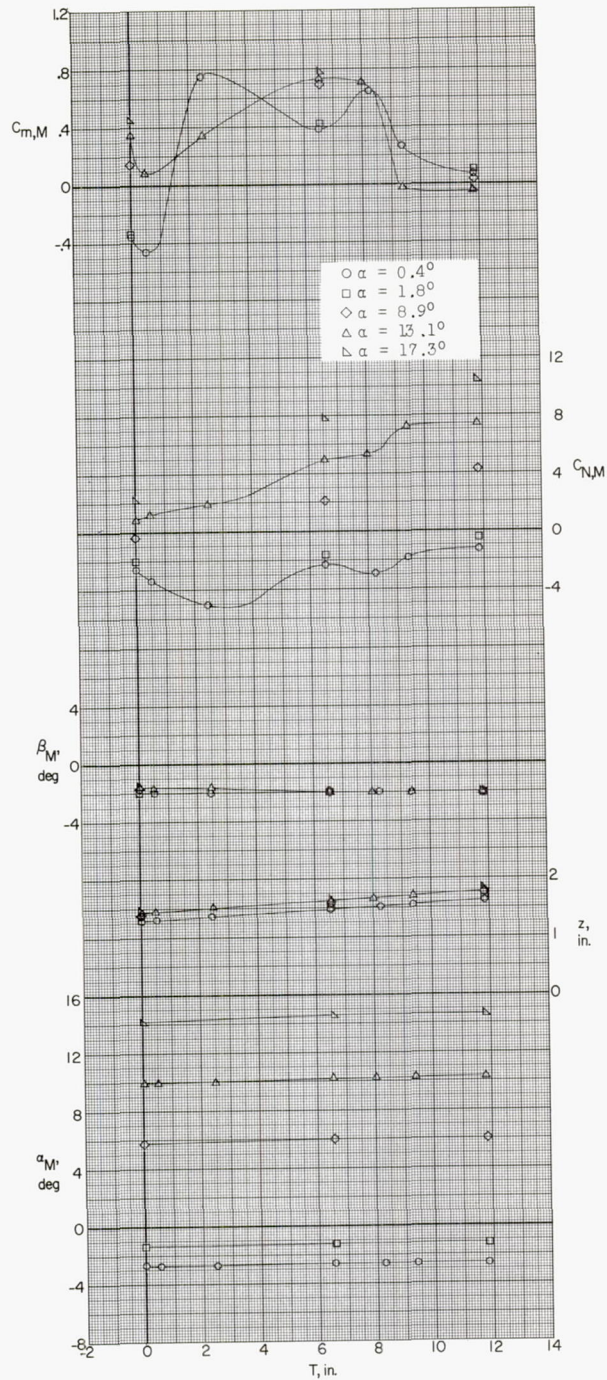
(b) Concluded.

Figure 15.- Continued.

(c)　M = 2.16; β = 0°.
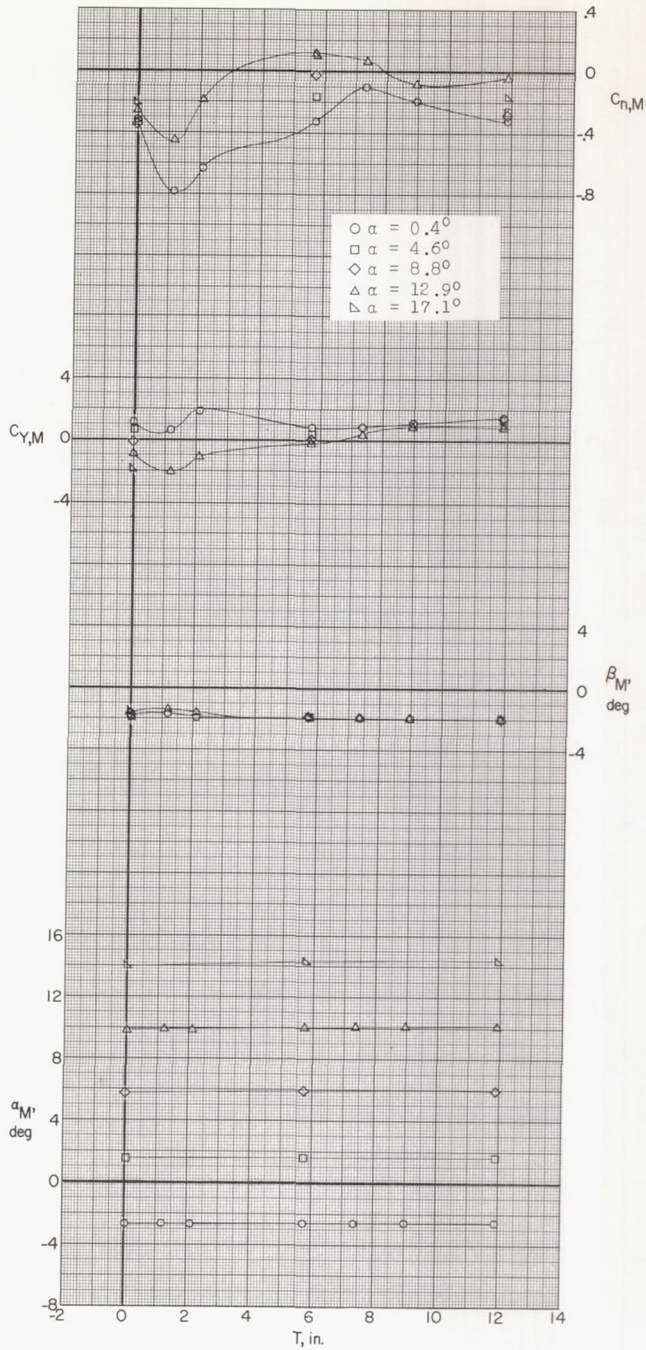
Figure 15.- Continued.

(c) Concluded.

Figure 15.- Concluded.
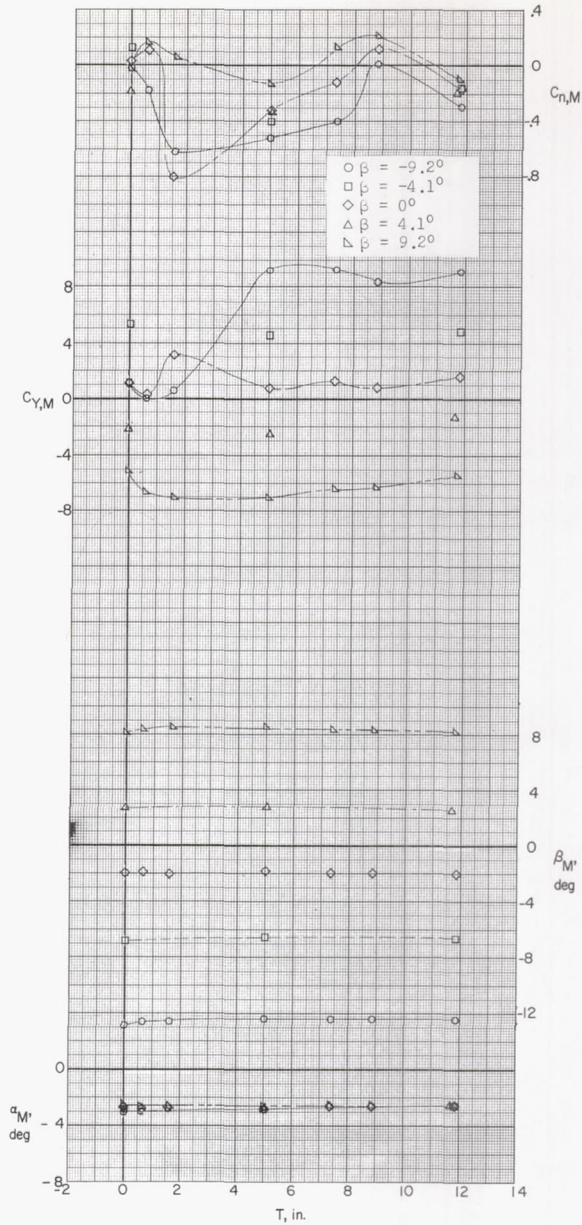
(a)   M = 1.57; α = 0°.

Figure 16.- Aerodynamic loads on the forward missile at various
traverse positions and angles of sideslip.
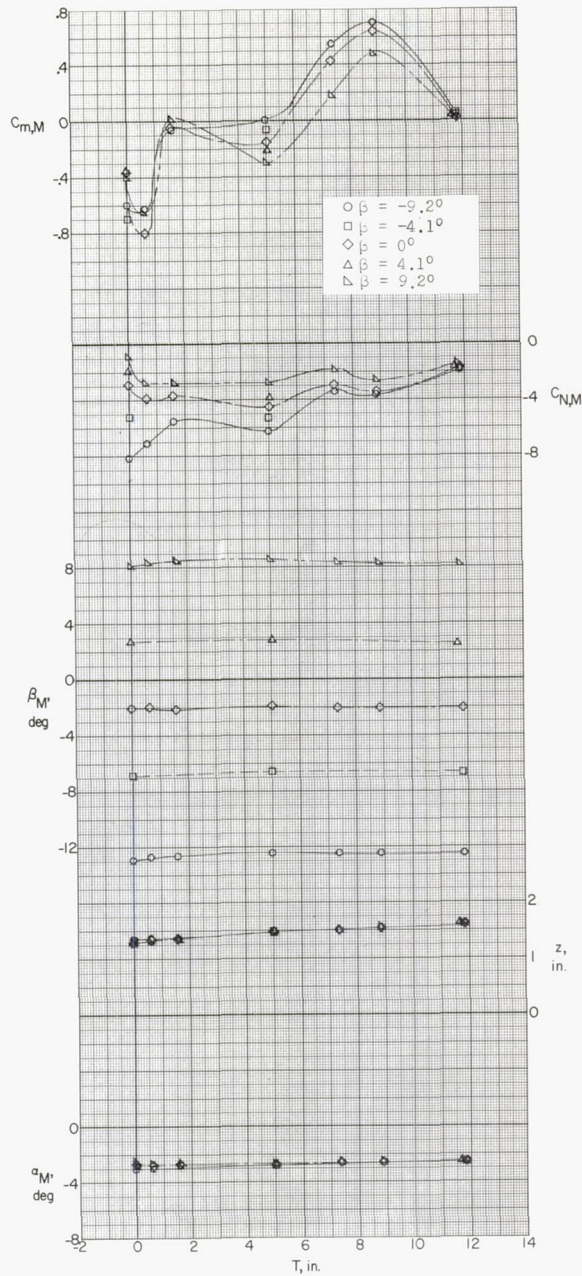
(a) Concluded.

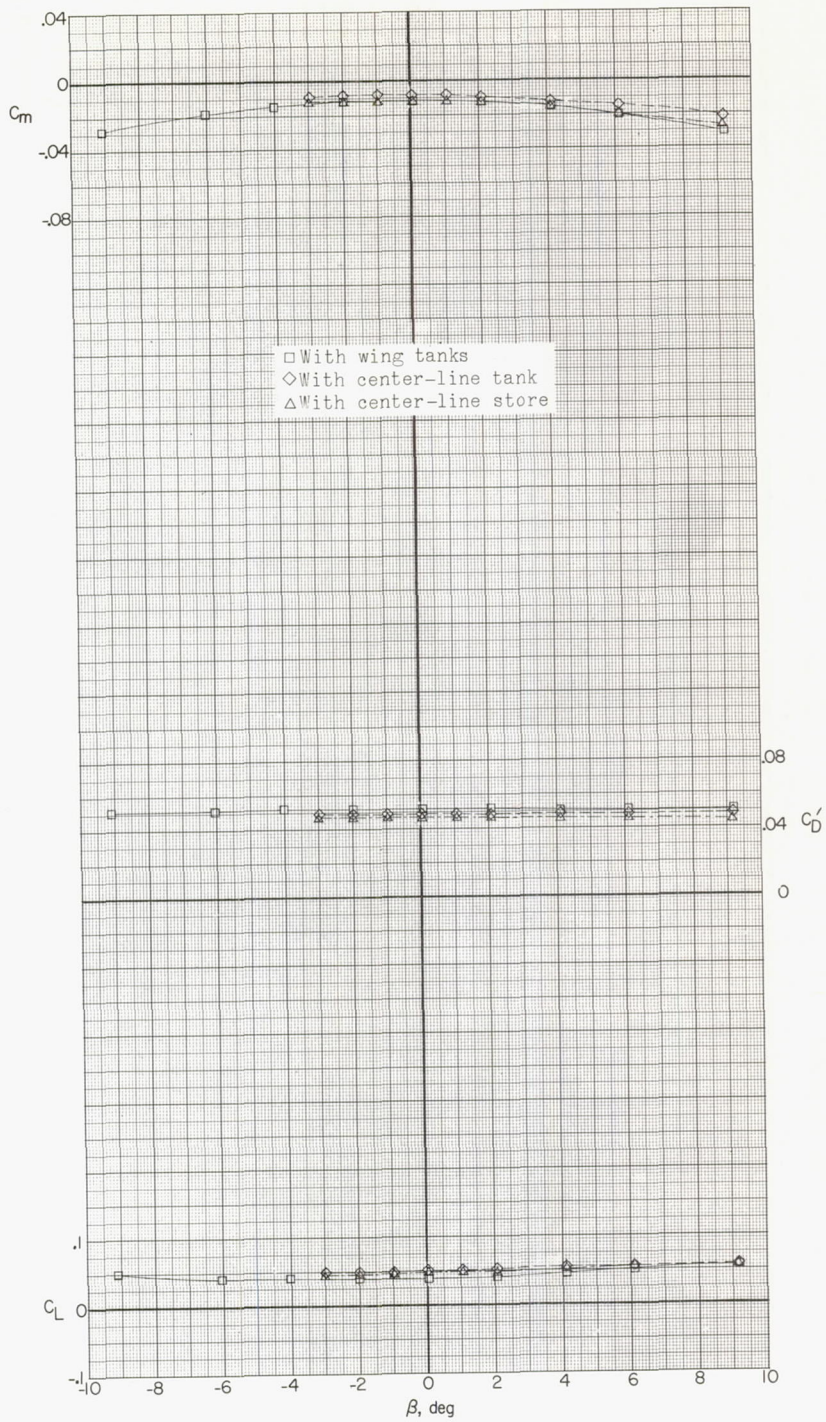Figure 16.- Continued.

(b) M = 1.87; α = 0°.
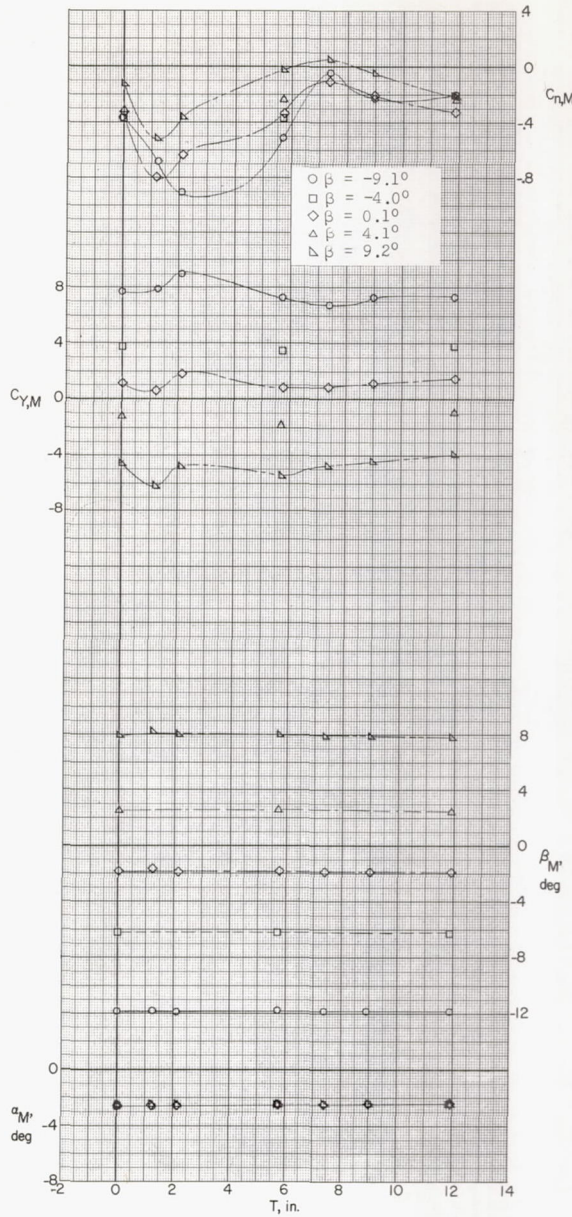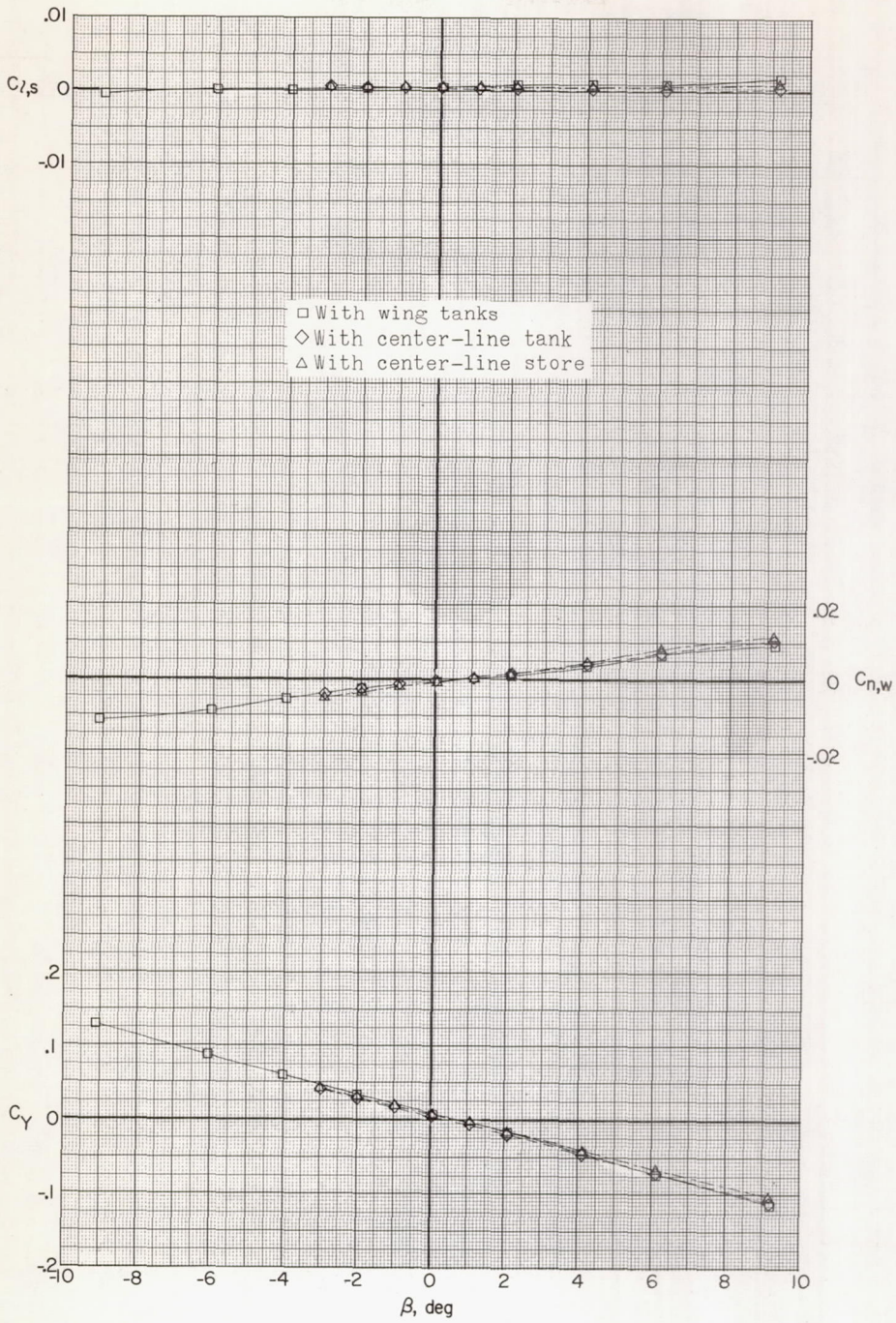
Figure 16.- Continued.
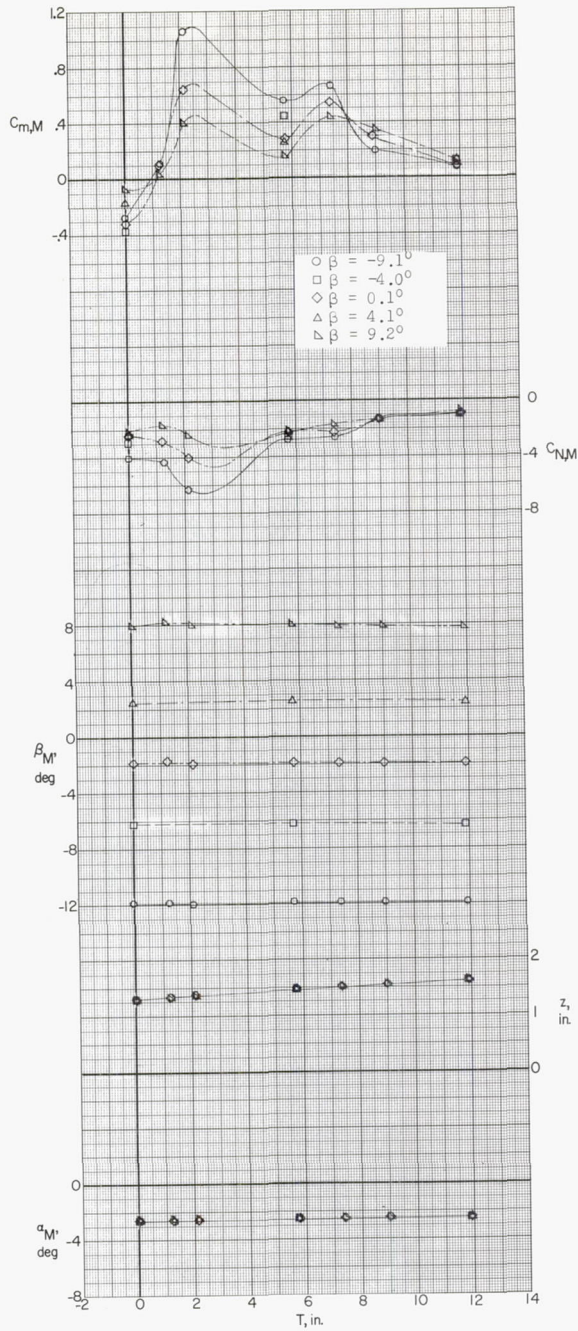
(b) Concluded.

Figure 16.- Continued.

(c) M = 2.16; α = 0°.
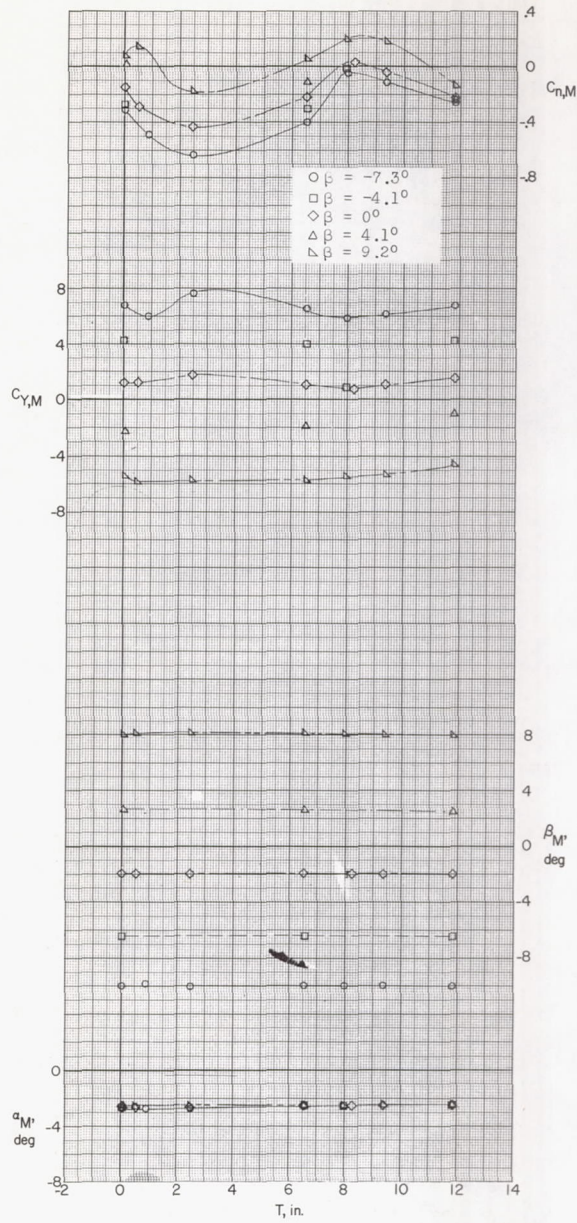
Figure 16.- Continued.

(c) Concluded.

Figure 16.- Concluded.
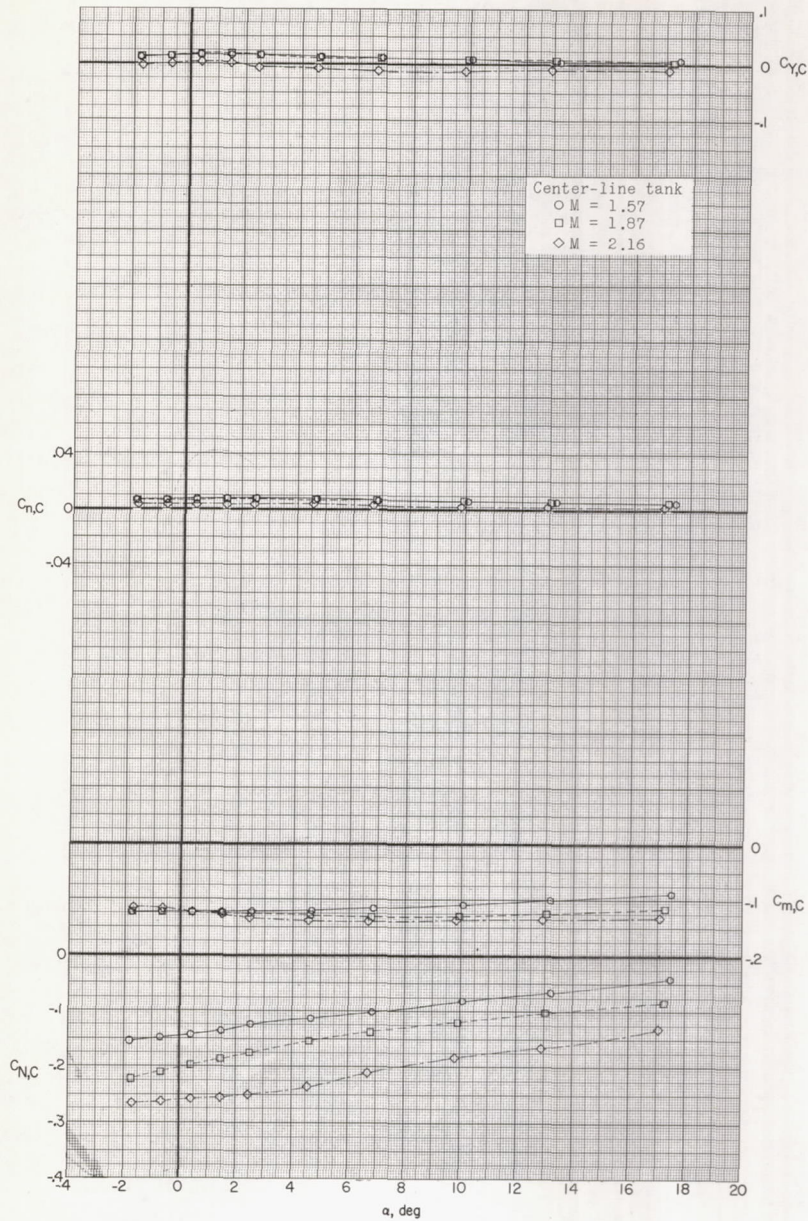
(a) Center-line tank.

Figure 17.- Aerodynamic loads on external stores in pitch.
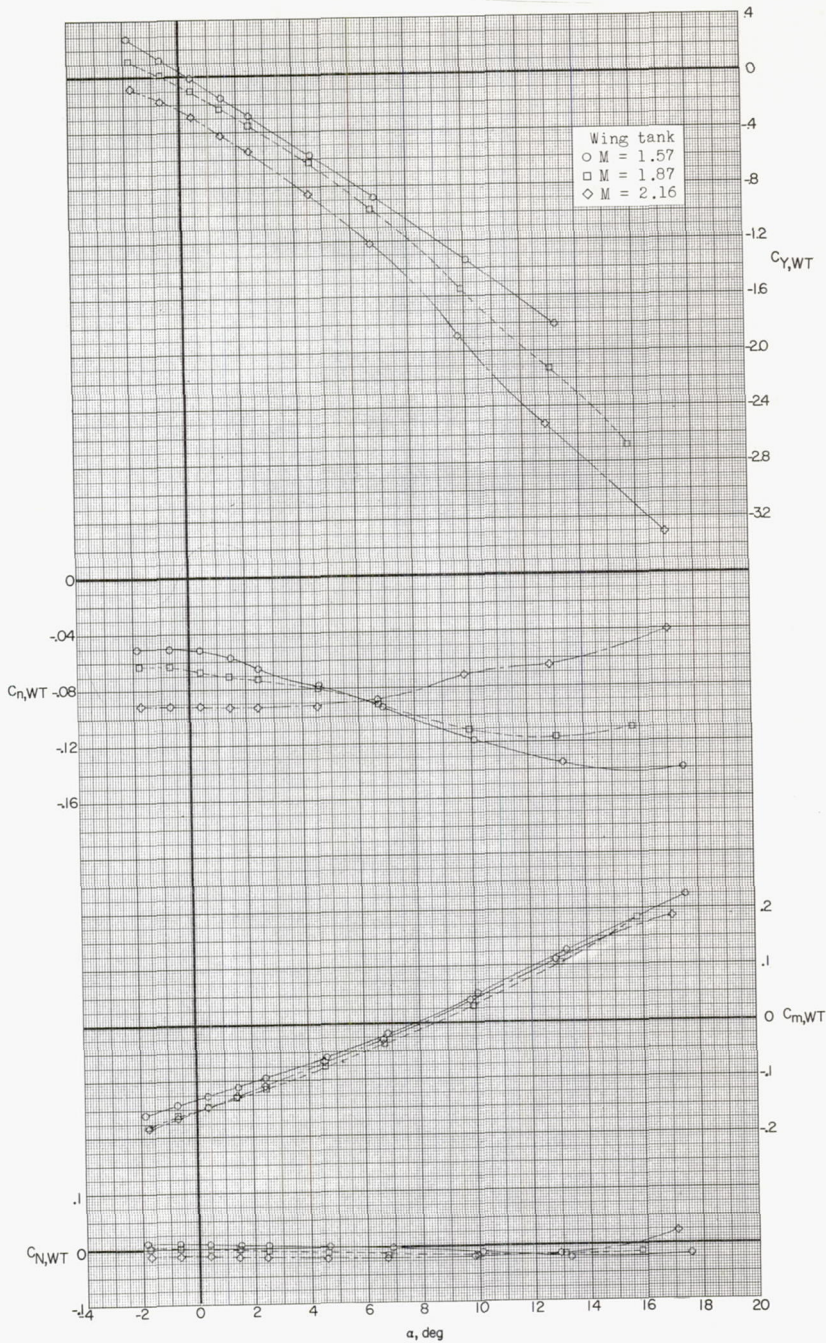
(b) Wing tank.

Figure 17.- Continued.

(c) Center-line store.

Figure 17.- Concluded.
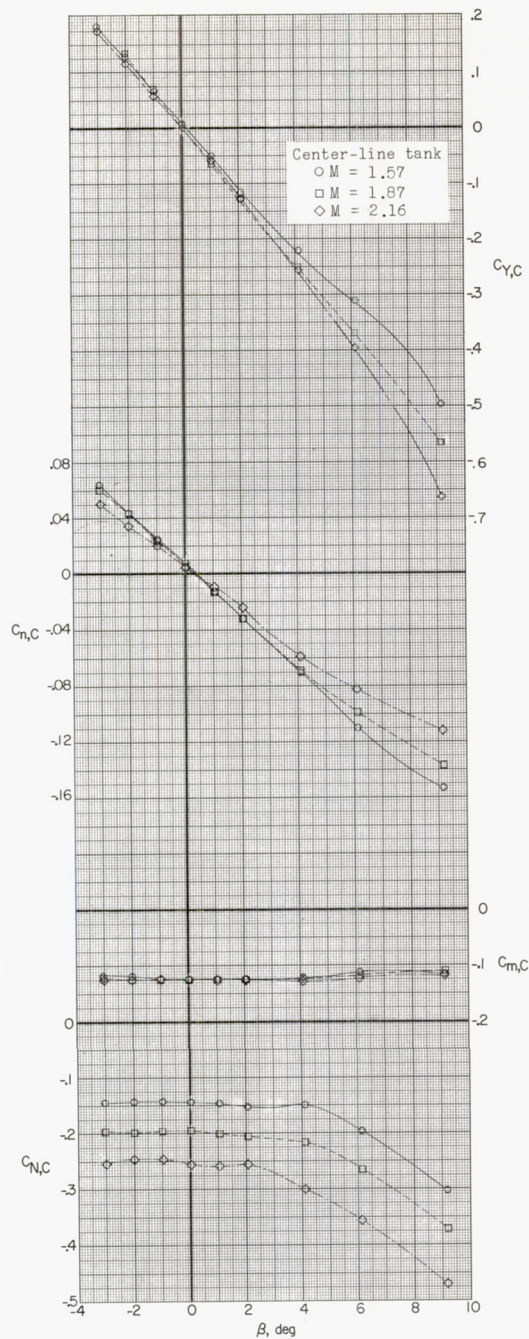
(a) Center-line tank.

Figure 18.- Aerodynamic loads on external stores in sideslip.
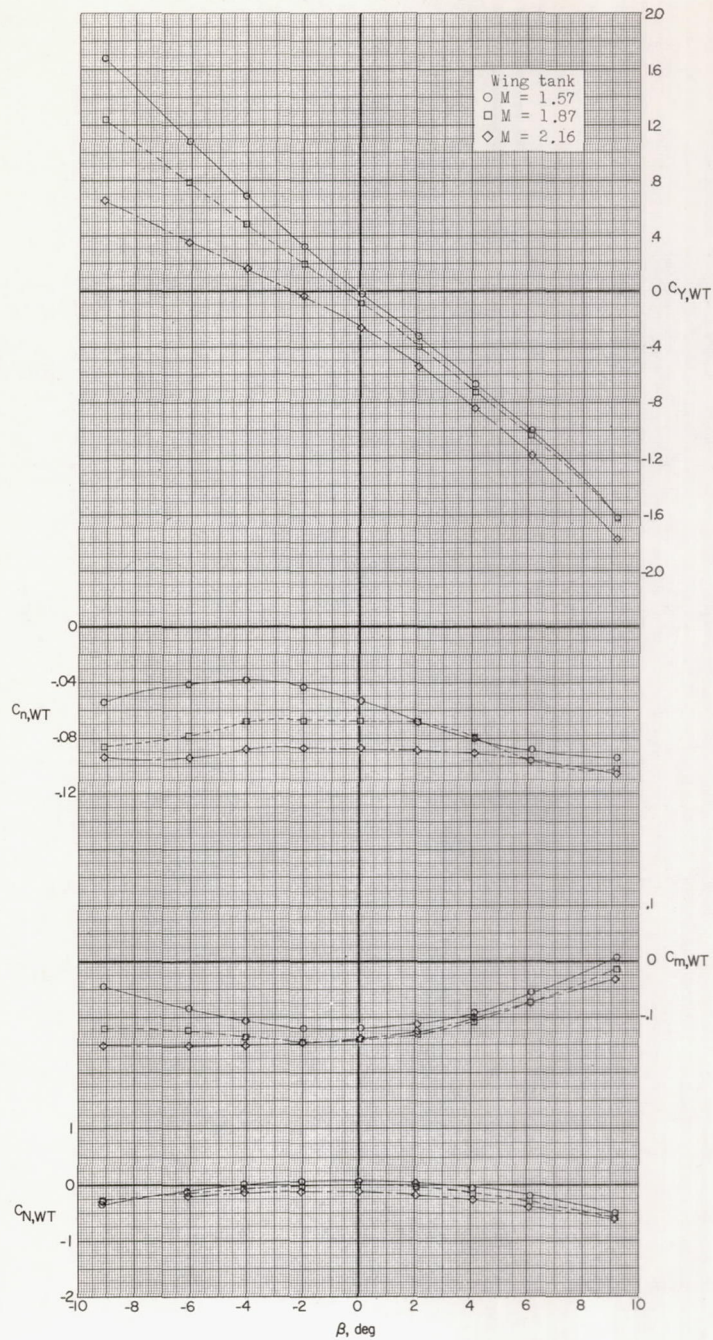
(b) Wing tank.

Figure 18.- Continued.
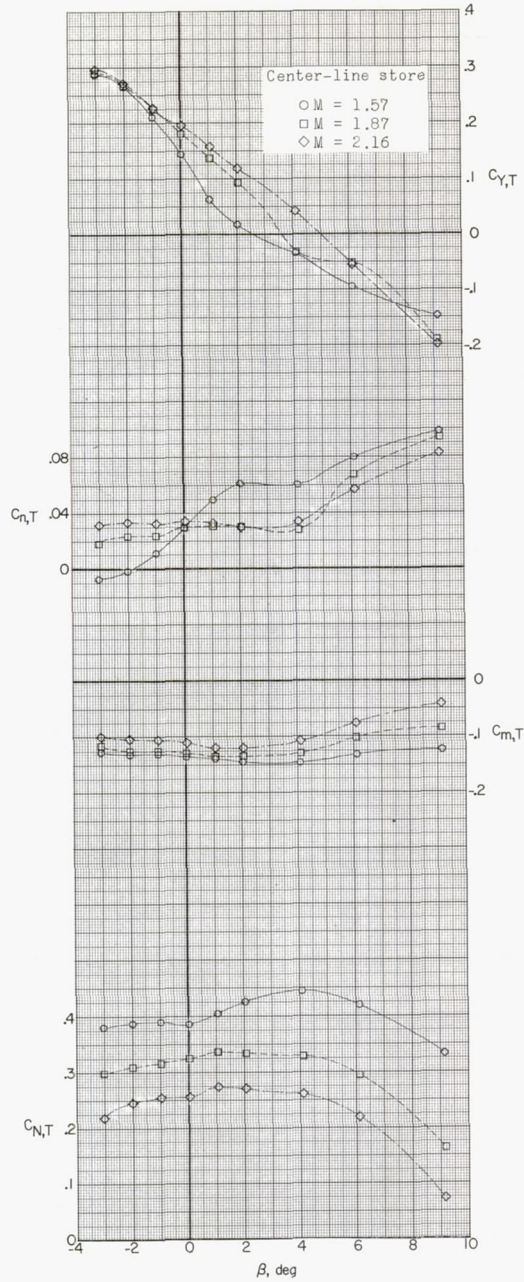
(c) Center-line store.

Figure 18.- Concluded.
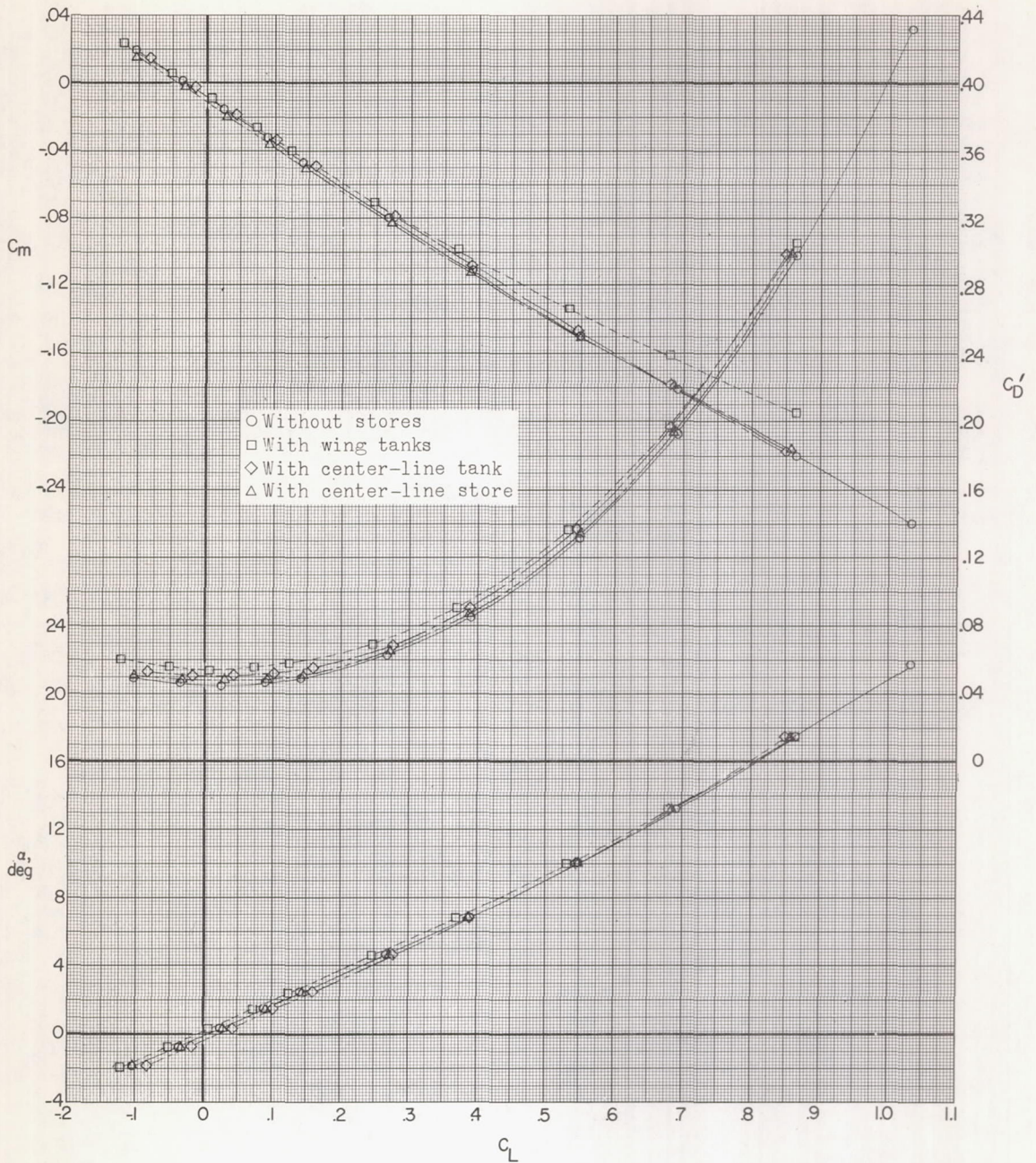
(a)　M = 1.57.

Figure 19.- Effect of external stores on aerodynamic characteristics in pitch.
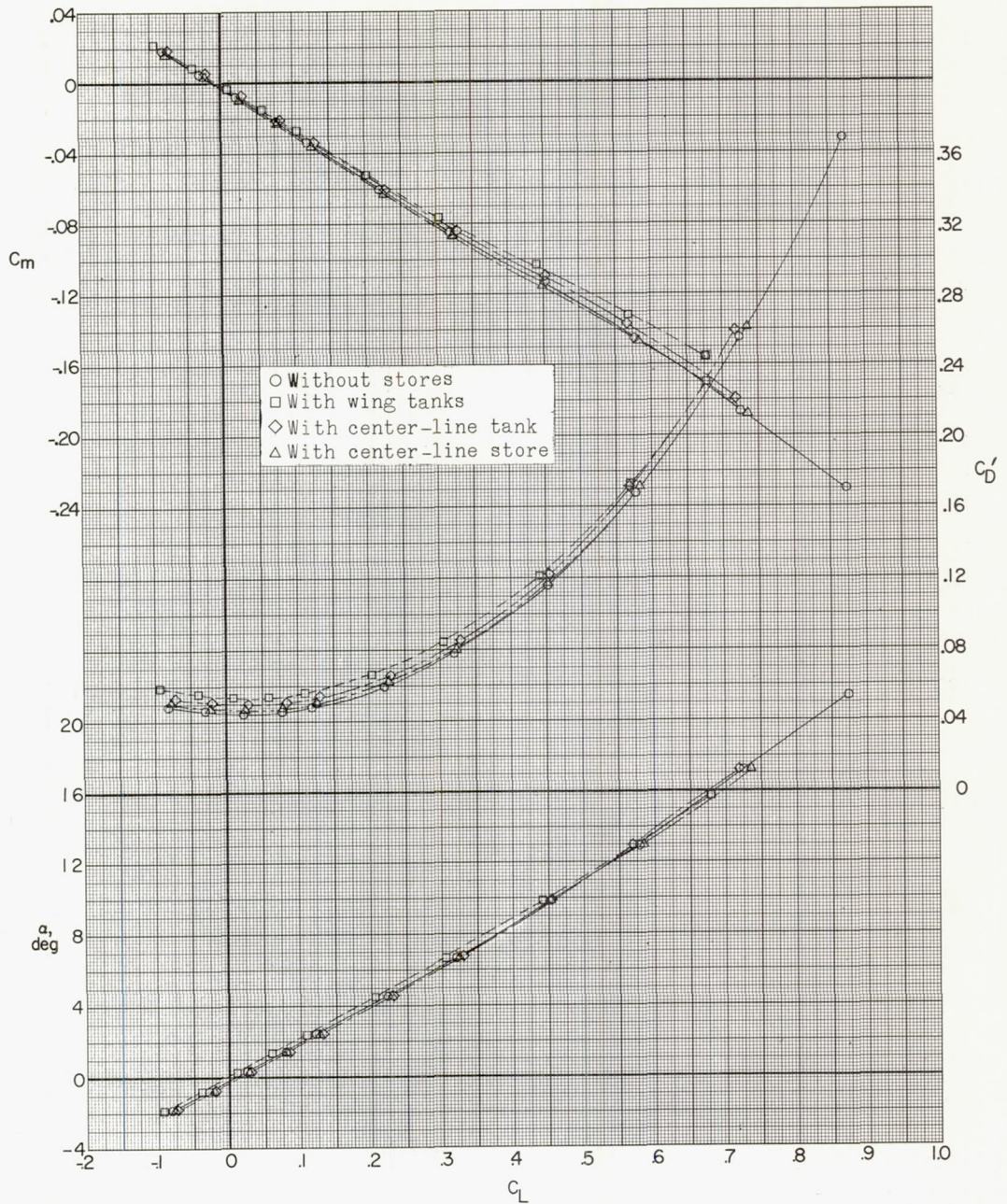
(b) M = 1.87.

Figure 19.- Continued.
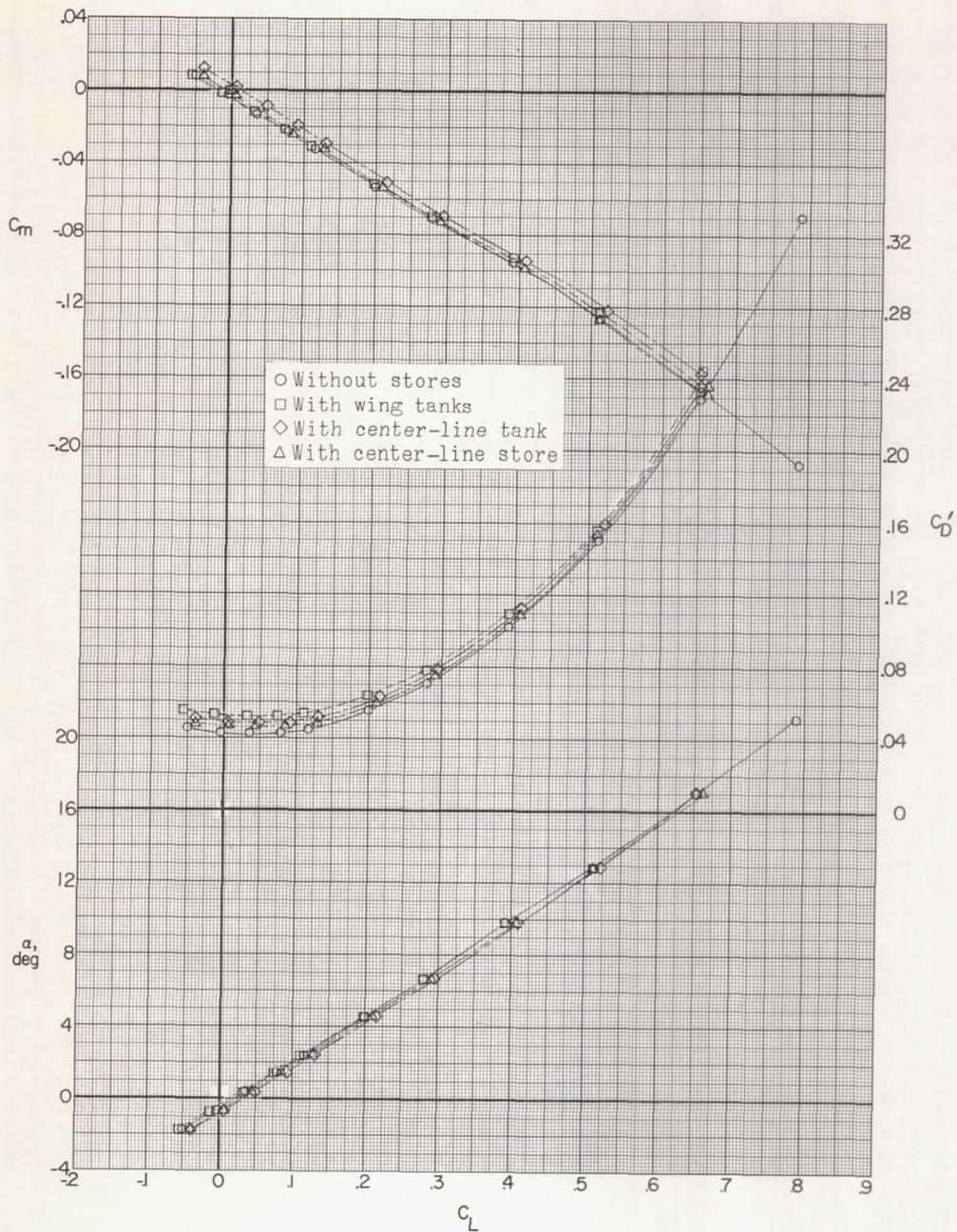
(c) M = 2.16.

Figure 19.- Concluded.
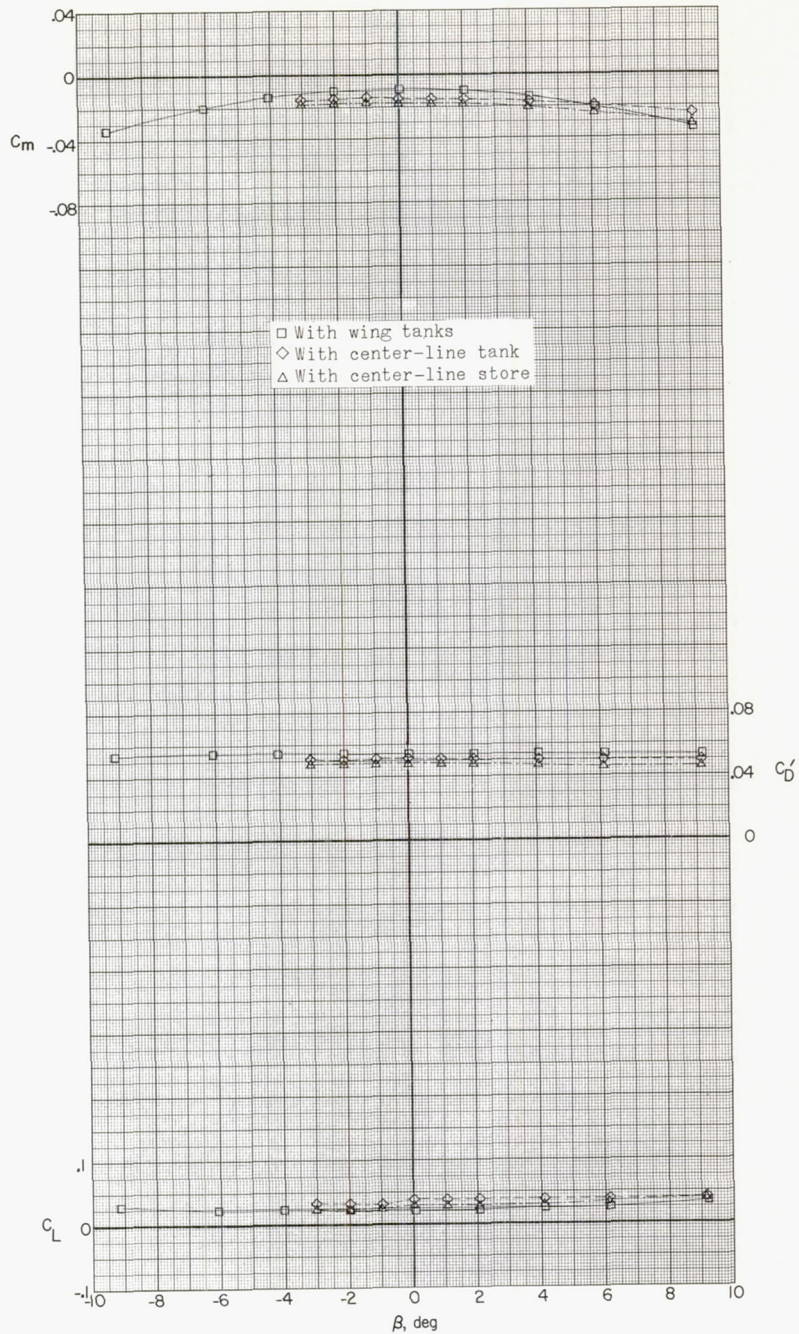
(a) M = 1.57.

Figure 20.- Effect of external stores on aerodynamic characteristics
in sideslip.
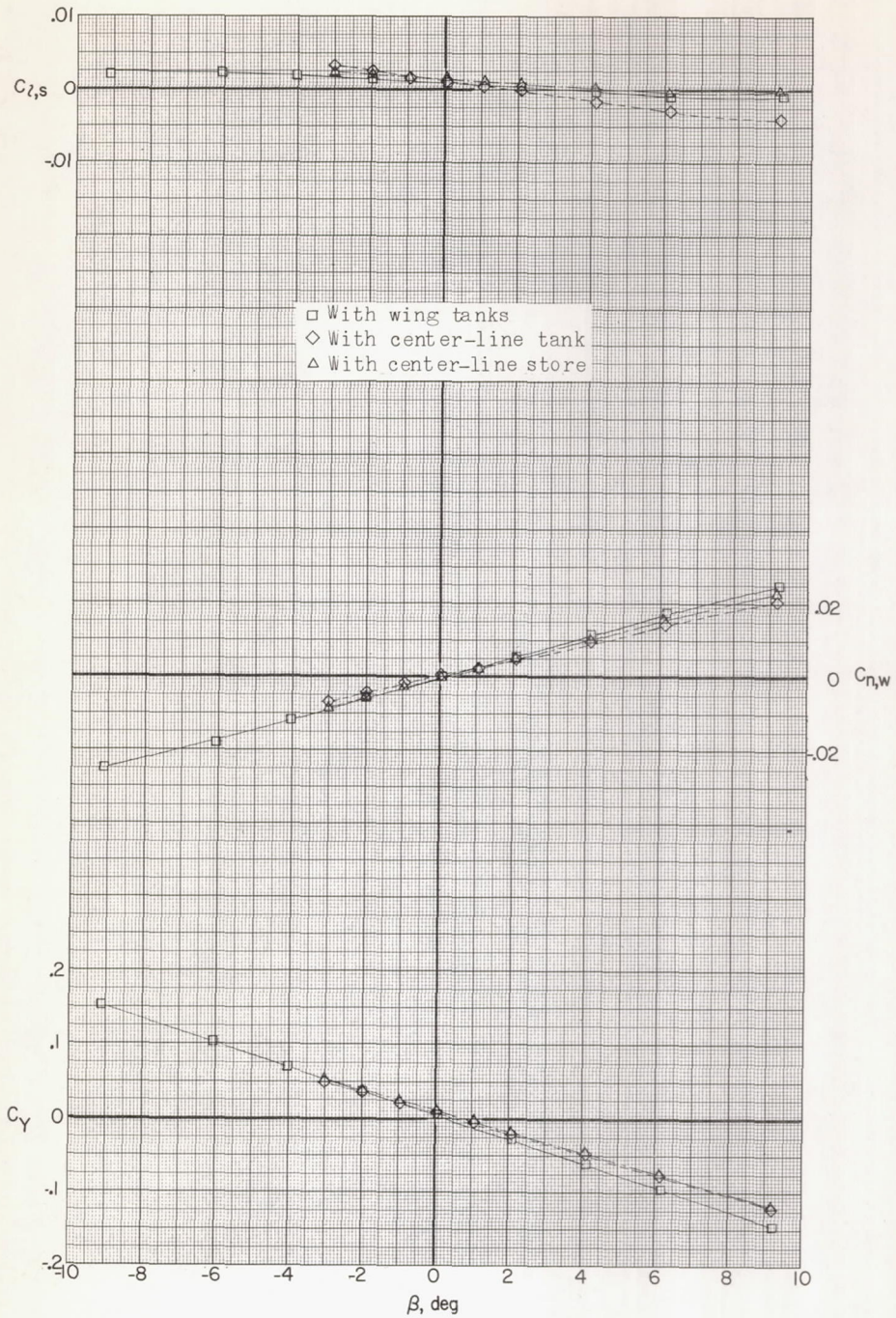
(a) Concluded.

Figure 20.- Continued.
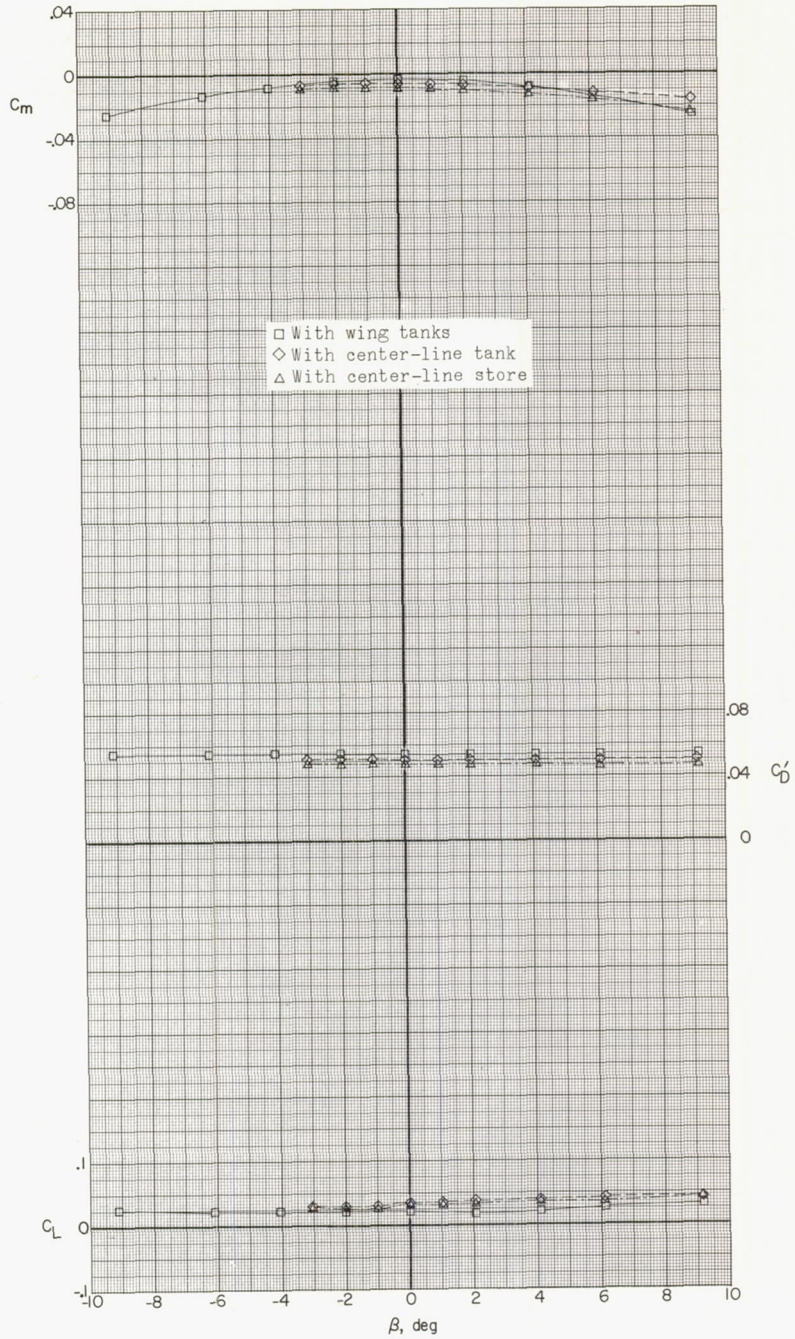
(b)   M = 1.87.

Figure 20.- Continued.
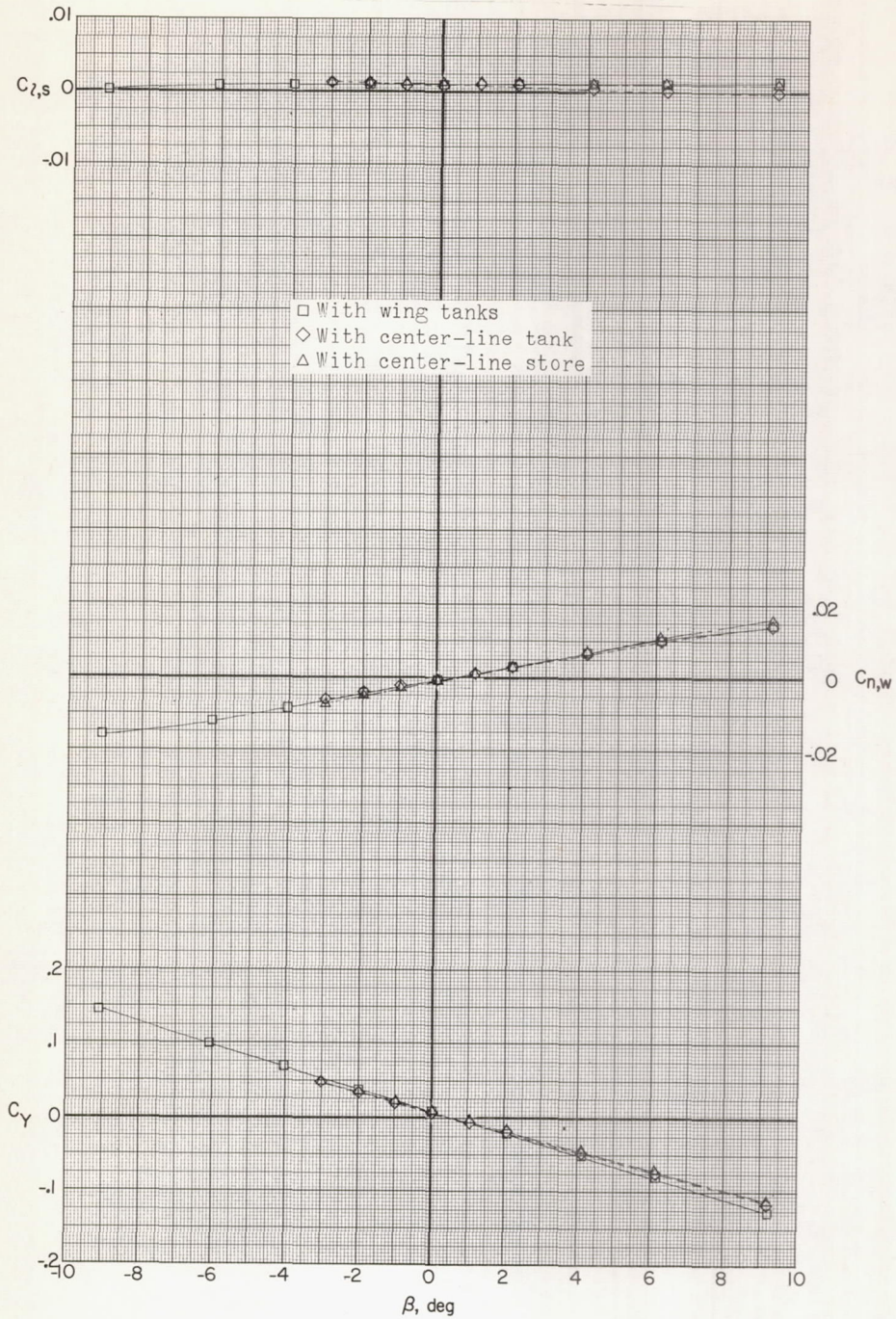
(b) Concluded.

Figure 20.- Continued.

(c)   M = 2.16.

Figure 20.- Continued.

(c) Concluded.

Figure 20.- Concluded.
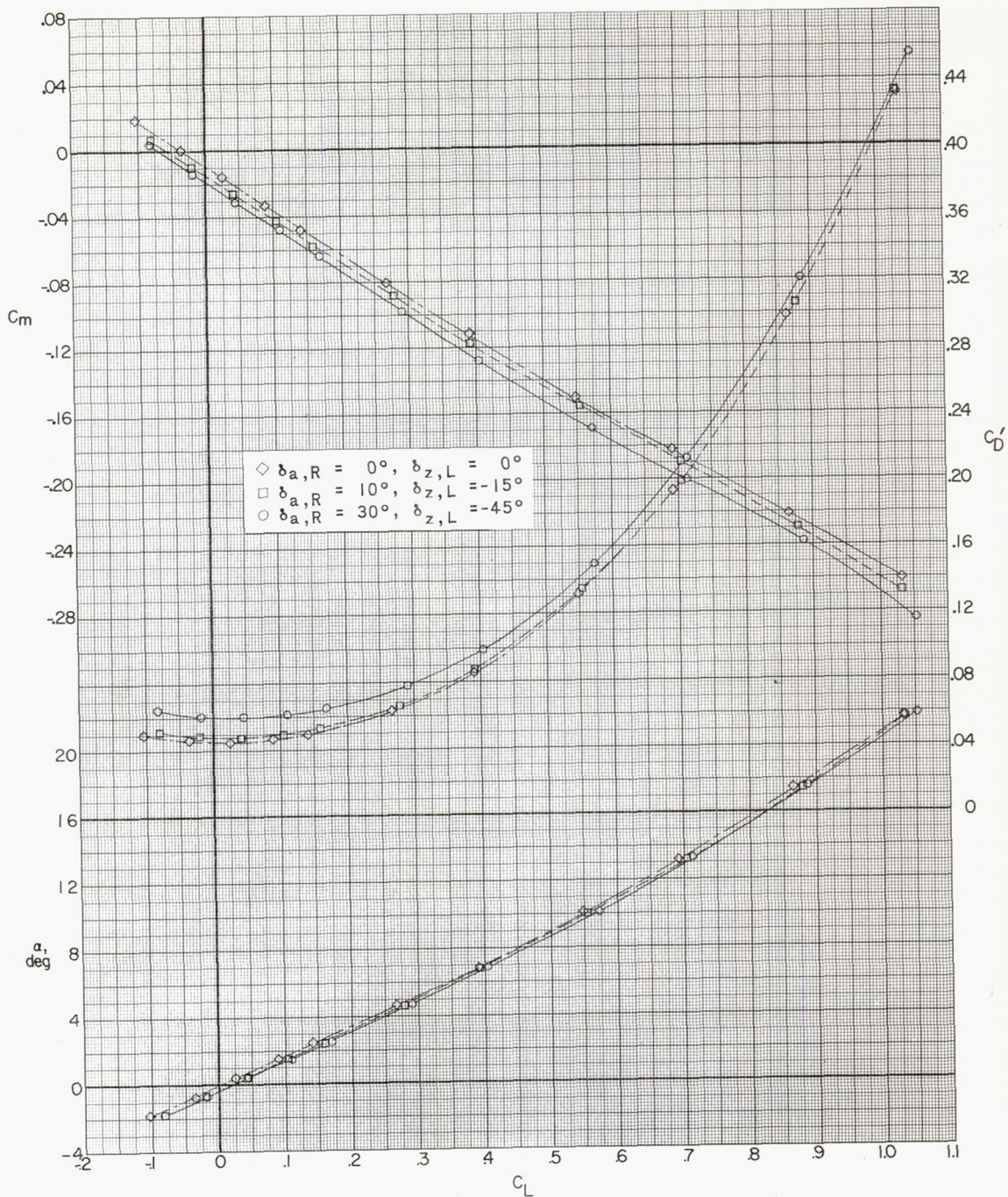
(a)   M = 1.57.

Figure 21.- Effect of aileron and spoiler deflections on aerodynamic
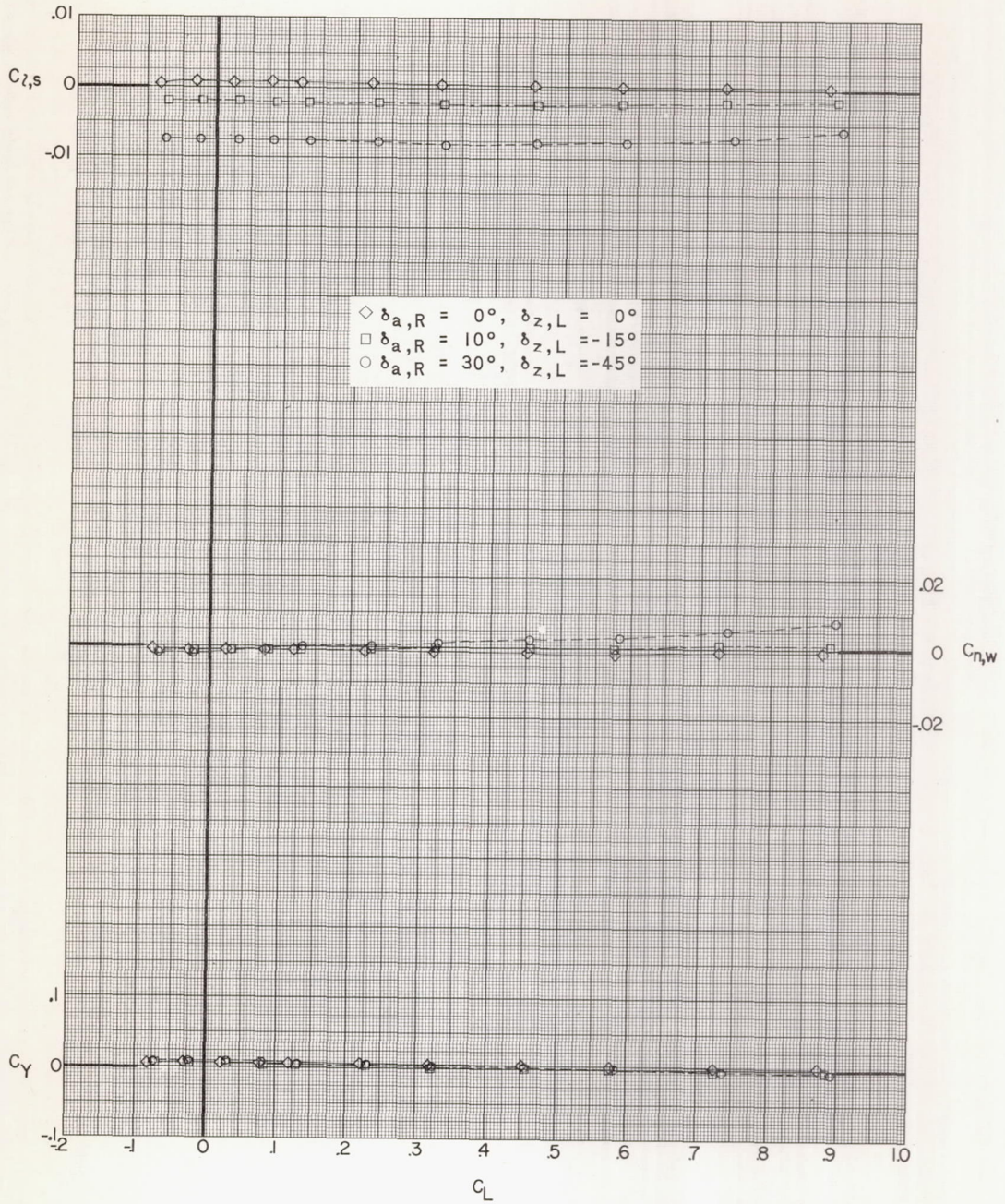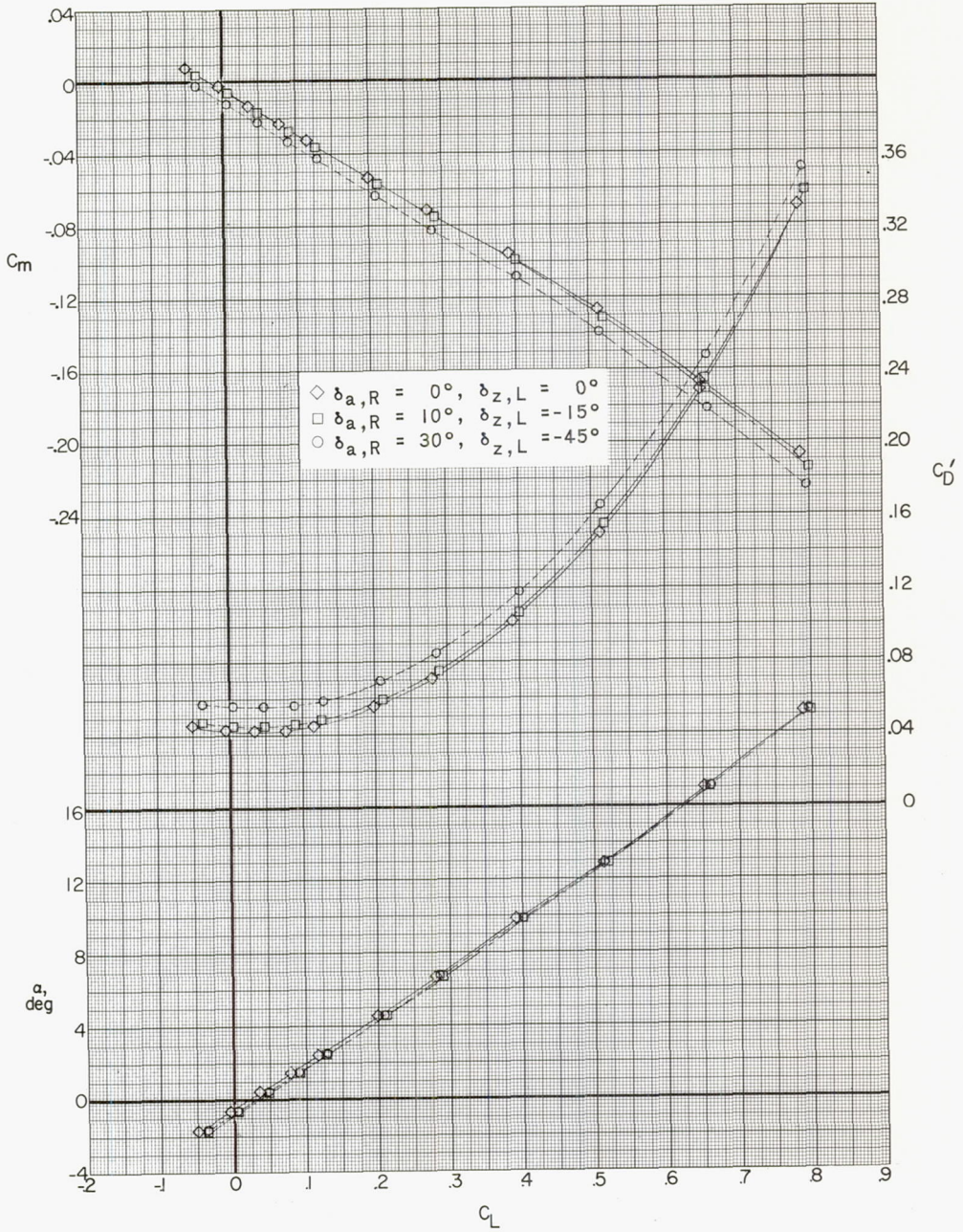characteristics in pitch.
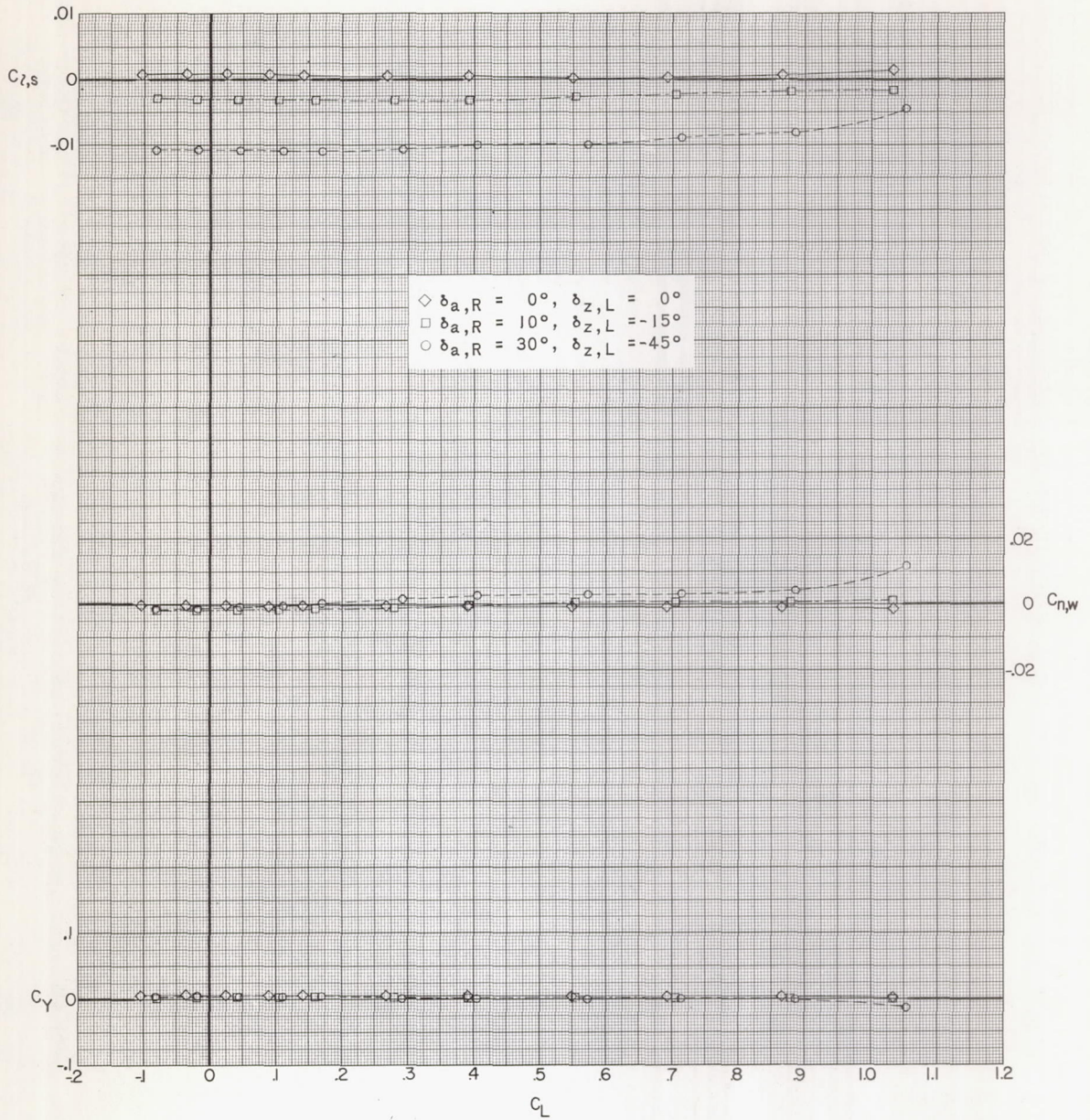
(a) Concluded.

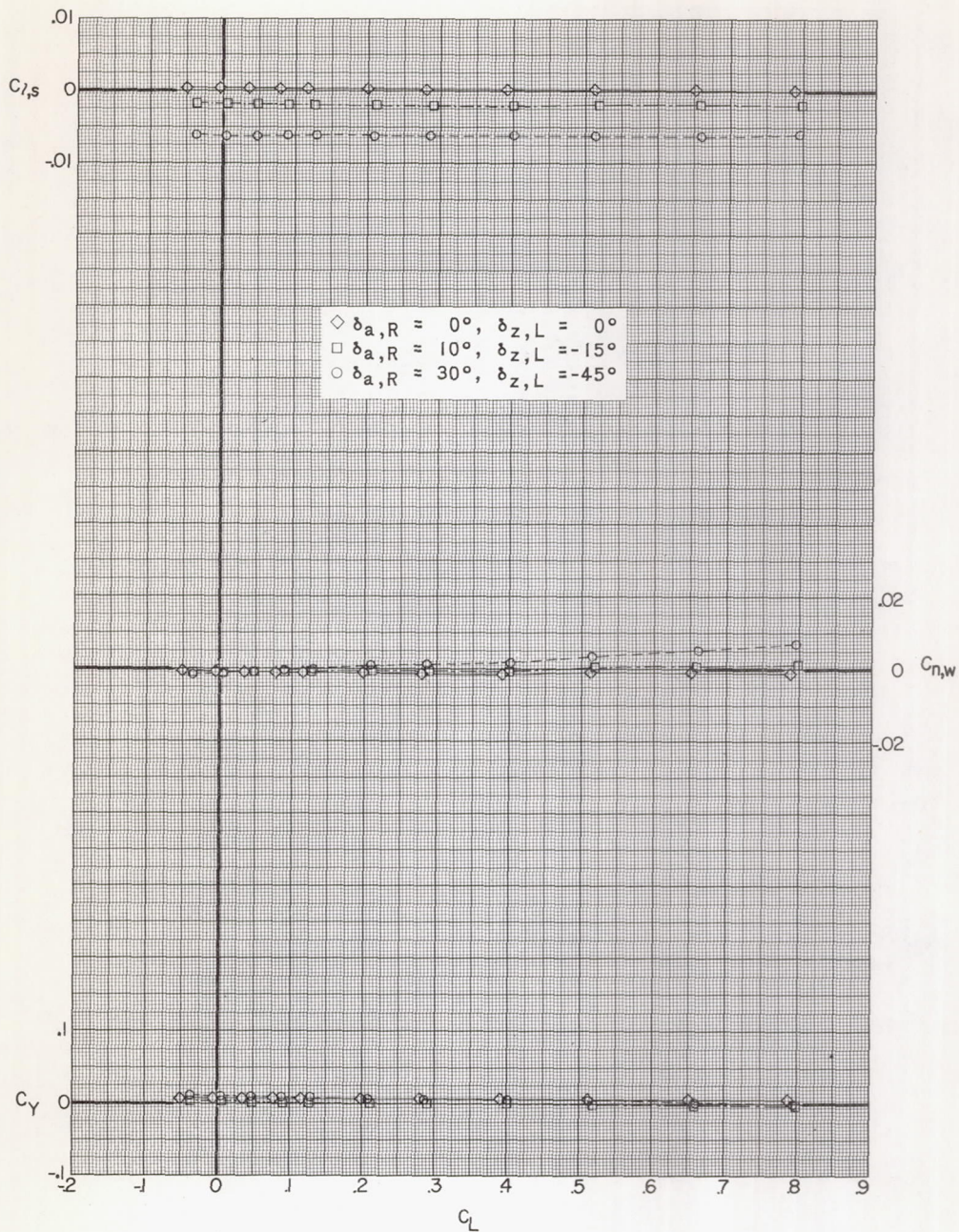Figure 21.- Continued.
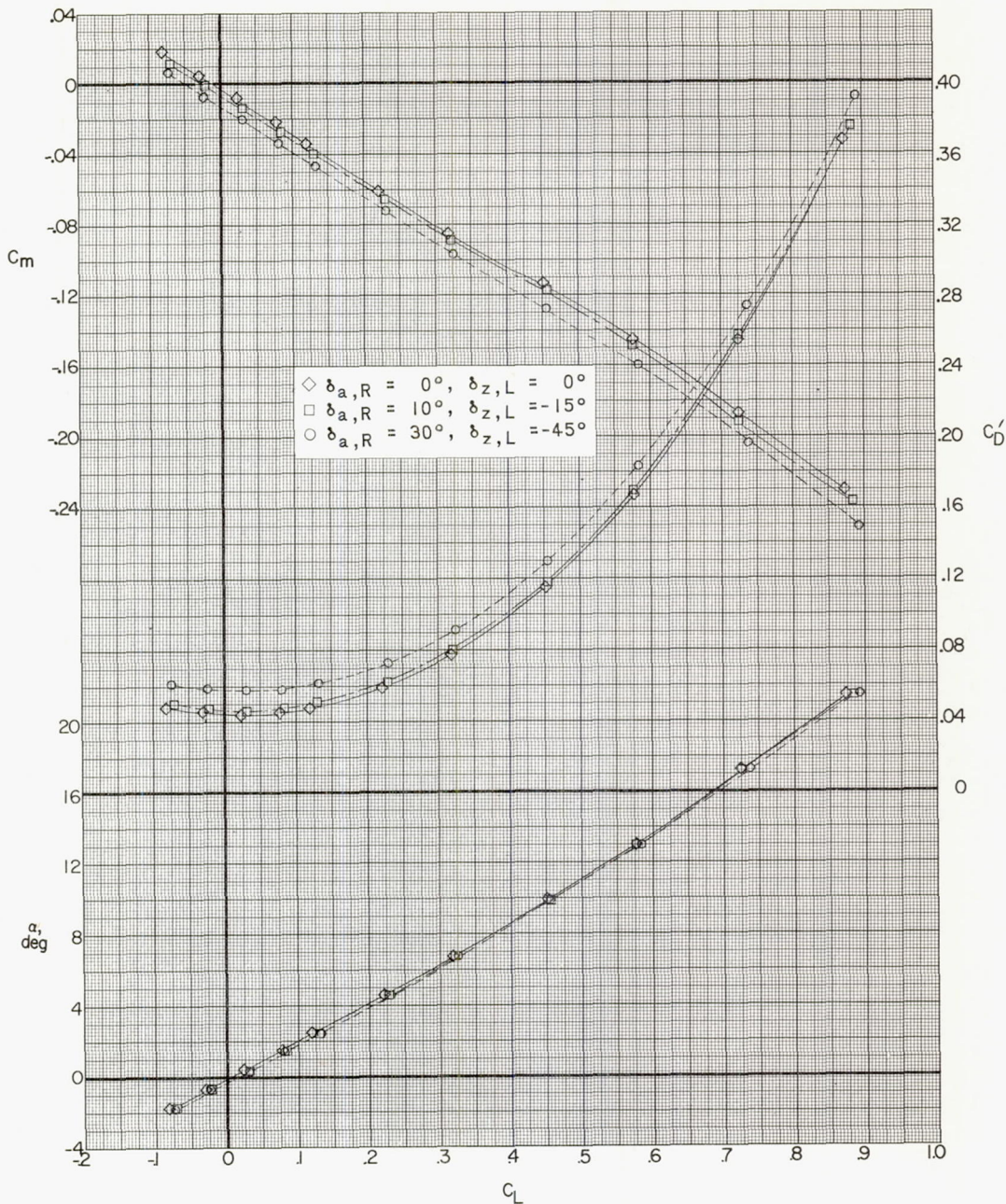
(b) M = 1.87.

Figure 21.- Continued.

(b) Concluded.

Figure 21.- Continued.

(c) M = 2.16.

Figure 21.- Continued.
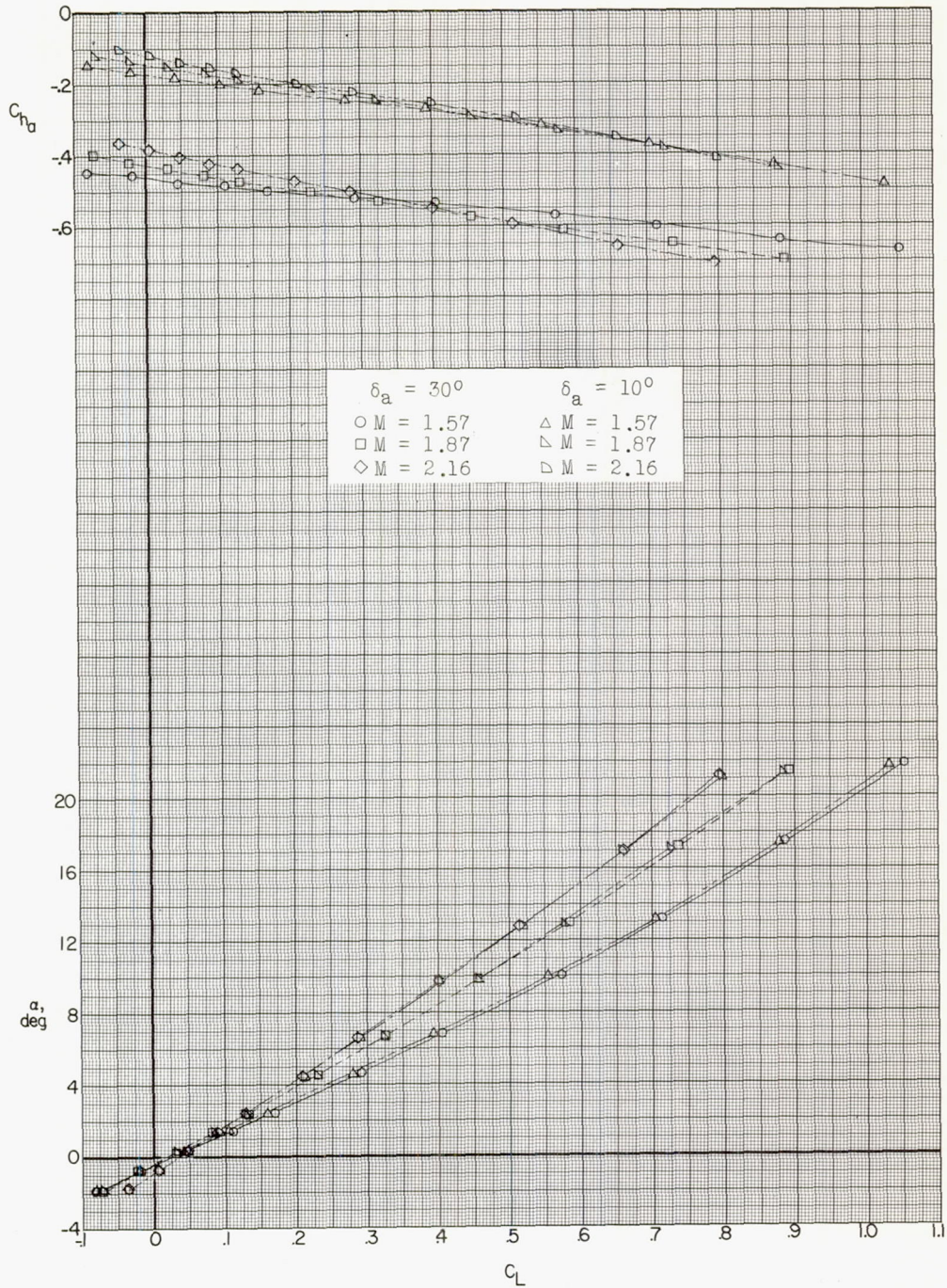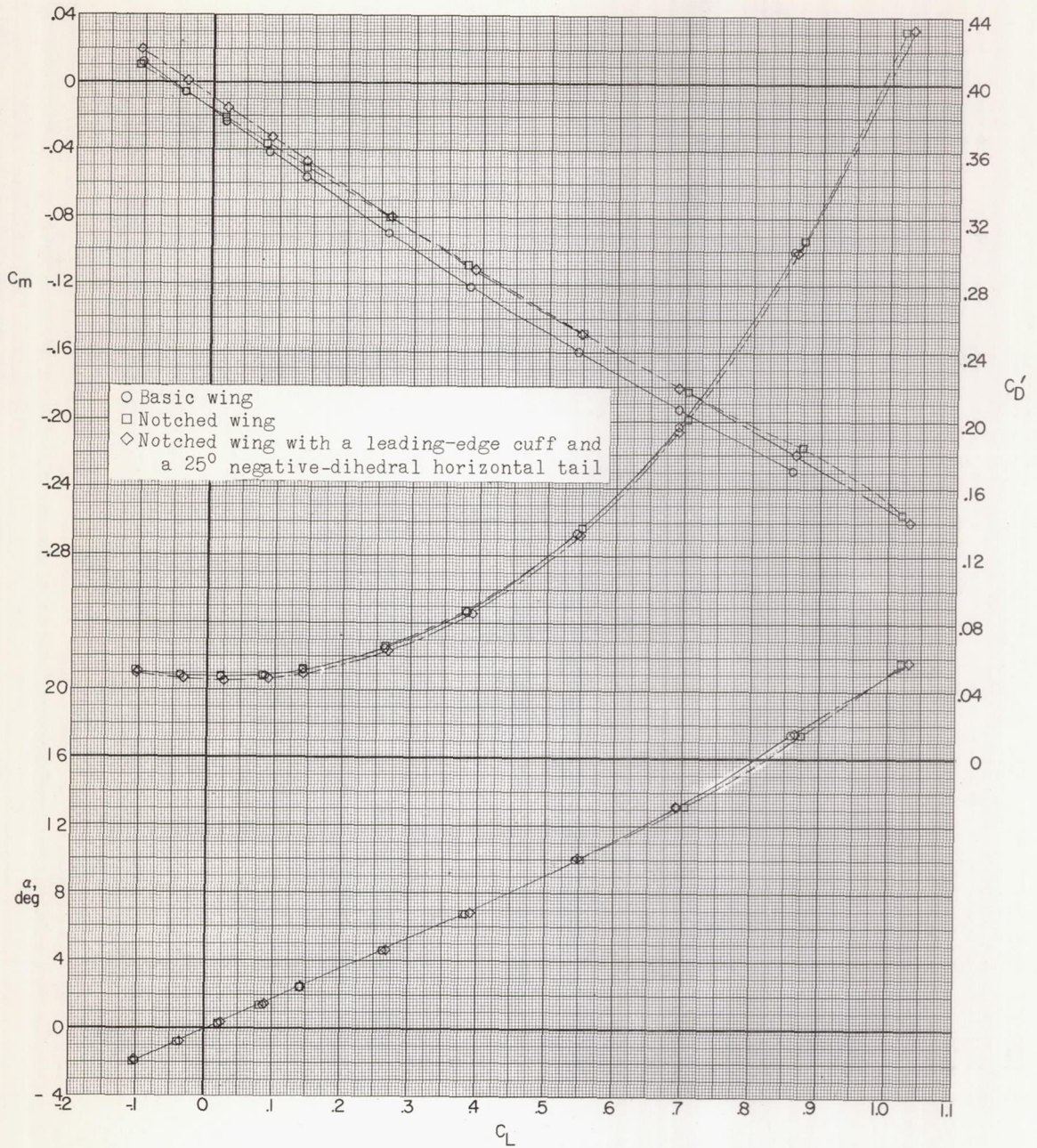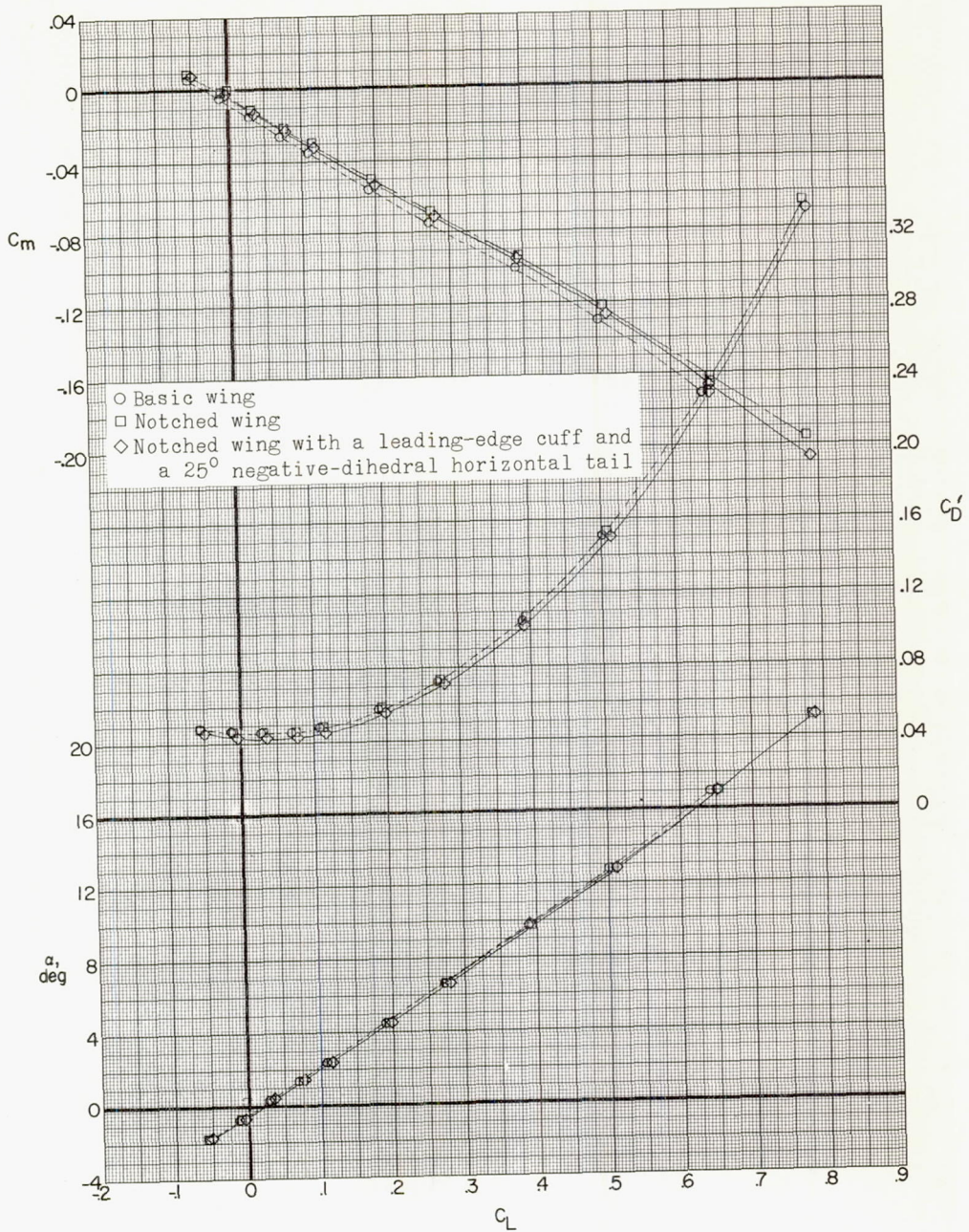
(c) Concluded.

Figure 21.- Concluded.

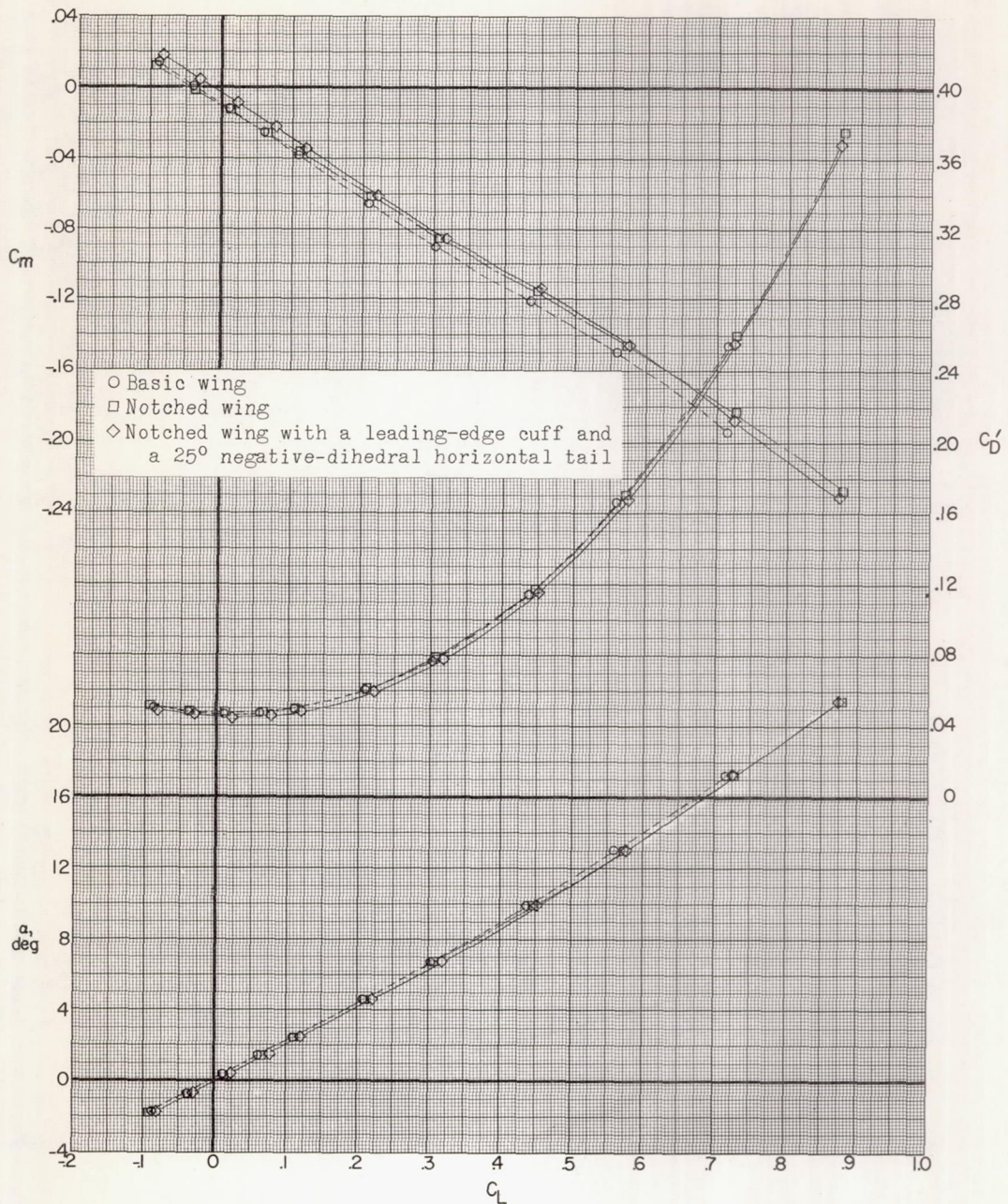Figure 22.- Effect of aileron deflection on aileron hinge-moment coefficient in pitch.

(a) M = 1.57.

Figure 23.- Effect of wing modifications on aerodynamic characteristics
in pitch.

(b)   M = 1.87.

Figure 23.- Continued.

(c) M = 2.16.

Figure 23.- Concluded.